PRODUCTION AND CHARACTERIZATION OF POLYPROPYLENE/ORGANOCLAY NANOCOMPOSITES

A THESIS SUBMITTED TO
THE GRADUATE SCHOOL OF NATURAL AND APPLIED SCIENCES
OF
MIDDLE EAST TECHNICAL UNIVERSITY

BY

SANİYE YAYLA

IN PARTIAL FULFILLMENT OF THE REQUIREMENTS
FOR
THE DEGREE OF MASTER OF SCIENCE
IN
CHEMICAL ENGINEERING

JUNE 2007

Approval of the Graduate School of Natural and Applied Sciences

_____

Prof. Dr. Canan Özgen
Director

I certify that this thesis satisfies all the requirements as a thesis for the degree of Master of Science

_____

Prof. Dr. Nurcan Baç
Head of Department

This is to certify that we have read this thesis and that in our opinion it is fully adequate, in scope and quality, as a thesis for the degree of Master of Science.

_____

Prof. Dr. Ülkü Yılmazer
Supervisor

Examining Committee Members

Prof. Dr. Güngör Gündüz (METU, CHE) _____

Prof. Dr. Ülkü Yılmazer (METU, CHE) _____

Prof. Dr. Nurcan Baç (METU, CHE) _____

Prof. Dr. Cevdet Kaynak (METU, METE) _____

Assoc. Prof. Dr. Göknur Bayram (METU, CHE) _____

I hereby declare that all information in this document has been obtained and presented in accordance with academic rules and ethical conduct. I also declare that, as required by these rules and conduct, I have fully cited and referenced all material and results that are not original to this work.

Name, Last name: Saniye Yayla

Signature:

ABSTRACT

PRODUCTION AND CHARACTERIZATION OF POLYPROPYLENE/ORGANOCLAY NANOCOMPOSITES

Yayla, Saniye

M.S., Department of Chemical Engineering

Supervisor: Prof. Dr. Ülkü YILMAZER

June 2007, 180 pages

Polypropylene, PP, based nanocomposites were produced via melt blending method by using twin-screw extrusion in this study. The effects of organoclay type, compatibilizer type, and mixing order of components on the morphology, thermal, mechanical and flow properties of ternary nanocomposites were investigated. Terpolymer of ethylene/butyl acrylate/maleic anhydride, ethylene/methyl acrylate/glycidyl methacrylate, and copolymer of ethylene/glycidyl methacrylate elastomers were used as compatibilizer, whereas Cloisite® 30B, Cloisite® 15A, and Cloisite® 25A were used as organoclay.

In order to determine the optimum amount of compatibilizer, PP/compatibilizer blends were produced with different compositions. The content of compatibilizer was determined as 5 wt % based on the mechanical tests. Then, ternary nanocomposites were prepared with 5 wt % compatibilizer and 2 wt % organoclay contents. In addition, neat PP and PP/organoclay composites were prepared in order to make comparison. After that, the samples were characterized.

According to the XRD analysis, the highest increase in the interlayer spacings of organoclays were observed in the PP/E-MA-GMA/Cloisite® 15A (23%) and PP/E-MA-GMA/ Cloisite® 25A (88.3%) ternary systems. SEM micrograms revealed that compatibilizer E-MA-GMA is the most compatible elastomer with PP. Thus, it was decided to investigate the effect of mixing order on the properties of these nanocomposites with E-MA-GMA.

DSC analysis showed that the melting behavior of the nanocomposites does not change significantly with the presence of organoclay and compatibilizer. In addition, compatibilizers and organoclays have no significant nucleation activity in PP.

The systems PP/E-MA-GMA/Cloisite® 15A and PP/E-MA-GMA/Cloisite® 25A have the highest improvements according to the results of mechanical tests. The results of mechanical tests showed that the mixing sequence (PEC), in which PP, organoclay and compatibilizer were compounded simultaneously in the first extrusion run, is the best sequence.

Keywords: polypropylene, compatibilizer, organoclay, nanocomposites

ÖZ

POLİPROPİLEN/ORGANİKKİL NANOKOMPOZİTLERİNİN ÜRETİLMESİ VE KARAKTERİZASYONU

Yayla, Saniye
Yüksek Lisans, Kimya Mühendisliği
Tez Yöneticisi: Prof. Dr. Ülkü YILMAZER

Haziran 2007, 180 sayfa

Bu çalışmada, polipropilen, PP, bazlı nanokompozitler, eriyik karışımı yöntemi ile çift vidalı ekstrüzyon kullanılarak üretilmiştir. Organik kil türü, uyum sağlayıcı tipi ve bileşenleri karıştırma sırasının, morfoloji, ısıl, mekanik ve akış özelliklerine olan etkileri incelenmiştir. Uyum sağlayıcı olarak etilen/bütil akrilat/maleik anhidrit, etilen/metil akrilat/glisidil metakrilat terpolimerleri ve etilen/glisidil metakrilat kopolimeri kullanılırken, organikkil olarak da Cloisite® 30B, Cloisite® 15A, ve Cloisite® 25A kullanılmıştır.

Uyum sağlayıcının en uygun miktarını belirleyebilmek için, farklı bileşenlerde PP/uyum sağlayıcı karışımları hazırlanmıştır. Mekanik test sonuçlarına

dayanarak, uyum sağlayıcı miktarı kütlece % 5 olarak saptanmıştır. Ayrıca, sonuçları karşılaştırabilmek için katkısız PP ve PP/organik kil kompozitleri de hazırlanmıştır. Daha sonra, tüm örnekler incelenmiştir.

XRD analizi sonuçlarına göre, organik killerin tabaka aralığındaki en yüksek artış, PP/E-MA-GMA/Cloisite® 15A (23%) ve PP/E-MA-GMA/Cloisite® 25A (88.3%) üçlü nanokompozitlerinde gözlemlenmiştir. SEM mikrografikleri ise PP ile en uyumlu terpolimerin E-MA-GMA olduğunu göstermiştir. Bu sonuca göre, karıştırma sırasının etkilerini E-MA-GMA içeren nanokompozitlerde incelenmesine karar verilmiştir.

DSC analizleri, organik kil ve uyum sağlayıcı varlığında, bileşenlerin erime davranışlarında önemli bir değişim olmadığını göstermiştir. Ayrıca, hem uyum sağlayıcı hem de organik killer, PP içinde çekirdekleşme aktivitesine sahip değildir.

PP/E-MA-GMA/15A ve PP/E-MA-GMA/25A sistemleri, mekanik test sonuçlarına göre en iyi değerleri vermişlerdir. Mekanik testlerin sonuçları, PP, organik kil ve uyum sağlayıcının ilk ekstrüzyonda eş zamanlı olarak karıştıkları, (PEC) serisinde en iyi sonucu vermektedir.

Anahtar sözcükler: polipropilen, uyum sağlayıcı, organik kil, nanokompozitler

To Oğuz and My Family

ACKNOWLEDGEMENTS

I would like to express my sincere gratitude to my supervisor, Prof. Dr. Ülkü Yılmazer, for his guidance, understanding, criticism, encouragement and patience throughout my thesis. I am greatly indebted to Assoc. Prof. Dr. Göknur Bayram from Department of Chemical Engineering for providing me every opportunity to use the instruments in her laboratory, Prof. Dr. Teoman Tinçer from Department of Chemistry for his permission to use the mechanical tetsing instrument in his laboratory.

I would sincerely thank Işıl Işık for her endless friendship, support, help in all parts of my thesis and for sharing her time and information about both thesis and life. I would also like to thank my dear friend Miray Mert who was beside me during all part of the experiments.

I express my special thanks to Güralp Özkoç for sparing his time and all his help during my experiments. I learned lots of things from him. I would like to thank to Fatma Işık Coşkunses for her encouragement, help and friendship. Thanks to my friends Sertan Yeşil, Mert Kılınç, Özcan Köysüren, İlknur Çakar who have always been up not only for support, but also for a good laugh during the laboratory time.

My deepest gratitude also goes to Yeliz Durak and Canan Kozu for their endless friendship, support, help in all parts of my life, making my stay in Ankara happy and memorable and being always right beside me.

And, a thanks to my family: to Mum and Dad - thank you for all your support over the years and belief in me; to Selim and Gözde, for being there no matter what. Last but not least, Oğuz, gave me his love, patience, support, understanding and encouragement in every step of my life. I would not have been able to complete this study without his love and support.

This study was supported by BAP-2006-03-04-06.

TABLE OF CONTENTS

LIST OF TABLES

LIST OF FIGURES

NOMENCLATURE

A_0 Original, undeformed cross-sectional area, mm^2

b Width of beam tested, mm

d Depth of beam tested, mm

d Plane spacing, Å

E Modulus of Elasticity, MPa

F Tensile Load, N

L Support span, mm

L_0 Initial gauge length, mm

ΔL Change in sample length, mm

m Slope of the tangent to the initial straight-line portion of the load deflection curve, N/mm

n Order of diffraction

P Load at a given point on the load-deflection curve, N

R Maximum strain in the outer fibers, mm/mm

S Stress in the outer fibers at midspan, MPa

T Thickness, mm

Tc Crystallization temperature, °C

Tg Glass transition temperature, °C

Tm Melting temperature, °C

Greek Letters

Є Tensile strain, mm/mm

Λ Wavelength, nm

Σ Tensile stress(nominal), MPa

σ_m Tensile strength, MPa

θ Scattering angle,°

Abbreviations

ASTM	American Society for Testing and Materials
CEC	Cation Exchange Capacity
DSC	Differential Scanning Calorimetry
E-GMA	Ethylene-Glycidyl Methacrylate
E-MA-GMA	Ethylene-Methyl Acrylate-Glycidyl Methacrylate
E-nBA-MAH	Ethylene-Butyl Acrylate-Maleic Anhydride
GMA	Glycidyl Methacrylate
HT	Hydrogenated Tallow
ISO	International Standards and Organization
MAH	Maleic Anhydrite
MFI	Melt Flow Index
MMT	Montmorillonite
MO	Mixing Order
OMLS	Organically Modified Layered Silicate
PP	Polypropylene
PLS	Polymer Layered Silicate
PLSNC	Polymer Layered Silicate Nanocomposites
PMC	Polymer Matrix Composites
SEM	Scanning Electron Microscopy
T	Tallow
TEM	Transmission Electron Microscopy
XRD	X-Ray Diffraction

CHAPTER 1

INTRODUCTION

Polymer systems are widely used due to their ease of production, light weight, and often ductile nature. However, polymers have lower modulus and strength with respect to metals and ceramics. In order to improve their mechanical properties, polymers are reinforced with inclusions (fibers, whiskers, platelets, or particles). Making composites with these inclusions, which gives material properties not achieved by either phase alone, has been a common practice for many years [1].

Composite materials have been utilized to solve technological problems for a long time. However, in the 1960's polymeric based composites started capturing the attention of industries. Since then, composite materials have become common engineering materials and are designed and manufactured for various applications including automotive components, sporting goods, aerospace parts, consumer goods, and in the marine and oil industries [2].

Nanocomposites, describing a two-phase material where suitable filler is dispersed in the polymer matrix at a nanometer (10^{-9}) scale, are a relatively new class of materials [3]. Polymer nanocomposites are a class of mineral- filled plastics that include small amounts (<10%) of nanometer-sized inorganic particles. Among them, silicates (clay minerals) which are used in the production of nanocomposites have a thickness of around only 1 nm.

Clay/polymer nanocomposites offer huge improvements in a wide range of physical, chemical and engineering properties such as superior mechanical properties, impact resistance, flammability properties, thermal properties and reduced permeability to gases [4].

In clay/polymer nanocomposites, smectite-type of clays, such as hectorite, montmorillonite, and synthetic mica are generally used. Smectite-type clays have layered structure. Each layer is constructed from tetrahedrally coordinated Si atoms fused into an edge-shared octahedral plane of either $Al(OH)_3$ or $Mg(OH)_2$. Thus, instead of “clay/polymer nanocomposite”, it can be called as “polymer layered silicate nanocomposites”.

In this study, montmorillonite is used as the layered silicate. It has a crystalline structure and belongs to the general family of 2:1 layered silicates. The layer thickness of the crystal structure is around 1 nm. These layers form stacks with a gap in between them called interlayer or gallery [3, 5]. Natural montmorillonite has to be modified organically by a simple cation exchange process in order to provide the compatibility between the polymer and clay, since montmorillonite is a hydrophilic material while most of engineering polymers are hydrophobic.

Polypropylene (PP) is a linear hydrocarbon polymer, expressed as C_nH_{2n}. PP is a polyolefin or saturated polymer. Polypropylene is one of those most versatile polymers available with applications, both as a plastic and as a fiber, in virtually all of the plastics end-use markets. To overcome the disadvantages of PP, such as low toughness and low service temperature, PP/layered silicate nanocomposites have been a subject of interest. The modified properties include higher modulus, improved dimensional stability, increased solvent resistance, and reduced gas permeability as compared to the base polymer [6].

Since PP has a non-polar structure, it is not compatible with organoclay. In order to provide compatibility between the polymer matrix and organoclay a third material called compatibilizer should be used in nanocomposites.

In production of nanocomposites, there are three methods: in-situ intercalative polymerization, solution intercalation and melt intercalation method. The melt intercalation method, which is favored in industry, is much easier than the others. In this method PP, compatibilizer and organoclay are compounded in the melt to form nanocomposites by extrusion.

The objective of this study is to investigate the effects of compatibilizer type, organoclay type and mixing order of the components on the properties of nanocomposites containing polypropylene, compatibilizer and organoclay. Three types of compatibilizers, terpolymer of ethylene – methyl acrylate – glycidyl methacrylate (E-MA-GMA), copolymer of ethylene – glycidyl methacrylate (E-GMA), and terpolymer of ethylene – n-butyl acrylate – maleic anhydride (E-nBA-MAH), and organoclays, Cloisite® 15A, Cloisite® 25A and Cloisite® 30B were used.

First, the compatibilizer concentration was selected as 5 wt% based on binary PP/compatibilizer blends. The concentration of organoclay was selected as 2% for all nanocomposite combinations. Then, ternary nanocomposites were produced by means of a co-rotating twin screw extruder with a two step mixing procedure. Finally, all standard test specimens were prepared by injection molding according to the standard of ISO 527-2 5A for characterization.

In order to investigate the morphology of nanocomposites X-Ray Diffraction (XRD), Scanning Electron Microscopy (SEM), Transmission Electron Microscopy (TEM) analysis were performed. Differential Scanning Calorimetry (DSC) was performed for thermal characterization of the nanocomposites. Tensile strength, tensile modulus, tensile strain at break, flexural strength, flexural modulus and impact strength of all samples were determined by mechanical characterization of nanocomposites. Finally, flow properties were determined by a Melt Flow Indexer.

CHAPTER 2

BACKGROUND

2.1. Composites

2.1.1. Definition of Composites

A composite is a structural material, which consists of combining two or more constituents. The components are combined at a macroscopic level and are not soluble in each other [8]. Although it is composed of several different materials, a composite behaves as a single product [7].

Early large-scale commercial applications of composite materials started during World War II (late 1940s and early 1950s) with marine applications for the military. Yet today, composite products are manufactured by a wide range of industries, including aerospace, automotive, marine, boating, sporting goods, consumer, infrastructure, and more. In recent years, the development of new and improved composite manufacturing processes has caused unlimited product development opportunities [2] since composites provide the advantages of low weight, high corrosion resistance, high fatigue strength and faster assembly, etc. [8].

Composites are necessary for optimization of material properties such as; mechanical (mainly strength and modulus), chemical and/or physical properties. In the latter, the optimization of thermal (thermal expansion, thermal conduction, specific heat, softening and melting points), electrical (electrical conductivity, electrical permittivity, dielectric loss), as well as optical and acoustical properties can be noted [9].

2.1.2. Types of Composites

One component of a composite is called the reinforcing phase and the one in which it is embedded is called the matrix. The reinforcing phase material may be in the form of fibers, particles, or flakes by the geometry of the reinforcement [8].

Particulate composites consist of particles immersed in matrices such as alloys and ceramics. They are usually isotropic since the particles are added randomly. Particulate composites may have advantages such as improved strength, increased operating temperature and oxidation resistance, etc.; typical examples include use of aluminum particles in rubber, silicon carbide particles in aluminum, and gravel, sand, and cement to make concrete [9].

Flake composites consist of flat reinforcement of matrices. Typical flake materials are mica, aluminum, and silver. Flake composites provide advantages such as high out-of-plane flexural modulus, high strength, and low cost. However, flakes cannot be oriented easily and only a limited number of materials are available for use [9].

Fiber reinforced composites are the most technologically important group, where the dispersed phase is in the form of a fiber [7, 9]. They consist of matrices reinforced by short (discontinuous) or long (continuous) fibers. Fiber reinforced composites are generally anisotropic. Examples of matrices are resins such as epoxy, metals such as aluminum, and ceramics such as calcium-alumino silicate. The fundamental units of continuous fiber matrix composite may be unidirectional or woven fiber laminas. Laminas are stacked on top of each other at various angels to form a multidirectional laminate [8].

2.1.3. Polymer Matrix Composites (PMC)

Polymers are mostly organic compounds based on carbon, hydrogen and other nonmetallic elements. PMC are the most developed composite materials group and they have found widespread applications. PMC can be easily fabricated into any large complex shape, which is an advantage [9]. Resins or matrices are divided into two major groups known as thermoset and thermoplastic. Thermoplastic resins become soft when heated, and may be shaped or molded while in a heated semi fluid state. Thermoset resins, on the other hand, are usually liquids or low melting point solids in their initial form. When used to produce finished goods, these thermosetting resins are “cured” by the use of a catalyst, heat or a combination of the two. Once cured, solid thermoset resins cannot be converted back to their original liquid form. Unlike thermoplastic resins, cured thermosets will not melt and flow when heated and once formed they cannot be reshaped [59]. In PMC applications, thermosetting and thermoplastic polymers can be used as the matrix component. PMC (also called reinforced plastics) are, in general, a synergistic combination of high performance reinforcing agent and matrices. In these systems, a reinforcing

agent provides the high strength and modulus while the polymer matrix transfers the load to the reinforcements and helps resistance to weathering and to corrosion [9].

2.2. Nanocomposites

2.2.1. Definition of Nanocomposites

The nanocomposite term can be defined as a two-phase material in which one of the phases is dispersed in the second one at a nanometer (10^{-9} m) level. Polymer nanocomposites are mineral-filled plastics that contain relatively small amounts (usually <10%) of nanometer-sized inorganic particles [10].

2.2.2. Polymer Layered Silicate (or clay) Nanocomposites (PLSNC or PCNC)

In polymer nanocomposites the additives can be one dimensional (examples include nanotubes and fibers), two dimensional (which include layered minerals like clay), or three dimensional (including spherical particles). Over the past decade, polymer nanocomposites have attracted considerable interest in both academia and industry, owing to their outstanding mechanical properties like stiffness, strength, and modulus with only a small amount of the nanoadditives. This is caused by the large surface area to volume ratio of nanoadditives when compared to micro- and macro-additives. Other superior properties of polymer

nanocomposites include barrier resistance, flame retardancy, wear resistance, as well as optical, magnetic and electrical properties [60].

Two major findings have stimulated the revival of interest in these materials: first, the report from the Toyota research group of a Nylon 6 (N6)/Montmorillonite (MMT) nanocomposite, for which very small amounts of layered silicate loadings resulted in pronounced improvements of thermal and mechanical properties; and second the observation by Vaia&Giannelis et al. [11, 55] that, it is possible to melt-mix polymers with layered silicates, without the use of organic solvent [12].

2.2.3. Structure and Properties of Layered Silicates

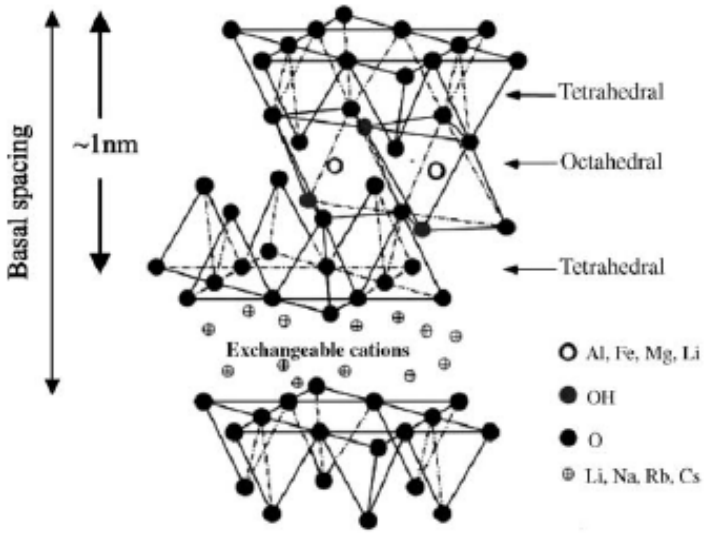

Figure 2.2.1 Structure of 2:1 phyllosilicates [12]

Polymer layered silicate (PLS) nanocomposites are hybrids between the polymer phase (an organic phase) and the silicate phase (an inorganic phase) [13]. The commonly used layered silicates for the preparation of PLS

nanocomposites belong to the same general family of 2:1 layered phyllosilicates, such as mica, talc, montmorillonite, vermiculite, hectorite, saponite, etc [12]. Their crystal structure consists of layers made up of two silica tetrahedral fused to an edge-shared octahedral sheet of either aluminum or magnesium hydroxide. The thickness of the layer is about 1 nm as shown in Figure 2.2.1. Stacking of the layers leads to a regular Van Der Waals gap between the layers called the interlayer or gallery [Giannelis 1998]. Isomorphic substitution within the layers (for example, Al^{3+} replaced by Mg^{2+} or Fe^{2+}, or Mg^{2+} replaced by Li^{1+}) generates negative charges that are counterbalanced by alkali and alkaline earth cations situated inside the galleries [12, 56]. Thus, all layered silicates have cation exchange capacity (CEC) to characterize the surface charge and generally expressed as mequiv/100 gm.

2.2.4. Organically Modified Layered Silicates

Since the layered silicates have a hydrophilic structure, they are incompatible with most polymers having organic structure. In order to overcome this situation the layered silicates should be organically modified. This makes the intercalation of many engineering polymers possible.

Organically modified layered silicates can be produced by replacing the cations originally present in the galleries with organic cations. Alkylammonium ions are mostly used as shown in Figure 2.2.2 to modify the surface of the layered silicates. In the presence of alkylammonium salts, the negative charge is on the surface of the silicate. Therefore, the cationic head of the alkylammonium is attached to the wall of the interlayer. Its aliphatic tail renders the normally hydrophilic silicate surface organophilic. Moreover, alkylammonium cations,

which increase the spacing between the layers and reduce the surface energy of the filler, provide functional groups that can react with the polymer to improve the strength of the interface between the inorganic component and the polymer. Therefore, these modified fillers can be called organically modified layered silicates (OMLS) or organoclay.

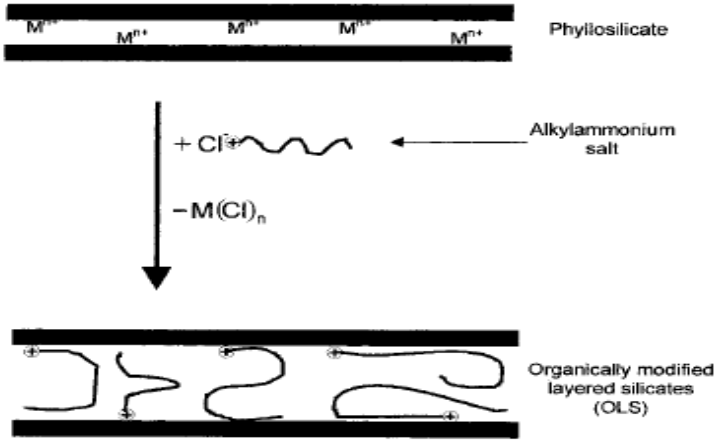

Figure 2.2.2. Schematic representation of a cation-exchange reaction between the silicate and an alkylammonium salt [13].

2.2.5. Types of PLS Nanocomposites

There are two main types of nanocomposite structure that depends on the nature of the components used, including polymer matrix, layered silicate and organic cation. As it is seen in Figure 2.2.3, when the polymer cannot intercalate between the silicate sheets, a microcomposite is obtained. However, intercalated structures are formed when a single (sometimes more) extended polymer chain is intercalated (sandwiched) between the silicate layers. The

result is a well ordered multilayer structure of alternating polymeric and inorganic layers.

If the silicates are completely and uniformly dispersed in the continuous polymer matrix, exfoliated or delaminated structures can be obtained. Since it maximizes the polymer-clay interactions, exfoliated configuration is of particular interest. It makes the entire surface of the layers available for polymer. Then, this provides the most significant changes in mechanical and physical properties [3].

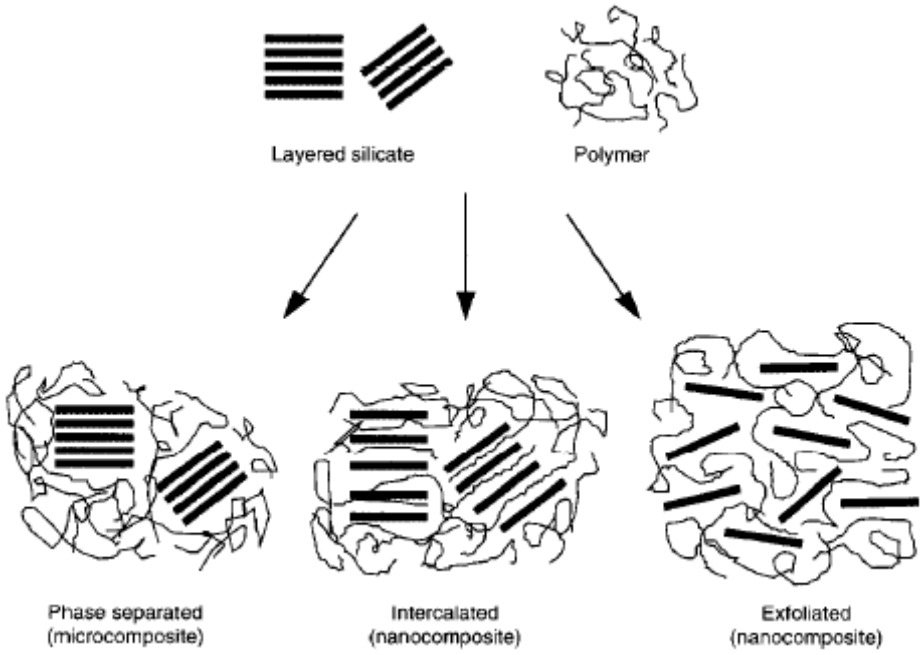

Figure 2.2.3. Possible Polymer/layered silicate structures [3].

2.2.6. Synthesis of PLS Nanocomposites

The preparation methods of the PLS nanocomposites can be divided into three main groups according to the starting materials and processing techniques:

“In-situ Polymerization” of the monomers confined in molecule-sized spaces has been used in the past to synthesize stereospecific polymers [13]. In this method, the layered silicate is swollen within the liquid monomer or a monomer solution. Then polymer formation occurs between the intercalated sheets. Polymerization can be initiated by either heat or radiation, by the diffusion of a suitable initiator, or by an organic initiator, or catalyst fixed through cation exchange inside the interlayer before the swelling step [12]. Generally, an exfoliated nanocomposite is formed with this method [37]. The process is illustrated in Figure 2.2.4.

Figure 2.2.4. Schematic representation of PLS obtained by in-situ polymerization [13].

In “solution method”, first the organo-modified clay is swollen in a polar organic solvent such as toluene or N, N-dimethylformamide. Then, the polymer, which is dissolved in the solvent, is added to the solution and it intercalates between the clay layers. After removing of the solvent by vaporization under vacuum, the process ends up (Figure 2.2.5).

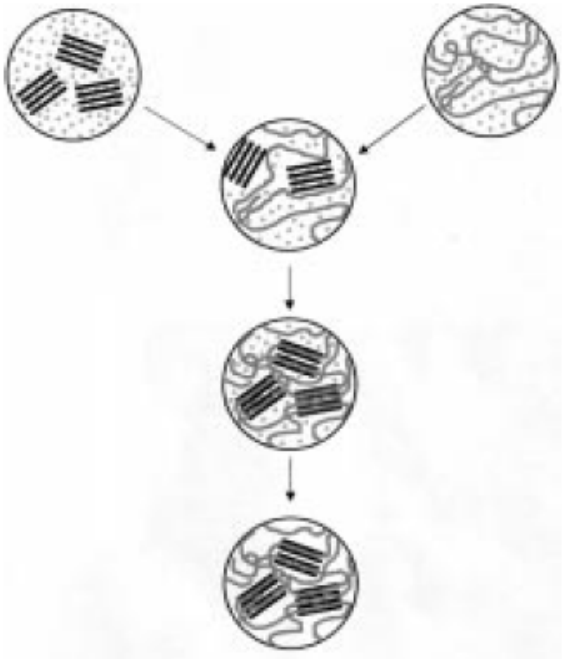

Figure 2.2.5. Schematic representation of PLS obtained by intercalation from solution [13].

This method has an important advantage since intercalated nanocomposites can be synthesized that is based on polymers with low or even no polarity. However, the solvent approach has a limitation. It is difficult to apply this method in industry owing to problems associated with the use of large quantities of solvents [3].

The last one is “melt intercalation method” (or melt-mixing) that involves annealing, statically or under shear, a mixture of the polymer and organo modified layered silicate above the softening point of the polymer [12] in order to optimize the polymer-clay interactions (Figure 2.2.6). The polymer chains have a significant loss of conformational entropy during the intercalation. This method is appreciated in industrial applications. Moreover, polymer-clay nanocomposites

have been successfully produced by extrusion in this method. A wide range of thermoplastics, including strongly polar polyamide-6, polystyrene etc. has been intercalated between clay layers. However polyolefins, that are the biggest volume of polymers produced, have so far only been successfully intercalated to a very limited extent [3].

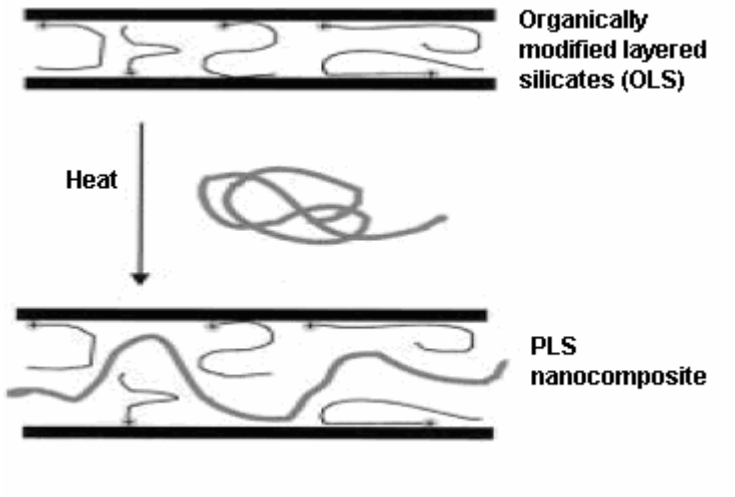

Figure 2.2.6. Schematic representation of PLS obtained by melt intercalation method [13].

2.3. Polypropylene

2.3.1. Structure of Polypropylene

Polypropylene (PP) was first produced by G. Natta, following the work of K. Ziegler, by polymerization of propylene monomer in 1954. Structurally, it is a vinyl polymer such that every other carbon atom in the backbone chain has a

methyl group attached to it (Figure 2.3.1). The macromolecule of PP contains 10,000 to 20,000 monomer units [15].

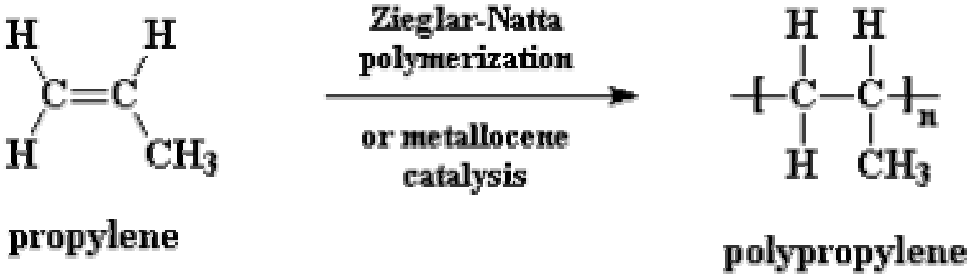

Figure 2.3.1. Synthesis of PP [15]

The steric arrangement of the methyl groups attached to the every second carbon atom in the chain may vary, which determines the tacticity of the PP. If all the methyl groups are on the same side of the winding spiral chain molecule, the product is referred to as isotactic PP. A PP structure where pendant methylene groups are attached to the polymer backbone chain in an alternating manner is known as syndiotactic PP. The structure where pendant groups are located in a random manner on the polymer backbone is the atactic form.

Atactic (at) PP lacks stereo regularity and is a soft, transparent, viscous liquid. This polymer has little used except as a softener for other polymers.

Isotactic PP, is a crystalline polymer in which the chains are present in helical conformations, with three repeating units per turn (Figure 2.3.2). Because of the added volume, which is left between the pendant methyl groups, this opaque polymer has a low specific gravity [16].

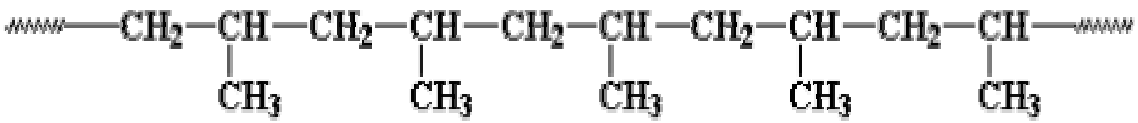

isotactic polypropylene

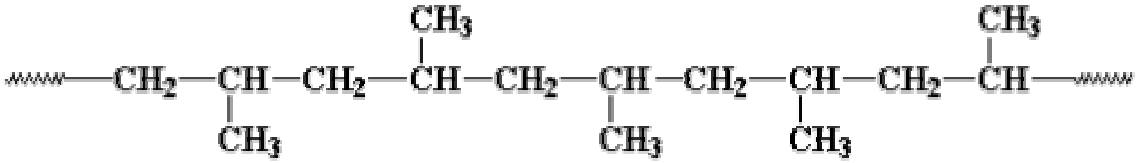

atactic polypropylene

Figure 2.3.2. The tacticity of PP [15]

2.3.2. Major Advantages of PP

PP is very popular as a high-volume commodity plastic. However, it is referred to as a low-cost engineering plastic. It exhibits higher stiffness at lower density and resistance to temperatures when not subjected to mechanical stress. Furthermore, PP offers good fatigue resistance, good chemical resistance, good environmental stress cracking resistance, good detergent resistance, good hardness and contact transparency and ease of machining, together with good processibility by injection molding and extrusion. The color is opaque and white, but it can be dyed in many colors [15, 17, 18].

2.3.3. Applications of PP

Typical applications of PP are listed in Table 2.3.1.

Table 2.3.1. Typical Applications of PP [15]

Sector	Typical Applications
Household goods	Buckets, bowls, bottle crates, toys, bottle caps, bottles, food processor housing, luggage
Automotive industry	Radiator expansion tanks, brake fluid reservoirs fittings, steering wheel covers, bumpers, bumper covers, side strips, spoilers, mudguards, battery cases, tool boxes
Fibers	Artificial sport surfaces, monofilaments for rope and cordage, stretched tapes, woven carpet backing, packaging sacks and tarpaulins, staple fibers, coarse fibers, filament yarns, fine fibers
Domestic appliances	Dishwasher parts, washing machine parts, refrigerator parts, irons and coffee maker body parts
Packaging	Margarine and ice cream tubs, films, dessert cups
Pipes and fittings	Solid rods, hot wire reservoirs, pressure pipes, heat exchanger
Furniture	Stackable chairs

2.4. PP/Layered Silicate Nanocomposites

2.4.1. Introduction

As it is mentioned above, PP is one of the most widely used plastics in large volume [19]. Its beneficial properties include relatively high thermal stability, low density, good processibility, and resistance to corrosion [18]. However, PP has some disadvantages such as; low toughness and low service temperature. As, it is tried to improve the properties of PP with nanotechnology.

Conventional fillers for PP such as talc and mica are used at a rather high loading of 20 to 40 wt.% to improve mechanical properties and dimensional stability while also increasing part weight. Silicate nanolayers have much larger aspect ratios and can enhance stiffness and scratch resistance significantly at a much lower loading. They are also impervious to gases. If they are well dispersed and oriented, they can yield greatly improved barrier properties as well as flame retardance in the composite. Therefore, developing of layered silicates such as montmorillonite as a multifunctional additive for polypropylene at 1 to 10 wt. % with minimal increase in weight is very attractive [33]. The enhanced properties are presumably due to the synergistic effects of the nanoscale structure and the maximized interaction between the fillers and PP molecules.

However, it is very difficult to disperse the silicate layers at the nanometer level since PP is a nonpolar molecule. Thus, in the synthesis of PP/layered silicate nanocomposites (PPLSN) a compatibilizer with functional groups must be used. For instance; in the synthesis of PPLSN which was suggested by Toyota, maleic

anhydride-grafted PP (PP-g-MA) can be used as an intermediate between PP and layered silicates. At the first stage, PP-g-MA and layered silicates are mixed in order to increase the basal spacing of the silicate by the intercalation of PP-g-MA into the silicate interlayer spaces. At the second stage, PP is inserted into the intercalated silicate galleries by mixing it with PP-g-MA/silicate compounds, and finally the PPLSN can be obtained [54]. Therefore, PP-g-MA provides the compatibilization between the silicate surface and the PP matrix.

2.4.2. Choices of Compatibilizer

Choices of polymeric compatibilizer are critical for optimizing the dispersion and properties of polypropylene clay nanocomposites. The interaction between the oxygen atoms on the clay surface and the polymeric compatibilizer must be stronger than the interaction between the clay surface and the surfactant in order to obtain delamination of the silicates. The polymeric compatibilizer must also be miscible with the bulk PP; this is a limitation on the extent of functionalization of the PP [33].

In this study, in order to provide the intercalation and exfoliation of PP through the organically modified silicate layers terpolymer of Ethylene-Methyl Acrylate-Glycidyl Methacrylate (E-MA-GMA), copolymer of Ethylene-Glycidyl Methacrylate (E-GMA), and terpolymer of Ethylene-nButyl Acrylate-Maleic Anhydride (E-nBA-MAH) have been used as compatibilizers.

2.4.2.1. GMA Functionality

Glycidyl Methacrylate (GMA) monomer whose chemical structure can be seen from Figure 2.4.1 contains acrylic and epoxy groups.

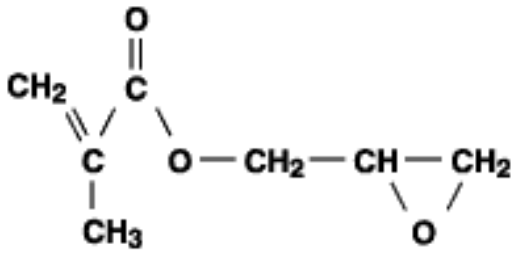

Figure 2.4.1. The Chemical structure of GMA [44]

Acrylic and vinyl groups on GMA structure allow copolymerization with variety of other vinyl monomers in aqeous and nonaqeous systems. Polymers obtained from copolymerization have a unique combination of epoxy functionality with an acrylic backbone. Besides, wide co-monomer selection provides easy control of physical and chemical properties such as glass transition temperature.

Epoxy group is capable of giving crosslinking reactions with amines, carboxylic acids, anhydrites and hydroxyl containing polymers. Also, when suitable catalyst is chosen wide range of cure temperatures can be used.

These acrylic and epoxy groups give greater flexibility and freedom in polymer design. Moreover, the benefits of GMA in the structure are to improve impact resistance, adhesive strength, water resistance, heat resistance and thermoplastic polymer blend compatibility.

2.4.2.2. Maleic Anhydride (MAH) Functionality

Maleic anhydride group introduces reactivity in the polymer chain and increases the adhesion onto polar substrates allowing the creation of chemical bonds. Chemical reaction occurs between the maleic anhydride and the hydroxyl groups of the organoclay as it is illustrated in Figure 2.4.2. This mechanism provides the intercalation of the silicate layers into the PP matrix. The major advantage of this group is to have excellent heat stability which allows high processing temperatures. Other properties of the maleic anhydride group are that it is moisture sensitive but not corrosive.

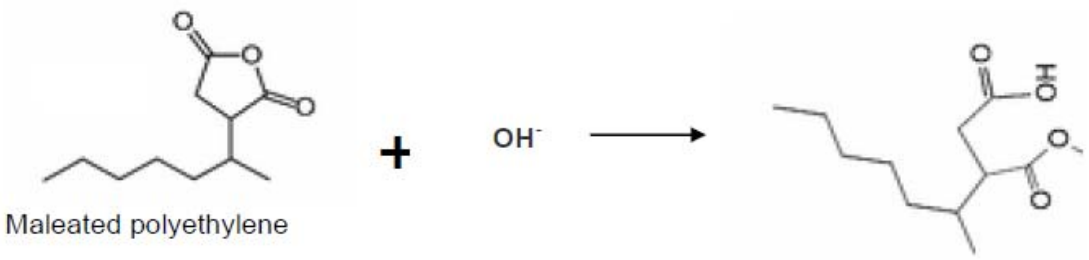

Figure 2.4.2. Reaction of Maleic Anhydride with hydroxyl group of clay.

2.5. Polymer Processing

One of the most excellent features of polymers is the ease of processing. A large part of polymer processing technology can be summed up in the statement: get the shape then set the shape [20]. There are wide range of processing methods for polymers such as extrusion and injection molding.

2.5.1. Extrusion

In order to describe extrusion, some terms which are related to extruder process should be defined (Figure 2.5.1). The main function of an extruder is to develop sufficient pressure in material to force the material through the die. The pressure necessary to force a material through the die depends on the geometry of the die, the flow properties of the material, and the flow rate. Basically, an extruder is a machine capable of developing pressure. In other words, an extruder is a pump.

Generally, in the extrusion process events can be summed up like this: The plastic, usually in the form of granules or powder, is fed from hopper on to the screw. It is then conveyed along the barrel where it is heated by conduction from the barrel heaters and shear due to its movement along the screw flights. The depth of the screw channel is reduced along the length of the screw so as to compact the material. At the end of the extruder, the melt passes through a die to produce an extrudate of the desired shape.

The extrusion process which is used to produce significant quantities of plastic products, such as plastic film, sheet, profiles and plastic granules (pellets) can be divided into two main parts depending on the number of screw: single screw extrusion and twin screw extrusion.

An extruder with one screw is called a single screw extruder. It is the most common machine in the plastics processing industry. In a screw extruder a screw rotates in a cylinder; the rotation of the screw creates a pumping action [21].

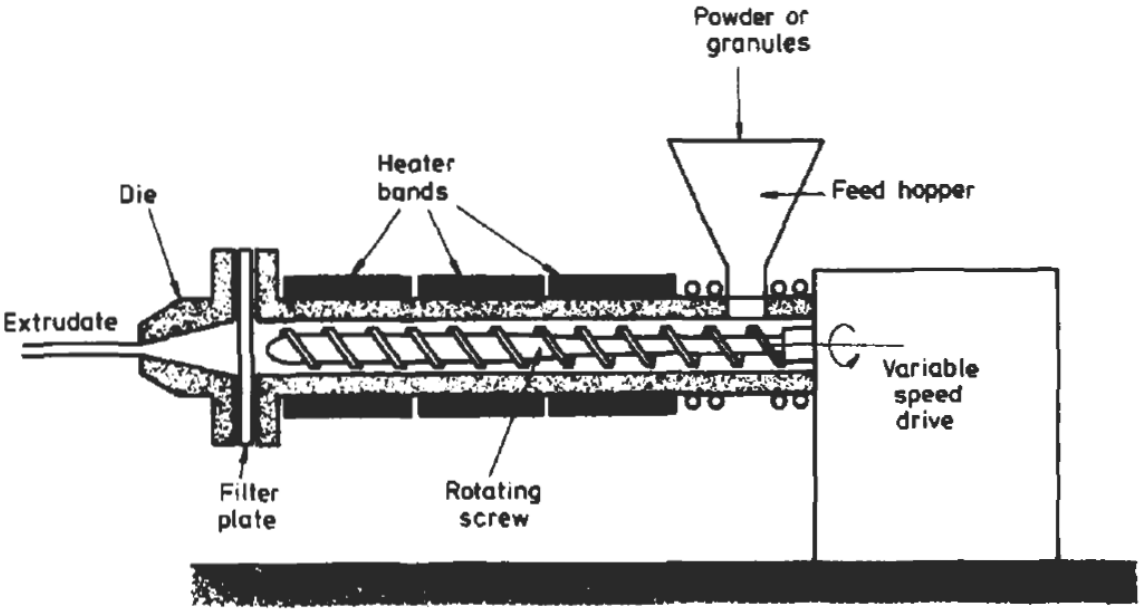

Figure 2.5.1. A schematic view of single screw extruder [21]

2.5.1.1. Function of Screw

The heart of the extruder is the extruder screw. This is a long cylinder with a helical flight wrapped around it, as seen in Figure 2.5.2. The screw is very important because conveying, heating, melting, and mixing of the plastic are mostly determined by the screw. The stability of the process and the quality of the extruded product are very much dependent on the design of the screw. The screw rotates in a cylinder that fits closely around it.

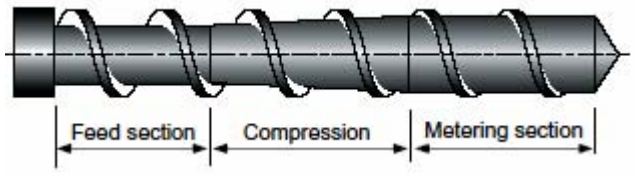

Figure 2.5.2. A single flighted extruder screw.

Generally, a screw includes three distinct sections; a feed section with a constant depth, a transition section with a varying depth, a metering section again with a constant depth.

The function of the feed zone is to preheat the plastic and convey it to the subsequent zones. The optimum design is related to the nature and shape of the feedstock, the geometry of the screw and the frictional properties of the screw and barrel in relation to the plastic. The frictional behavior of the feed-stock material has a considerable influence on the rate of melting which can be achieved [21].

In compression zone, the screw depth gradually decreases so as to compact the plastic. This compaction has the dual role of squeezing any trapped air pockets back into the feed zone and improving the heat transfer through the reduced thickness of material.

In metering zone, the screw depth is again constant but much less than the feed zone. In this zone, the melt is homogenized in order to supply at a constant rate, material of uniform temperature and pressure to the die.

2.5.1.2. Twin Screw Extrusion

In recent years, there has been a steady increase in the use of twin screw extruders that have two screws in a heated barrel. In this machine, there are wide ranges of possibilities in terms of output rates, mixing efficiency, heat generation, etc compared with a single screw extruder. Although the term “twin-screw” is used almost universally for extruders having two screws, the screws need not be identical. There are large varieties of machine types. Figure 2.5.3

shows some of the possibilities with counter-rotating and co-rotating screws. In addition, the screws may be conjugated or non-conjugated. A non-conjugated screw configuration is one in which the screw flights are a loose fit into one another so that there ample space for material between the screw flights.

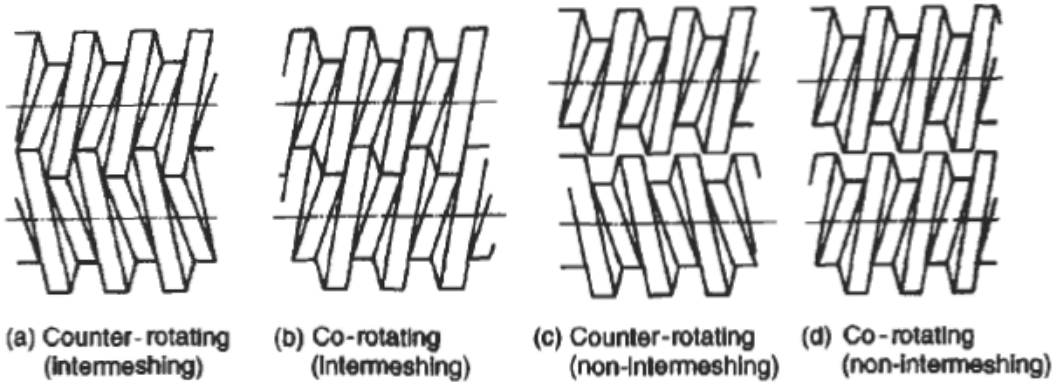

Figure 2.5.3. Different types of twin screw extruder [21].

In a counter-rotating twin screw extruder the material is sheared, pressurized and effectively squeezed between counter-rotating rolls. In a co-rotating system, the material is transferred from one screw to the other in a Figure-of-eight pattern as shown in Figure 2.5.4.

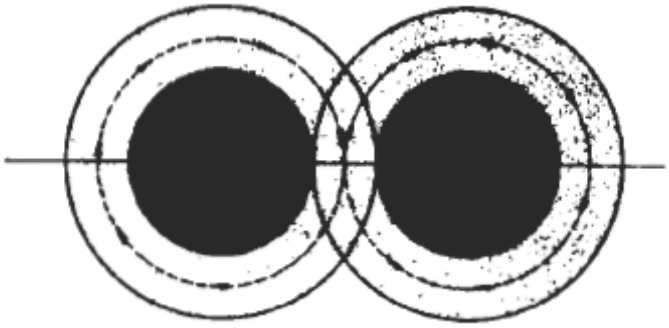

Figure 2.5.4. Material flow path with co-rotating screws [21].

In order to produce nanocomposites generally, co-rotating twin screw extruders are used which can be seen in Figure 2.5.5.

A control panel, feeders, two screws, barrel and a die are the components of the extruder that has been used in the study. The control panel has indicators in order to control the extrusion process such as temperature, screw speed and feed rate. In addition to this pressure of the die, barrel temperatures and torque can be controlled with control panel.

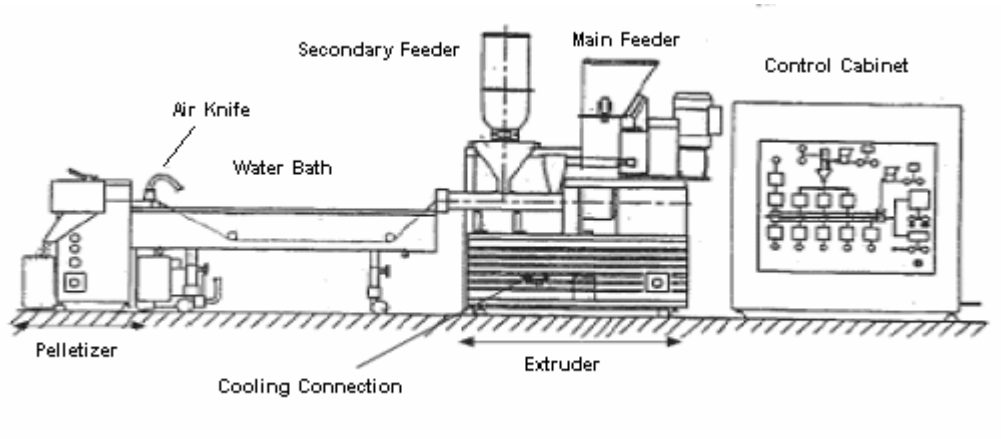

Figure 2.5.5. Co-rotating twin screw extruder used in nanocomposite production in this study.

The function of screw has been explained in details above. As for barrel, it is normally heated to melt the polymer or initiate the process. The barrel is of constant inner diameter and has heavy walls to withstand high pressures. A heating element is usually wrapped around the outside of the barrel. The barrel runs the entire length of the screw from the hopper, where its upper side is fitted to the hopper, to the die where it narrows, with the only opening being through the die. In the die zone, the polymer melt is shaped and distributed in the flow

channel in such a way that the material exits from the die with a uniform velocity. The pressure can be determined by the extruder die.

2.5.2. Injection Molding

Injection molding is one of the most common processing methods for plastics. It is used to produce finished articles which range from household appliances to automobile front-end assemblies. Also, it is one of the most important polymer flow processes due to the significant fraction of the total industrial output of plastics that is injection molded [22].

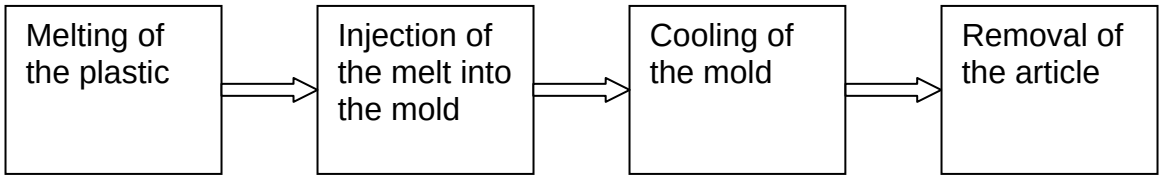

Figure 2.5.6. Stages in the injection molding process

The basic steps or stages of injection molding process are indicated in Figure 2.5.6. The solid plastic is melted, and the melt is injected into the mold under high pressure. In order to solidify the article the mold is cooled. Finally, the mold is opened and the article is ejected [22].

The original injection molding machines were based on the pressure die casting technique for metals. The first machine is reported to have been patented in the United States in 1872, specifically for use with Celluloid. This was an important invention, but probably before its time because in the following years, very few developments in injection molding processes were reported and it was not until the 1920s, in Germany, that a renewed interest was taken in the process. The

first German machines were very simple pieces of equipment and relied totally on manual operation. The next major development in injection molding, i.e. the introduction of hydraulically operated machines, did not occur until the late 1930s when a wide range of thermoplastics started to become available. In 1950s a new generation of equipment was developed. These machines catered more closely for the particular properties of polymer melts, and modern machines are of the same basic design, although of course the control systems are very much more sophisticated nowadays [21].

Although the process of injection molding is very simple, injection molding machines and molds are very costly due to the high pressure needed for injection of the thermoplastic melt and the associated complex controls [15].

Molding conditions are quite unique to the article being molded and depend on the part configuration, mold design, material properties, choice of the material and properties required from the finished part. For example, PP can be injection molded at a melt temperature of 200-300 °C and a mold temperature of 20-90 °C. However, a melt temperature of 220-260 °C and mold temperature of 20-40 °C are quite normal [15].

2.6. Characterization of Nanocomposites

2.6.1. Morphological Analysis

In morphogical analysis of the nanocomposite systems, X-ray Diffraction that provides quantitative data, Scanning Electron Microscopy (SEM) that gives the

appearance of the material surface and Transmission Electron Microscopy (TEM) that enable to analyze materials qualitatively were used in this study.

2.6.1.1. X-ray Diffractometer (XRD)

X-rays were discovered by Roentgen in 1895. The new X-rays were first applied to crystalline substances in 1912 and 1913, following the suggestion by Von Laue that crystalline substances ought to act as a three-dimensional diffraction grafting for X-rays [23].

X-rays are electromagnetic waves with very short wavelength. For instance, the X-rays used in polymer studies have wavelengths of about 0.1-0.2 nm. When waves of any kind are scattered from structures with which they interact, the angles of scatter are large when the lengths within the structure are comparable to the wavelength, and small when the lengths are large compared with the wavelength of the waves. There are two types of X-ray scattering used in the study of polymers, wide-angle X-ray scattering, or WAXS, and small-angle X-ray scattering, or SAXS, depending on the scale of the features studied. Scattering from structures of any size is regular, i.e. it takes place at well defined angles, only when the structures are periodic. The scattering is then usually called diffraction [24].

Diffraction occurs when a wave encounters a series of regularly spaced obstacles which are capable of scattering the wave spacing that are comparable in magnitude to the wavelength of the radiation. X-rays have high energies and wavelengths which are of the order of the atomic spacings for solids. When a beam of X-rays encounters a solid, a portion of the beam is scattered in all directions by the electrons associated with each atom which lie within the path of the beam [25].

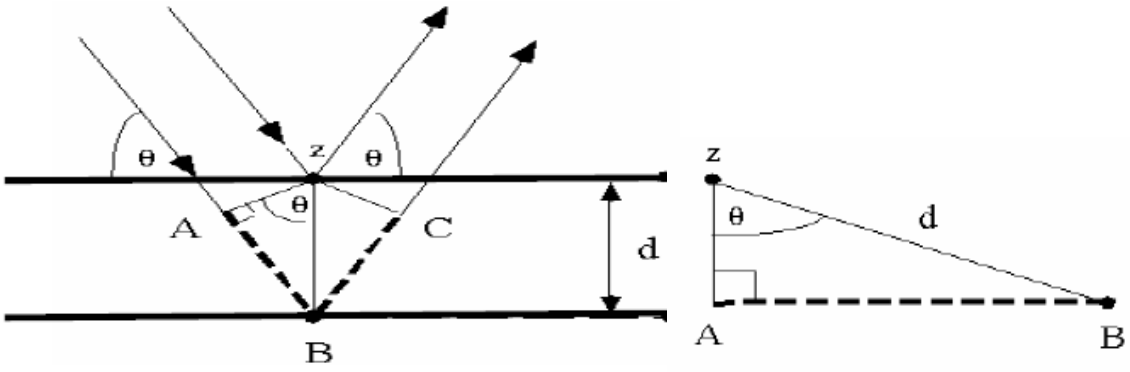

Figure 2.6.1. Principal of X-ray diffraction

X-ray diffraction is carried out by using a diffractometer. The intensities of the diffracted beams are detected by a counter. Its angular position is measured in terms of 2θ. When the counter moves at a constant angular velocity, a recorder plots the diffracted beam intensity as a function of 2θ [25]. In polymers, crystallites diffract X-ray beams from parallel planes for incident angles (θ) determined by using the Bragg equation; as follows:

$$n\lambda = 2d\sin\theta \qquad (2.6.1)$$

where λ is the wavelength of the radiation, d is the distance between the parallel planes in the crystallites and n is an integer indicating the order of diffraction which is illustrated in Figure 2.6.1.

In order to determine the dispersion of the clay platelets in the polymer matrix the quantitative analysis can be done by XRD. The d spacing of the clay platelets is calculated by Bragg's equation. The increase of the d spacing of the clay platelets and the shift to lower angles of the clay peak demonstrate that

polymer chains enter the clay gallery in intercalated systems. When the clay platelets are randomly dispersed throughout the polymer matrix no peak is observed in the XRD pattern in exfoliated systems.

2.6.1.2. Scanning Electron Microscopy (SEM)

Scanning electron microscopy (SEM) constitutes one of the older, and one of the most widely used, instruments for surface analysis. Because SEM provides a three-dimensional visual image, the qualitative analysis is relatively straightforward. SEM forms its image by scanning a focused electron beam probe across the specimen of interest [23].

In this technique, a fine electron beam (5-10 nm in diameter) is scanned across the sample surface in synchronization with a beam from a cathode-ray tube. The scattered electrons produced can then result in a signal which modulates this beam. As polymers tend not to be good conductors, they need to be coated with a thin layer of a conducting material such as gold or silver [25].

SEM has been used for a broad range of polymer studies and applications, including surface roughness, adhesive failures, fractured surfaces, networks, and phase boundaries in blends.

SEM is limited to a surface view only. It does not give any information about the interior of the specimen.

2.6.1.3. Transmission Electron Microscopy (TEM)

TEM is a very effective technique for the study of polymer morphology [25]. Both XRD and TEM are essential tools for evaluating the nanocomposite structure. However, TEM gives qualitative information on the sample such as internal structure, distribution of the various phases, whereas peaks in XRD allow quantification of changes in layer spacing [12].

TEM is often used with thin samples of materials in which different phases within the sample absorb electron differently [24]. Figure 2.6.2 shows the schematic structure of TEM. It includes illumination system, a specimen stage, an objective lens system, magnification system, data recording system and chemical analysis system. The illumination system in which the electron gun is used is composed of condenser lenses that are very important for forming a fine electron probe. The objective lens determines the limit of image resolution. There are intermediate lenses and projection lenses in the magnification system that gives a magnification up to 1.5 million. The data recording system allows quantitative data processing and quantification. Finally, chemical analysis system is the energy dispersive X-ray spectroscopy and electron energy-loss spectroscopy [57, 58].

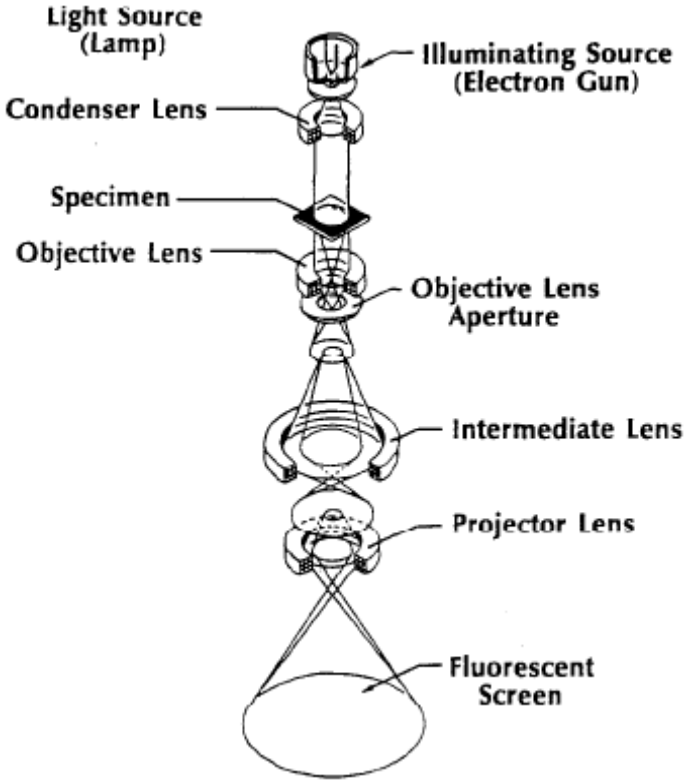

Figure 2.6.2. Schematic representation of a transmission electron microscope (TEM) [57]

2.6.2. Mechanical Tests

When a polymer is used as a structural material, it is important that it should be capable of withstanding applied stresses and resultant strains over its useful service life [16].

There are a number of fundamental techniques used to characterize the mechanical properties of polymers. In this study, tensile and flexural tests were performed.

2.6.2.1. Tensile Test

Tensile tests measure the force required to break a specimen and the extent to which the specimen stretches or elongates to that breaking point. Tensile tests produce a stress-strain diagram, which is used to determine tensile modulus. The data are often used to specify a material, to design parts to withstand application force and as a quality control check of materials. Since the physical properties of many materials (especially thermoplastics) can vary depending on ambient temperature, it is sometimes appropriate to test materials at temperatures that simulate the intended end use environment.

The tensile test employs samples of a specified shape, typically a dog bone. The sample is clamped at one end and pulled at a constant rate of elongation until the center of the specimen fails. The mechanism of tensile test is shown in Figure 2.6.2, and stress-strain curve, which is used to determine tensile modulus and the strength of the material, can be obtained. By examining the stress-strain curve the mechanical behavior of polymers can be understood.

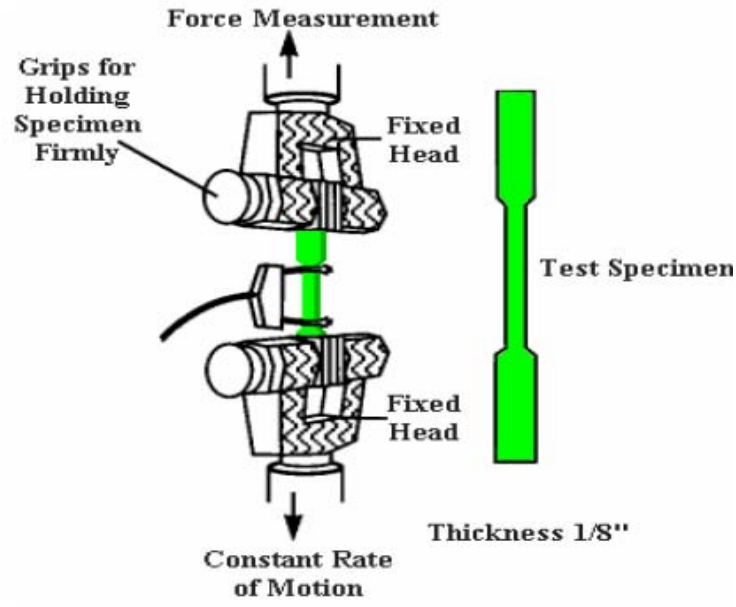

Figure 2.6.3. Tensile test procedure and test specimen.

Tensile stress, σ is the tensile load per unit area perpendicular or normal to the applied force, and tensile strain, ε is the ratio of change in gage length of a specimen in the direction of applied load stress to its original gage length.

$$\sigma = \frac{F}{A_0} \tag{2.6.2}$$

$$\varepsilon = \frac{\Delta L}{L_0} \tag{2.6.3}$$

where, F is the measured value (N) at the fixed end as a function of elongation, and A_0 is the original cross-section area of the gage region (mm^2), ΔL is the

change in gage length (mm), and L_0 is the original gage length of the specimen (mm).

The tensile strength, σ_m of a material is the maximum amount of tensile stress that it can be subjected to before it breaks during a tensile test and is reported in MPa. If the maximum stress occurs at break, it is called tensile strength at break.

The area under the stress-strain curve can be called as toughness. This area has units of energy per unit volume and is the work expended in deforming the material. The deformation may be elastic, and recoverable, or permanent (irreversible deformation). Elastic energy is stored in the sample in terms of energy per unit volume.

For most tensile testing of materials, you will notice that in the initial portion of the test, the relationship between the applied force, or load, and the elongation the specimen exhibits is linear. In this linear region, the line obeys the relationship defined as "Hooke's Law" where the ratio of stress to strain is a constant, or

$$E = \frac{\sigma}{\varepsilon} \tag{2.6.4}$$

E is the slope of the line in this region where stress (σ) is proportional to strain (*ε*) and is called the "Modulus of Elasticity"" or "Young's Modulus".

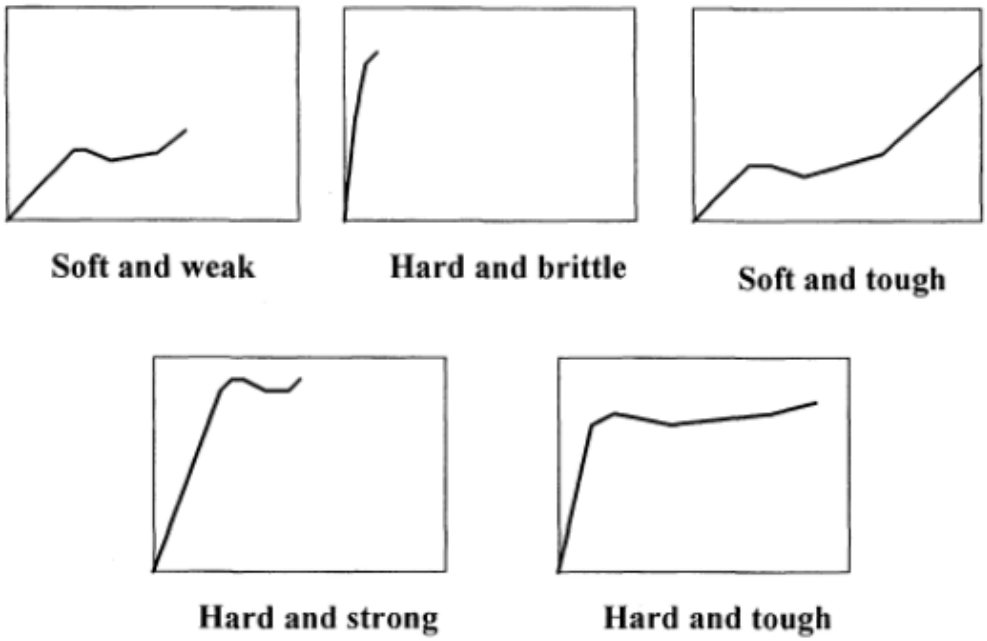

Figure 2.6.4. Stress-strain curves of several polymeric materials.

Figure 2.6.4 shows classification of polymers based on their mechanical properties.

2.6.2.2. Flexural Test

Flexural (or bending) tests are used to measure the rigidity of polymers.

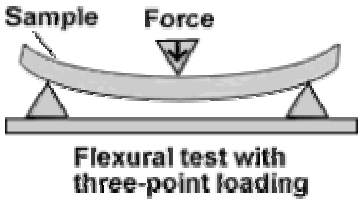

Figure 2.6.5. Schematic view of flexural test.

In flexural tests, rectangular bars of the sample to be evaluated are placed on supports and a load is applied to the sample at a specified rate according to the ASTM D-790 or ISO 178. As illustrated in Figure 2.6.5 the three points bending tests are done in this study.

Flexural strength is defined as the maximum fiber stress. It is the ability of the material to resist bending forces applied perpendicular to its longiditual axis. This stress may be calculated for any point on the load-deflection curve by the following equation.

$$S = \frac{3PL}{2bd^2} \tag{2.6.5}$$

where; S is the stress in the outer fibers at midspan and may be represented in MPa, P is the applied load at a given point on the load-deflection curve (N), L is the length of support span (mm), b is the width of the specimen (mm), and d is the depth of the specimen (mm). In this study flexural yield strength values are calculated.

The following equation represents the maximum strain in the outer fibers at midspan;

$$r = \frac{6Dd}{L^2} \tag{2.6.6}$$

where; r is the maximum strain, D is the maximum deflection of the center of the beam(mm), and L is the length of the support span (mm), and d is the depth of the specimen (mm).

Flexural modulus is calculated from the slope of the stress vs. deflection curve as demonstrated in equation 2.6.7. In addition to this, the flexural modulus is used in order to indicate the stiffness of the material when it is flexed. For calculation of the flexural modulus the following equation can be used:

$$E_b = \frac{L^3 m}{4bd^3} \tag{2.6.7}$$

where; E_b represents the flexural modulus (MPa), L is the support span (mm), m is the slope (Figure 2.6.6) of the tangent to the initial straight-line portion of the load-deflection curve (N/mm), b is the width of beam tested (mm), and d is the depth of the beam (mm).

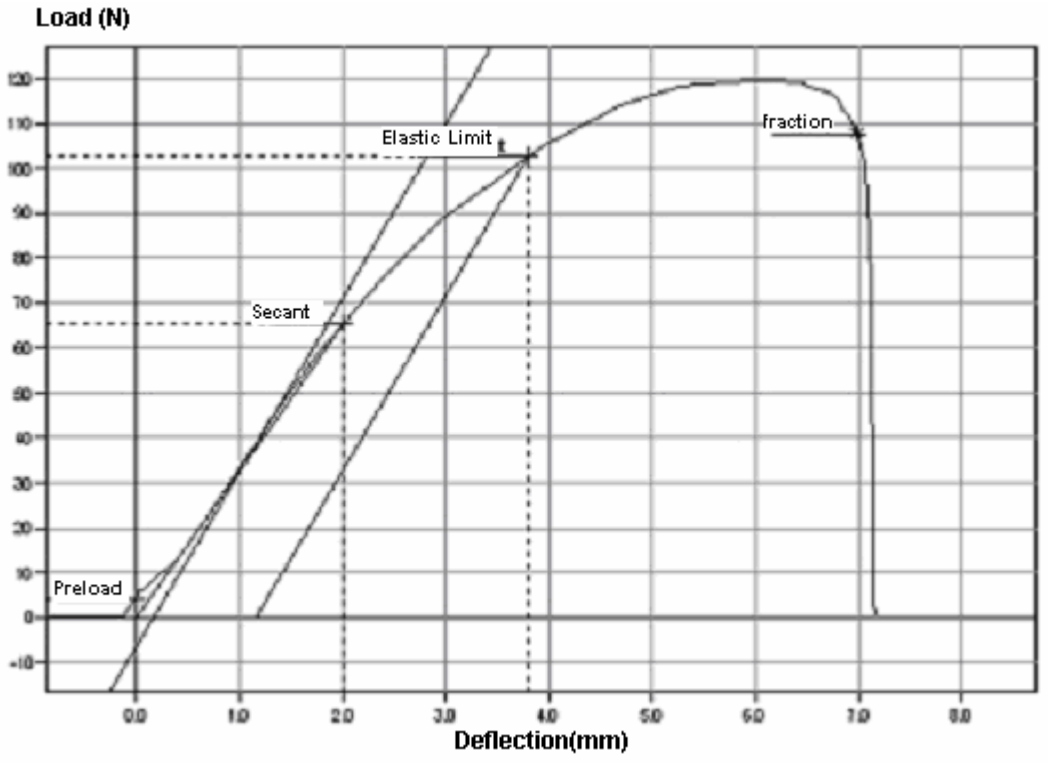

Figure 2.6.6. Typical graph showing 3 point bend strength test.

2.6.2.3. Impact Test

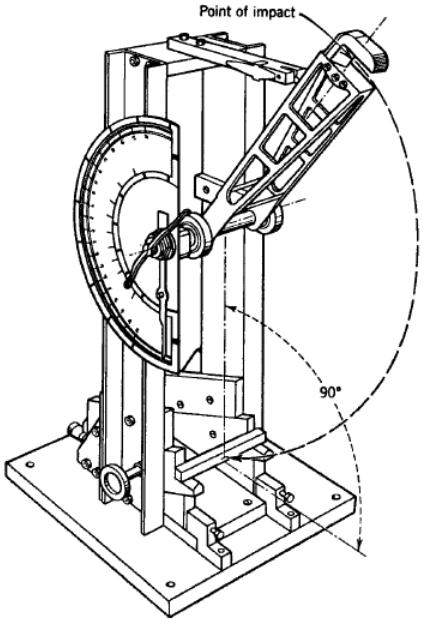

Figure 2.6.7. Charpy type impact instrument.

Impact tests are performed in order to measure the response of a material to dynamic loading. The impact test is also a method for evaluating the toughness and notch sensitivity of thermoplastics. Impact resistance is defined in terms of the energy required to fracture a sample. The impact energy measured by the impact test is the work done to fracture the specimen.

Resistance to impact loading may be measured by using specially designed universal testing machines, which permit very high rates of loading, or, more commonly, by using one of two types of instruments: the Izod and the Charpy impact test machines. In both tests a pendulum strikes the specimen. The Charpy instrument is illustrated in Figure 2.6.7. In both cases, the sample is often notched to provide a standardized weak point for the initiation of fracture.

2.6.2.3.1. Charpy Impact Test

The charpy impact test measures the energy absorbed by the high strain rate fracture of a standard notched specimen. In the Charpy experiment, the specimen is supported on both ends and struck in the middle. The notch is on the side away from the striker. The specimen is broken by the impact of a heavy pendulum hammer, falling through a fixed distance (constant potential energy) to strike the specimen at a fixed velocity (constant kinetic energy).

Charpy testing is usually reported in units of kJ/m^2, or energy required creating a unit area of crack. The striker is released from an elevated position. On striking the sample, part of the momentum of the striker goes into the creation of new surface area.

2.6.3. Thermal Analysis

Differential Scanning Calorimetry (DSC) analysis has been used in this study in order to determine melting temperature and crystallinity of the polymeric material.

2.6.3.1. Differential Scanning Calorimetry (DSC)

Differential scanning calorimetry (DSC) is a thermoanalytical technique in which the difference in the amount of heat required to increase the temperature of a sample and reference are measured as a function of temperature. Both the sample and reference are maintained at very nearly the same temperature throughout the experiment. Generally, the temperature program for a DSC

analysis is designed such that the sample holder temperature increases linearly as a function of time. The reference sample should have a well-defined heat capacity over the range of temperatures to be scanned.

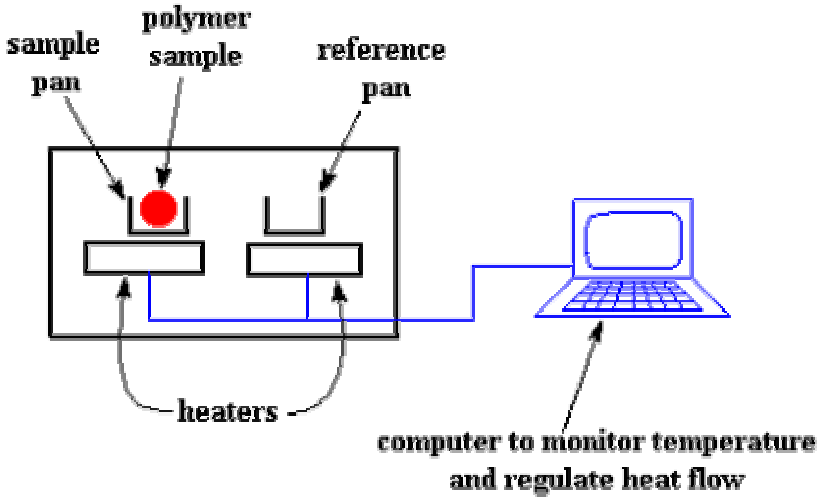

Figure 2.6.8. Schematic view of the DSC equipment.

As shown in Figure 2.6.8 there is two pans, one of which is the sample pan. The other is the reference pan that is empty. Each pan sits on top of a heater. After the computer turns on the heaters the two pans heat at a specific rate such as 5 °C per minute noticing that heating rates stay exactly the same throughout the experiment.

The basic principle underlying this technique is that, when the sample undergoes a physical transformation such as phase transitions, more (or less) heat will need to flow to it than the reference, to maintain both at the same temperature. Whether more or less heat must flow to the sample depends on whether the process is exothermic or endothermic. For example, the glass transition temperature (T_g) of a polymer can be detected from the endothermic

shift during DSC analysis. Such a change results from an increase in heat capacity due to the increased molecular motions in the material. The melting point (T_m) of a polymer corresponds to a change from the solid to liquid state. This gives rise to an endothermic peak in the DSC curve. In Figure 2.6.9 the exothermic and endothermic curves can be seen.

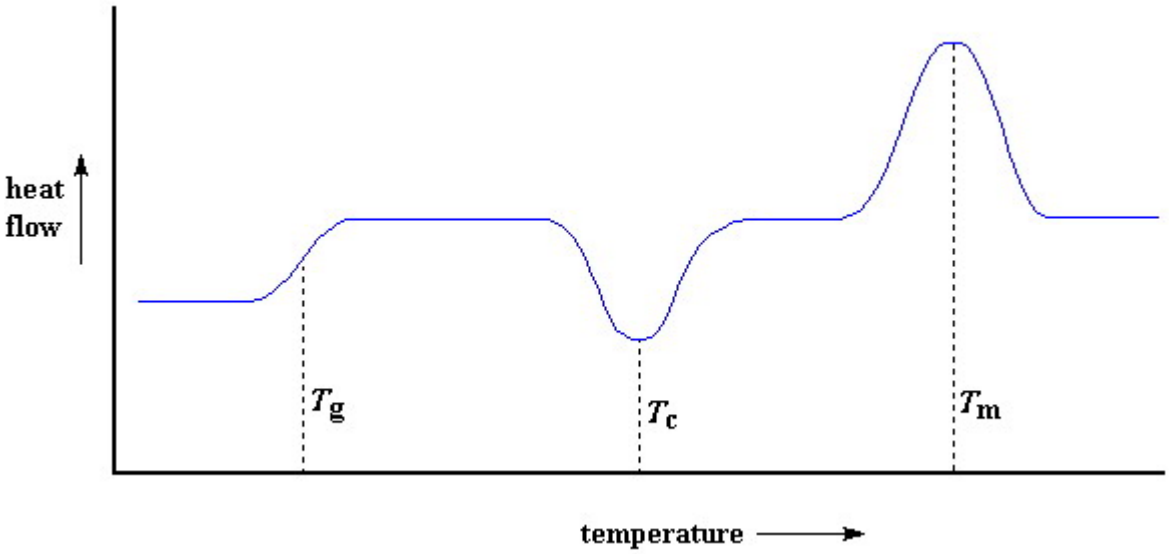

Figure 2.6.9. A representative drawing of DSC analysis output.

2.6.4. Flow Characteristics

2.6.4.1. Melt Flow Index (MFI) Test

Melt flow index (MFI) is defined as the weight of the polymer in grams flowing in a specific time, generally 10 minutes, through a capillary of specific diameter and length by a pressure applied via prescribed alternative gravimetric weights for alternative prescribed temperatures [47].

Melt flow index test, also known as melt flow rate (MFR) test, is used to characterize polymer melts. It is an indirect measure of molecular weight, high MFI corresponding to low molecular weight. At the same time, the melt flow rate is a measure of the ability of the material's melt to flow under pressure. The melt flow rate is inversely proportional to the viscosity of the polymer melt. If the melt index is low then its melt viscosity and melt flow resistance is high.

The melt flow index machine is, in effect, a single point ram extruder. The polymer sample is heated in the barrel and then extruded through a standard die using a standard weight on the piston. Then, the weight of the polymer (in grams) extruded in ten minutes is quoted as melt flow index [21].

2.7. Previous Studies

Zhang et al. [26] prepared polypropylene/montmorillonite nanocomposites via melt intercalation by using organomontmorillonite and conventional twin screw extrusion. They investigated the dispersibility of silicate layers of the montmorillonite in the composites. The particles of the silicate layers were dispersed at the nanometer level according to the XRD and TEM results. In their study, the tensile strength of nanocomposites is not increased much compared with that of polypropylene and conventional filled composite. However, the impact strength was greatly improved.

Koo et al. [28] prepared three types of maleated polypropylene-layered silicate nanocomposites with different dispersion states of layered silicate (deintercalated, intercalated and exfoliated states) from two kinds of

polypropylenes with different molecular weights, organically modified layered silicate and pristine montmorillonite. They investigated the effect of final morphology of the nanocomposite on the rheological and mechanical properties. They showed that maleated polypropylene with high molecular weight intercalates slowly and the other with low molecular weight exfoliates fast into the organophillic layered silicates. They showed rheological properties has close relationship with the dispersion state of layered silicates. They also showed that the exfoliated nanocomposite shows the largest increase and the deintercalated nanocomposites shows almost no change in relative shear, complex viscosities and dynamic storage modulus with the clay content.

Polypropylene nanocomposite, containing 4 wt % of an organomontmorillonite, was prepared and characterized by Ellis et al. [27] and its properties were compared with those of talc-filled (20-40 wt %) composites. The major driving force behind their work was weight reduction, with maintained or even improved flexural and tensile modulus, especially at temperatures up to 70 °C. PP nanocomposite exhibited a weight reduction of approximately 12% in comparison with the 20% talc-filled PP, while maintaining comparable stiffness.

Hambır et al. [29] prepared PP/clay nanocomposites by using different grades of PP, compatibilizers and organically modified clay via melt intercalation method. They used two grades of maleic anhydrite (MAH) modified PP one of which contains 1%MAH. The other one includes 0.65% MAH. Their results showed that the extent of intercalation/exfoliation depended on the type of compatibilizer used. The compatibilizer including 1%MAH was found to be more effective. According to their results of dynamic mechanical analysis, the storage modulus of PP/clay nanocomposites showed significant improvement, which is ascribed to the increase in the apparent aspect ratio of clay layers.

Zhang et al. [32] investigated the effect of elastomeric nano-particles (ENP) on the mechanical and crystallization behaviour of polypropylene. They achieved a good balance of toughness and stiffness of PP via blending PP with a small amount of ENP. Based on the measurements, mechanical properties of the blends studied both the toughness of PP at room temperature and at -20 °C showed substantial increase. In addition to this, the stiffness of the PP blends retains or even possesses a slight enhancement. They pointed out that one of the reasons for this improvement is due to the fact that the ENP is not only a toughening modifier but also a nucleation agent for the PP.

Ton-That et al. [30] investigated the effect of crystallization on intercalation of clay-polyolefin nanocomposites and their performance. They used two types of PP with different levels of crystallinity in order to prepare clay/PP nanocomposites. Their results demonstrated the impact of crystallization on the level of clay intercalation. They determined that it is essential to reduce the degree of crystallinity in order to improve exfoliation. However, this might result in a loss of mechanical performance. They reported that exfoliation of PP nanocomposites is complex, and to achieve exfoliation by melt compounding, one needs to overcome different challenges in terms of chemistry, thermodynamics, crystallization, and processing.

A novel fabrication method for polypropylene/clay nanocomposites were investigated by Kim et al. [31]. They reported that the exfoliated structure of PP/clay nanocomposites could be obtained without using any compatibilizer when exposed to the electric field. They regulated the degree of dispersion and exfoliation by controlling the amount of clay loading, the strength of electric field, the time exposed to the electric field. In their study, they tried to produced PP/clay nanocomposites via continuous processing like extrusion. They

presented a novel method to continuously produce PP/clay nanocomposites using the electric melt pipe equipped with a twin-screw extruder. They applied an AC electric field of 1kV. mm^{-1} and 60 Hz during processing. In their study, only a partial intercalation was achieved through continuous processing. However, they claimed the possibility to produce nanocomposites by this approach.

CHAPTER 3

EXPERIMENTAL

3.1. Materials

3.1.1. Polymer Matrix

Polypropylene used in this study was purchased from Petkim Petrokimya Holding A.Ş, İzmir, Turkey. Polypropylene whose trade name is MH-418 was sold in the form of white pellets in a 25 kg polyethylene bags. Properties of MH-418 can be seen from Table 3.1.1.

Table 3.1.1 Properties of polymer matrix, PP, MH-418

Property	**Unit**	**Value**
Melt Flow Rate (MFR) (2160 g, 230°C)	g/10min	4.0 -6.0
Density, 25 °C	g/cm^3	0.85
Tensile Strength (ASTM-638, TS-1398)		
At Yield	kg/cm^2	320
At Break	kg/cm^2	430

3.1.2. Organoclays

Three different organically modified montmorillonites were used in this study as the filler. These organoclays whose trade names are Cloisite® 15A, Cloisite® 25A, and Cloisite® 30B were modified by the manufacturer with a quaternary ammonium salt.

Cloisite® clays consist of organically modified nanometer scale, layered magnesium aluminum silicate platelets. The silicate platelets that Cloisite® clays are derived from are 1 nanometer thick and 70 – 150 nanometers in width. The surface modification of the platelets allows dispersion into the thermoplastic systems for which they were designed to improve.

These three Cloisite® clays were purchased from Southern Clay Products, Texas-U.S.A. and they are all additives for plastics to improve various physical properties, such as mechanical, thermal, and barrier properties.

3.1.2.1. Cloisite® 30B

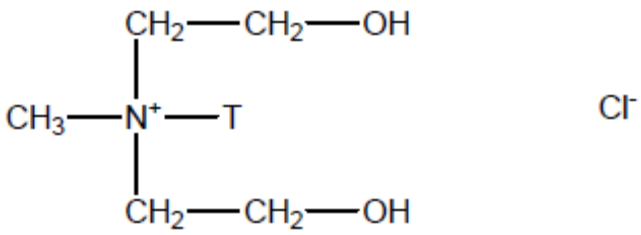

Figure 3.1.1. The chemical structure of Cloisite® 30B.

Figure 3.1.1. shows the chemical structure of Cloisite® 30B where T is Tallow (~65% C18; ~30% C16; ~5% C14) and the anion is chloride. This structure can be written as MT2EtOH: methyl, tallow, bis-2-hydroxyethyl, quaternary ammonium. Typical physical properties of Cloisite® 30B are listed in Table 3.2.

Table 3.1.2. Typical physical properties of Cloisite® 30B

Property	**Cloisite® 30B**
Organic Modifier	MT2EtOH
Modifier concentration	90 meq/100 g clay
% Moisture	<2%
% Weight loss on ignition	30 %
Color	Off white
Density:	
Loose bulk, Ibs/ft^3	14.25
Packed bulk, Ibs/ft^3	22.71
Specific Gravity, g/cc	1.98
X-ray results	d_{001}=18.5 Å
Dry particle sizes (microns, by volume):	
	10% less than 2 µm
	50% less than 6 µm
	90% less than 13 µm

3.1.2.2. Cloisite® 15A

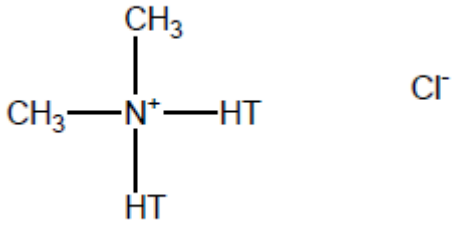

Figure 3.1.2. The chemical structure of Cloisite® 15A.

The chemical structure of Cloisite® 15A where HT is Hydrogenated Tallow (~65% C18; ~30% C16; ~5% C14) is shown in Figure 3.1.2. The name of this structure can be written as 2M2HT: dimethyl, dehydrogenated tallow, quaternary ammonium.

Table 3.1.3. Typical physical properties of Cloisite® 15A

Property	**Cloisite® 15A**
Organic Modifier	2M2HT
Modifier concentration	125 meq/100 g clay
% Moisture	<2%
% Weight loss on ignition	43 %
Color	Off white
Density:	
Loose bulk, Ibs/ft^3	10.79
Packed bulk, Ibs/ft^3	18.64
Specific Gravity, g/cc	1.66
X-ray results	d_{001}=31.5 Å
Dry particle sizes (microns, by volume):	
	10% less than 2 µm
	50% less than 6 µm
	90% less than 13 µm

The physical properties of Cloisite® 15A which was used in this study are listed in Table 3.1.3.

3.1.2.3. Cloisite® 25A

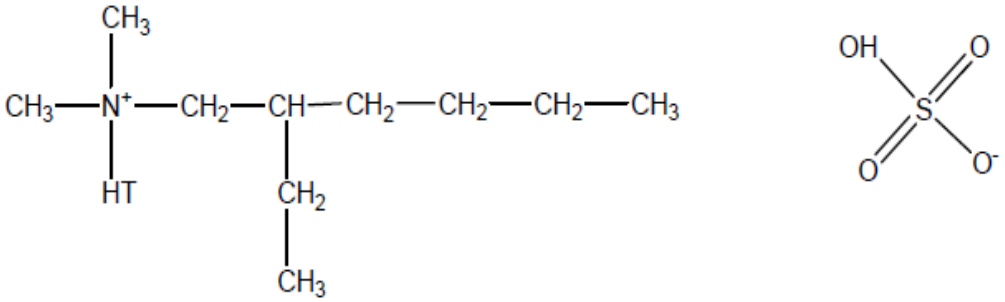

Figure 3.1.3. The chemical structure of Cloisite® 25A.

The chemical structure of Cloisite® 25A is illustrated in Figure 3.1.3 where HT is Hydrogenated Tallow (~65% C18; ~30% C16; ~5% C14) and the anion is methyl sulfate. This can be written as 2MHTL8: dimethyl, dehydrogenated tallow, 2-ethylhexyl quaternary ammonium. Typical physical properties of Cloisite® 15A can be seen in Table 3.1.4.

Table 3.1.4. Typical physical properties of Cloisite® 25A

Property	**Cloisite® 25A**	
Organic Modifier	2MHTL8	
Modifier concentration	95 meq/100 g clay	
% Moisture	<2%	
% Weight loss on ignition	34 %	
Color	Off white	
Density:		
Loose bulk, Ibs/ft^3	12.08	
Packed bulk, Ibs/ft^3	20.48	
Specific Gravity, g/cc	1.87	
X-ray results	d_{001}=18.6 Å	
Dry particle sizes (microns, by volume):		
	10% less than	2 µm
	50% less than	6 µm
	90% less than	13 µm

3.1.3. Compatibilizers (Elastomers)

Compatibilizers were used in order to provide interaction between the polypropylene matrix and the organoclays. Moreover, they are necessary to facilitate the opening of the silicate layers so that the PP matrix can enter through the layers.

In this study, Lotader® grades were used as the compatibilizer. The Lotader® grades which were used in this study include ethylene, acrylic ester and functional reactive groups such as maleic anhydride or glycidyl methacrylate.
The reasons why Lotaders® were used are their good reactivity and elastomeric properties that make Lotaders® excellent impact modifiers or compatibilizer materials for technical polymers. Lotaders® are also compatible with polyolefins like PP owing to their olefinic chain structure.

Lotader® grades have polar structure allowing these polymers to adhere to other materials and be compatible with different types of polymers. These structures confer Lotader® molecules have outstanding heat stability, allowing processing conditions of up to 320 °C. Furthermore, Lotader® grades are not corrosive for processing machines even in the case of accidental degradation.

Acrylic ester content of Lotaders® used in this study is between 0 to 25% in weight, which may decrease crystallinity and have a large influence on mechanical and thermal properties.

The reactive groups with up to 3.5% MAH or 8% GMA give strong reactivity to Lotader® which can then bond to polar substrates or polymers with functional groups.

In this study, three types of Lotader® grades whose trade names are Lotader® AX8900; terpolymer of Ethylene – Methyl Acrylate – Glycidyl Methacrylate (E-MA-GMA) , Lotader® AX8840; Copolymer of Ethylene – Glycidyl Methacrylate (E-GMA), and Lotader® 2210; terpolymer of Ethylene – nButyl Acrylate – Maleic Anhydride (E- nBA-MAH) were chosen. They were all purchased from Arkema Inc., France.

3.1.3.1. Lotader® 2210

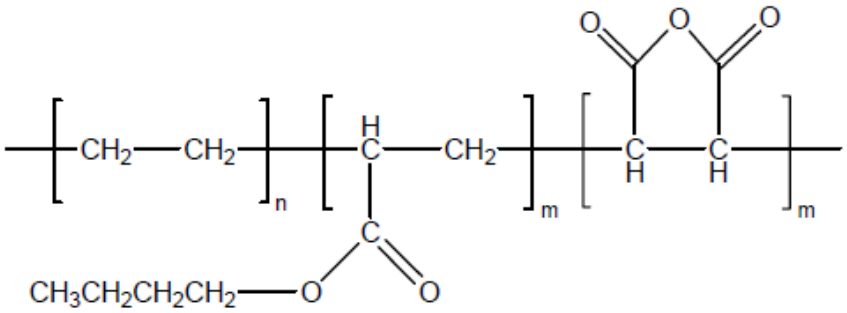

Figure 3.1.4. The chemical structure of Lotader® 2210 (E-nBA-MAH).

The chemical structure and physical properties of Lotader® 2210 can be seen in Figure 3.1.4 and Table 3.1.5, respectively. It is terpolymer of Ethylene – nButyl Acrylate – Maleic Anhydride (E- nBA-MAH). Lotader® 2210 contains maleic anhydride group as a reactive group which gives polarity to the structure, increases adhesion onto polar substrates and helps formation of chemical bonds with substrates such as metals, polymers metallized products.

Table 3.1.5. Properties of Lotader® 2210

Property	**Lotader® 2210**
n-butyl acrylate content (%wt)	8
MAH content (%wt)	2.6
MFI (190 ° 2.16 kg ASTM D 1238) (g/10 min)	3
Melting Point (ASTM D 2117) (°C)	107
Vicat Softening Point (ASTM D 1525) (°C)	80
Flexural Modulus (ASTM D 638) (MPa)	120
Tensile Strength at Break (ASTM D 638) (MPa)	12
Elongation at Break (ASTM D 638) (%)	600

3.1.3.2. Lotader® AX8900

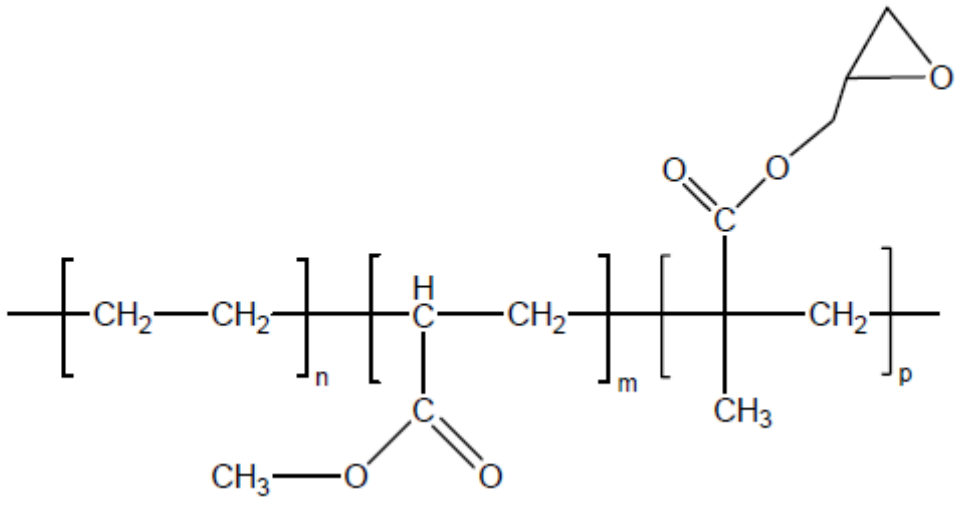

Figure 3.1.5. The chemical structure of Lotader® 8900 (E-MA-GMA).

Lotader® 8900 whose chemical structure is seen in Figure 3.1.5. is the terpolymer of Ethylene – Methyl Acrylate – Glycidyl Methacrylate (E-MA-GMA). Here epoxy groups can react with substances such as hydroxyl, (OH) containing materials, carboxylic acids (COOH), and amines. On the other hand, the acrylic group may reduce the crystallinity of the PP matrix. Table 3.1.6 shows the typical specifications of Lotader® 8900.

Table 3.1.6. Properties of Lotader® 8900

Property	**Lotader® 8900**
Acrylic Ester content (%wt)	25
GMA content (%wt)	8
MFI (190 ° 2.16 kg ASTM D 1238) (g/10 min)	6
Melting Point (ASTM D 2117) (°C)	60
Vicat Softening Point (ASTM D 1525) (°C)	<40
Young's Modulus (ASTM D 638) (MPa)	8
Tensile Strength at Break (ASTM D 638) (MPa)	4
Elongation at Break (ASTM D 638) (%)	1100
Hardness Shore A (ASTM D 2240)	70

3.1.3.3. Lotader® AX8840

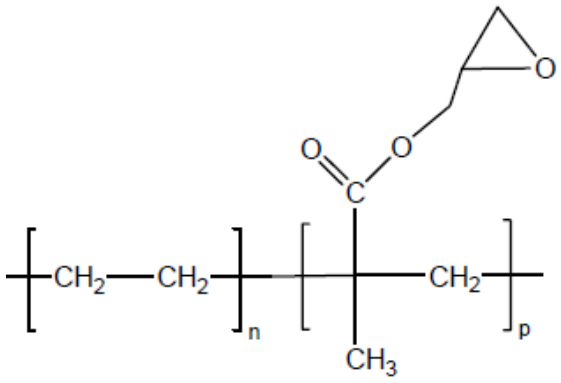

Figure 3.1.6. The chemical structure of Lotader® 8840 (E-GMA).

Lotader® 8840 contains GMA functional group like Lotader® 8900. It is copolymer of ethylene and glycidyl methacrylate as it is seen in Figure 3.1.6. The typical properties of Lotader® 8840 are shown in Table 3.1.7.

Table 3.1.7. Properties of Lotader® 8840

Property	**Lotader® 8840**
Acrylic Ester content (%wt)	0
GMA content (%wt)	8
MFI (190 ° 2.16 kg ASTM D 1238) (g/10 min)	5
Melting Point (ASTM D 2117) (°C)	105
Vicat Softening Point (ASTM D 1525) (°C)	87
Young's Modulus (ASTM D 638) (MPa)	104
Tensile Strength at Break (ASTM D 638) (MPa)	8
Elongation at Break (ASTM D 638) (%)	420
Hardness Shore A (ASTM D 2240)	92

3.2. Experimental Set-up and Procedure

3.2.1. Extrusion Process and Melt Blending

In the production of all blends and ternary nanocomposites, a co-rotating twin screw extruder was used in this study. The extruder model is Thermoprism TSE 16 TC with L/D = 24, screw diameter = 16 mm. The length of barrel and die of the extruder is 384 and 16 mm, respectively. Also, the extruder has 500 rpm maximum screw speed, 12 Nm maximum torque capability. As it is seen in Figure 3.2.1 (a) and (b), the extruder that was used in this study has a control panel in order to set barrel and die temperatures, screw speed, feed flow rate of main feeder and side feeder. In addition to these, the control panel provides control process parameters, such as screw speed, temperature profile of the barrel, during extrusion.

Figure 3.2.1.a. Thermo Prism TSE 16 co-rotating twin screw extruder.

Figure 3.2.1.b. The die and control panel of Thermo Prism TSE 16.

3.2.2. Injection Molding

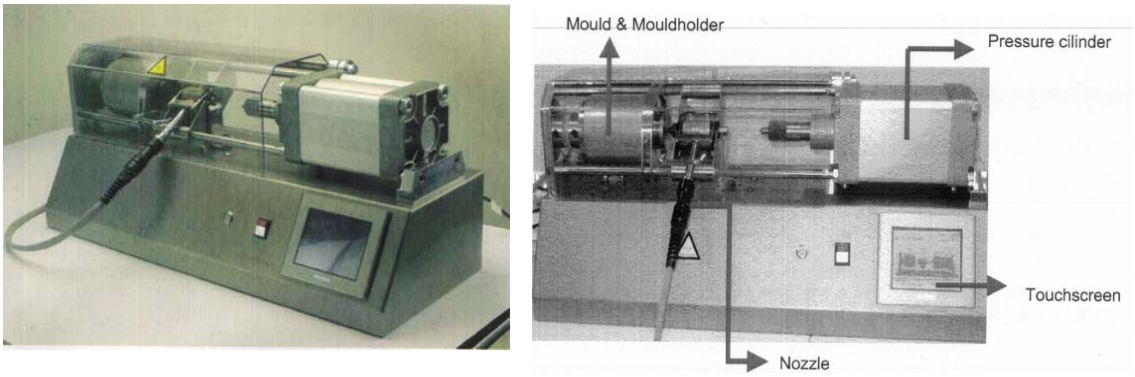

Figure 3.2.2. DSM Xplore injection molding.

The specimens were prepared by using laboratory scale DSM Xplore (micro 10cc) injection molding machine (Figure 3.2.2) in order to perform characterization. Injection molding apparatus used in this study consists of a mold on the left hand side and a pressure cylinder on the right hand side. A nozzle is connected to the machine. There is also a control panel on the machine in order to set the nozzle (melt) temperature, mold temperature and injection pressure. The maximum injection pressure of this machine is 16 bars.

3.2.3. Experimental Procedure

In this study, ternary nanocomposites of PP/organoclay/compatibilizer (elastomer) were produced. Type of compatibilizer, type of montmorillonite and mixing order of materials were the process parameters.

First of all, all materials (except PP) were dried in an oven at suitable temperatures (Table 3.2.1). Drying temperatures and duration were determined

from the literature by considering the melting point of the raw materials. After drying process, initially pure PP and PP/compatibilizer blends were extruded. The content of compatibilizer was chosen as 5, 10 and 15 wt % in the blends in order to select the best percentage to produce the nanocomposites. Having determined the best percentage, ternary nanocomposites were then produced. Also, PP/montmorillonite mixtures were prepared in order to make comparison.

All sets were extruded twice to provide long duration of shear and high level of exfoliation. After the first extrusion process, the melts were pelletized by using a pelletizer and then they were dried in order to remove the moisture. While the polymer melt was flowing from the extruder die in the second extrusion process, it was taken to the barrel of the injection molding machine and injection was done immediately. This process is called the continuous process.

Table 3.2.1. Drying Conditions

Materials	**Drying Temperature (°C)**	**Drying Time (h)**
Before First Extrusion Process		
PP	-	-
Cloisite® 30B Cloisite® 15A Cloisite® 25A	80	12-16
Lotader® 2210 Lotader® 8900 Lotader® 8840	40	12-16
Before Second Extrusion Process		
PP	100	4
PP + Clay	100	4
PP + Elastomer	100	4
Elastomer + Clay	40	4
PP + Elastomer +Clay	100	4

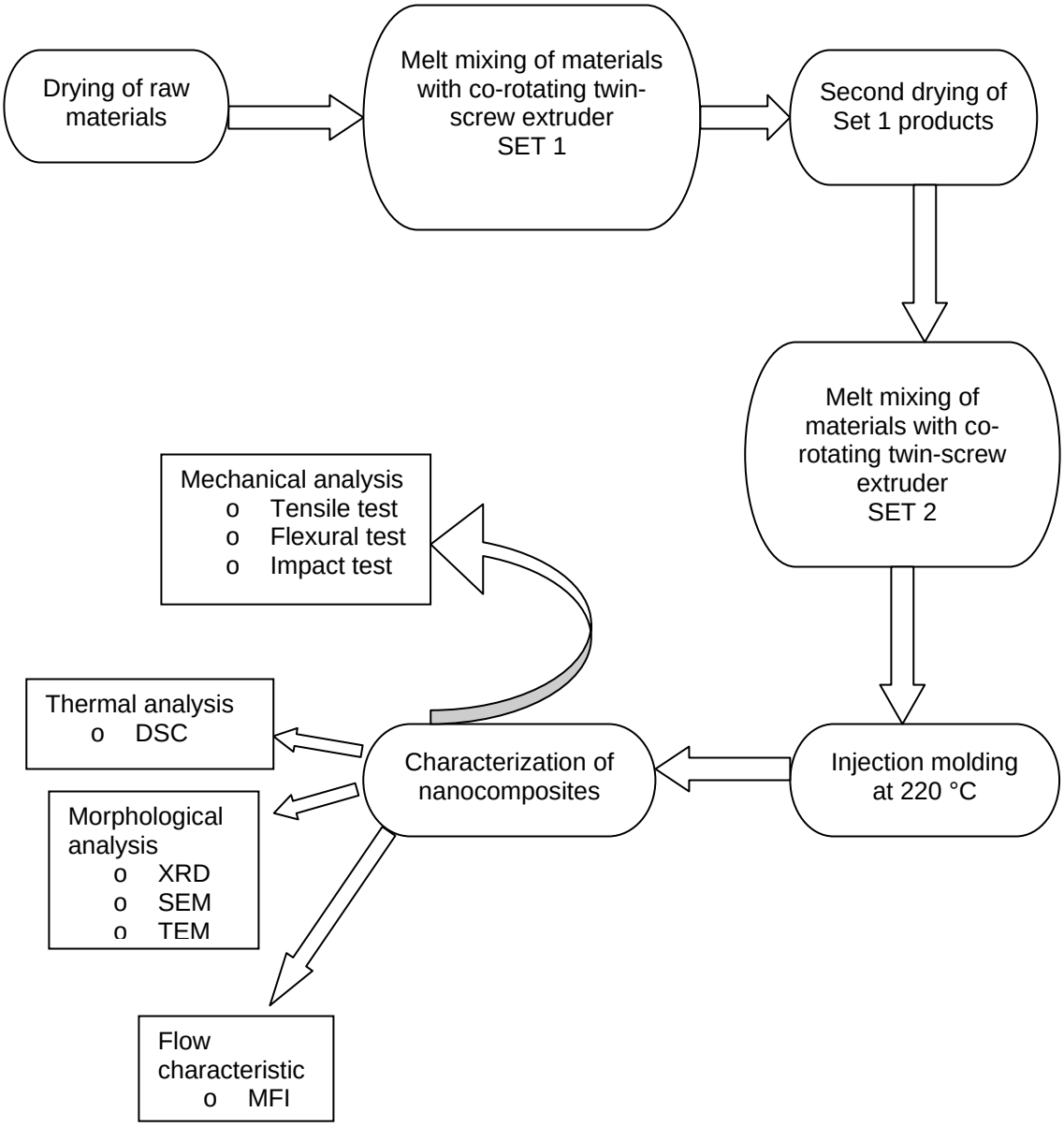

Figure 3.2.3. Flow chart of experimental procedure

3.2.4. Extrusion Process

3.2.4.1. First Extrusion Process

The summary of the experimental procedure flow chart is shown in Figure 3.2.3.

In this study, feed flow rate, screw speed and temperature profiles were not selected as the process parameters. They were all held constant.

Feed flow rate was 25 g/min for each run. Clay was fed to the system from the side feeder, whereas all of other raw materials such as PP, PP/compatibilizer blends were fed from the main feeder. For each run, the extrusion process was started with 500 g of raw material. Inlet flow rates of main and side feeder were calibrated before each run in order to get the desired compositions.

The screw speed was held constant at 250 rpm for each run during the extrusion process.

There are five temperature zones through the barrel (from the hopper to the die). All of them were set to 200 °C during extrusion. The polymer melt leaving the extrusion die was cooled by passing through a water bath. After the bath, there is an air blower in order to remove the water coming from the bath. Polymer surface was dried with this air blower. Finally, the product was sent to a pelletizer and collected in the plastic bags.

3.2.4.2. Second Extrusion Process

The procedure explained above was same for second extrusion until the product came out of the die.

In the second extrusion, the polymer melt was taken into the barrel of injection molding machine in order to obtain specimens. This procedure is called the continuous process. Since the product did not enter the water bath, it did not need a second drying process. Furthermore, the product was taken in the melt form so that waiting for melting was not necessary. Briefly, it can be said that the continuous process is a time-saving process and it minimizes thermal degradation.

3.2.4.3. Effect of Mixing Order in the Processes

In changing the mixing order of processing, there were four different variations by using the raw materials of PP / Lotader® AX8900 / Cloisite® 15A, and PP / Lotader® AX8900 / Cloisite® 25A. After many series of experiments and some characterization it was decided to use these raw materials. The letters P, E and C represent PP, elastomer (compatibilizer) and clay, respectively.

Mixing Order 1 (PEC)

RUN 1: Pellets of elastomer and PP were mixed in desired compositions and fed to the extruder from the main feeder, while powder of organoclay was fed to the extruder from the side feeder in the first extrusion process. The streams of main

and side feeder were calibrated for a total flow rate of 25 g/min. The product contained all of the raw materials.

RUN II: After drying the product of the first extrusion process, (EPC) pellets were fed to the extruder from the main feeder for the second extrusion process.

Mixing Order 2: (PE)C

RUN I: Pellets of PP and elastomer were put in the main feeder in desired compositions. After calibration for feed flow rate of 25 g/min, the blend of PP/elastomer was extruded.

RUN II: In the second extrusion (PE) blend was fed to the extruder from the main feeder and clay was fed to the system from the side feeder.

Mixing Order 3: (PC)E

RUN I: Pellets of PP were fed to the extruder from the main feeder, whereas powders of clay were fed to the system from the side feeder in desired compositions in the first extrusion process. The flow rates of PP and clay streams were maintained as 25 g/min in total.

RUN II: The product of run I process and the pellets of elastomer were mixed mechanically in the main feeder required compositions, and extruded again after drying.

Mixing Order 4: (EC)P

RUN I: While the pellets of elastomer were put in the main feeder, the powders of clay were located in the side feeder. The total flow rate of the system was calibrated as 25 g/min.

RUN II: The product of run I process and pellets of PP were mixed mechanically in the main feeder and the second extrusion process was performed by the calibration of the total feed flow rate of 25 g/min.

Table 3.2.2. Summation of the Mixing Order Protocols

RUN	**Main Feeder**	**Side Feeder**	**Product**
RUN I	P + E	C	(PEC)
	P + E	-	(PE)
	P	C	(PC)
	E	C	(EC)
RUN II	(PEC)	-	(PEC)
	(PE)	C	(PE)C
	(PC) + E	-	(PC)E
	(EC) + P	-	(EC)P

Table 3.2.3. Compositions of PP Blends and Binary Nanocomposites

SET	PP	Compatibilizer	Organoclay
PP	100	-	-
PP + 2210 **PP + 2210** **PP + 2210**	95 90 85	5 10 15	- - -
PP + 8900 **PP + 8900** **PP + 8900**	95 90 85	5 10 15	- - -
PP + 8840 **PP + 8840** **PP + 8840**	95 90 85	5 10 15	- - -
PP + 30 B	98	-	2
PP + 15 A	98	-	2
PP + 25 A	98	-	2

Table 3.2.4. Compositions of Ternary nanocomposites

SET	PP (wt %)	Compatibilizer (wt %)	Organoclay (wt%)
PP + 2210 + 30B PP + 8900 + 30B PP + 8840 + 30B	93	5	2
PP + 2210 + 15A PP + 8900 + 15A PP + 8840 + 15A	93	5	2
PP + 2210 + 25A PP + 8900 + 25A PP + 8840 + 25A	93	5	2
(PP + 8900) + 15A (8900 + 15A) + PP (PP + 15A) + 8900	93	5	2
(PP + 8900) + 25A (8900 + 25A) + PP (PP + 25A) + 8900	93	5	2

Summary of the experimental conditions are shown in Tables 3.3.2, 3.3.3 and 3.3.4.

3.2.5. Injection Molding Process (Specimen Preparation)

The specimens were molded by injection molding process in order to perform characterization. The molding process began by taking the polymer melt to the barrel of injection molding machine as it comes out of the extruder.

Table 3.2.5. Parameters of injection molding

Parameter	**Unit**	**Value**
Melt Temperature	°C	220
Mold Temperature	°C	30
Injection Pressure	bar	15

After each molding process two specimens were obtained one of which had the shape of dogbone according to the ISO 527-2 5A, whereas the other one was a sample of impact or flexural test bar according to ISO 178. The injection molding parameters are shown in Table 3.2.5.

3.3. Characterization

In this study, synthesis of PP/organoclay/compatibilizer ternary nanocomposites by melt blending method was carried out and the samples were characterized. In addition, the effects of compatilizer type, organoclay type and mixing protocols of materials on the final properties of nanocomposites were examined. In order to characterize the materials not only morphological, thermal, mechanical analysis were performed, but also hardness and flow characteristics were determined.

3.3.1. Mechanical Analysis

In mechanical analysis tensile, flexural and impact tests were performed at room temperature in laboratory conditions. For each set, five samples were tested. The results of tests and the average and standard deviation values were determined. Tensile strength, young's modulus and strain at break were obtained from the tensile tests; flexural strength and flexural modulus were determined from the flexural tests according to the ISO standards. Also, from the impact tests, impact strength was evaluated according to the ISO standards. The specimens were molded according to the standards of ISO 527-5A for tensile tests and ISO 178 for impact and flexural tests.

3.3.1.1. Tensile Test

Tensile tests were performed on five samples for each compositions according to the standards of EN-ISO 527-1 and EN-ISO 527-2 (international standards and organization) by using a Lloyd LR 30 K Universal Testing machine. The shape and dimensions of the specimens ISO 527-2 5A are shown in Table 3.2.6.

The distance between the grips was taken as 50 mm while performing the tests. Since the gauge length and crosshead speed was taken as 20 mm and 10 mm/min, respectively, the strain rate was calculated as 0.5 min^{-1}. At the end of these tests, stress versus strain curves were obtained, which provided determination of tensile strength, tensile modulus and elongation at break.

Table 3.2.6. Dimensions of specimen ISO 527-2 5A

Dimensions	**Value (mm)**	**Shape**
Gauge length (L_o)	20	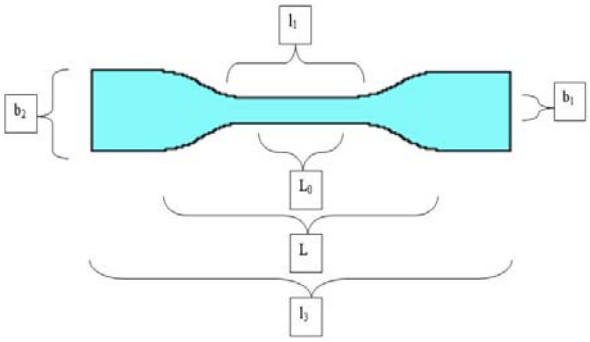
Distance between grips (L)	50	
Length of narrow parallel-sided portion (l_1)	25	
Overall length (l_3)	>=75	
Width of narrow portion(b_1)	4	
Width at ends (b_2)	12.5	
Thickness (h)	>=2	

3.3.1.2. Flexural Tests

The shape and the dimensions of the specimens for flexural tests were molded according to ISO 178. In addition, these tests were performed according to the standards of ISO 178-1975 (E) (Plastics-Determination of Flexural Properties of Rigid Plastics) with LR 30 K Universal Testing machine. Three points bending was carried out with the span length of 50 mm and the strain rate of $0.5min^{-1}$. The rate of cross-head motion was calculated as 52.083 mm/min. The dimensions of the flexural tests specimens are shown in Table 3.2.7. During flexural tests no failure was observed. The tests were continued until the specimens leaned against the base of the supports. At the end of tests, load

versus deflection diagrams were obtained in order to determine the flexural strength and flexural modulus.

Table 3.2.7. Dimension of specimen ISO 178

Dimensions	**Value (mm)**
Overall length (L_0)	80
Support span (L)	50
Width of beam (b)	10
Depth of beam (d)	4

3.3.1.3. Impact Tests

Charpy impact tests of one sided notched specimens were performed according to the standard of ISO 179-2 (Plastics – Determination of Charpy Impact Strength) with pendulum Ceast Resil Impactor.

The dimensions and shape of the specimens that were used in impact tests were the same as the flexural tests specimens (ISO 178), and each specimen had a notch of 2 mm. ISO impact strength is expressed in kJ/m^2. Impact strength was calculated by dividing impact energy in J by the area under the notch. The results were obtained typically on five specimens, and the averages are reported.

Table 3.2.8. Impact Test Specimen Dimensions

Term	Specimen Dimensions (mm)
Length, L	80
Thickness, t	4
Total Width, w_1	10
Unnotched Width, w_2	8
Notch Type and Angle	v, 45°

The dimensions and shape of the specimens that were used in impact tests were the same as the flexural tests specimens (ISO 178), and each specimen had a notch of 2 mm. ISO impact strength is expressed in kJ/m^2. Impact strength was calculated by dividing impact energy in J by the area under the notch. The results were obtained typically on five specimens, and the averages are reported.

3.3.2. Morphological Analysis

In order to determine d-spacing of clays and dispersion of clay particles in the PP matrix, X-ray Diffraction (XRD) analysis was performed. Also, in order to see the surface of the composites Scanning electron microscopy (SEM) photographs were taken.

3.3.2.1. X-Ray Diffraction (XRD) Analysis

Clay containing composites were analyzed by using a RIGAKU D/MAX 2200/PC X-ray diffractometer. Cu Kα (λ = 1.54Å) radiation, generated at a voltage of 40 kV and current of 40 mA was used as the X-Ray source. The diffraction angle 2θ was scanned from 1° to 10° at a scanning rate of 1°/min and a step size of 0.01°. The molded specimens were used as the X-ray diffraction samples.

3.3.2.2. Scanning Electron Microscopy (SEM) Analysis

JEOL JSM-6400 low voltage scanning electron microscope was used in SEM analysis. The surfaces which were obtained from the impact tests were used for the SEM photographs. In order to have conductive surface, the fractured surfaces were coated with a thin layer of gold. This treatment was necessary for taking the SEM photographs. SEM analyses were used to see the elastomer domains in the structure and investigate the effect of compatibilizer and organoclay on the morphology of the nanocomposites. In this study, SEM photographs were taken at x250 and x3000 magnifications for each specimen.

3.3.2.3. Transmission Electron Microscopy (TEM) Analysis

In this study, TEM analysis is needed in order to investigate the dispersion of clay particles in the PP matrix and determine the nanocomposite structure whether intercalated or exfoliated.

Philips CM200 Transmission Electron Microscope (TEM) in DSM Research, Holland is used at an acceleration voltage of 120 kV to examine the samples.

Ultra thin sections of 70 nm in thickness are cryogenically cut with a diamond knife at a temperature of –100 ºC. All samples are trimmed parallel to the molding direction.

3.3.3. Thermal Analysis

3.3.3.1. Differential Scanning Calorimetry (DSC) Analysis

In this study, differential scanning calorimetry was performed with differential scanning calorimeter General V4.1.C DuPont 2000, at the temperature range of 30 °C to 250 °C. Measurements were carried out under nitrogen atmosphere with a heating rate of 5 °C/min. In order to determine the melting points of samples and the degree of crystallinity, DSC analysis was necessary. The value of heat of fusion (ΔH) of 100% crystalline PP was taken as 209 J/g [38].

3.3.4. Flow Characteristics

3.3.4.1. Melt Flow Index (MFI) Test

Melt flow index (MFI) test was performed by using an Omega Melt Flow Indexer according to the ISO R1133 shown in Figure 3.3.1. The MFI experiments were carried out at 230 °C with a load of 2.16 kg. The MFI machine looks like an extruder. Pellets of polymer enter into the machine. After waiting for a while they melt in the machine. The amount of polymer melt was weighed after flow of 10

min, which is defined as the melt index. The results were recorded in grams/10min.

Figure 3.3.1. Omega Melt Flow Indexer.

CHAPTER 4

RESULTS AND DISCUSSION

4.1. Morphological Analysis

In order to examine the structure of nanocomposites XRD, SEM and TEM analysis were carried out.

4.1.1. X-Ray Diffraction (XRD) Analysis

XRD is a rather simple and widely employed technique for the characterization of clay dispersibility. It is a very useful method for examining the intercalation and exfoliation of clay by monitoring the reflections from the silicate layers in the clay. According to the position, shape and intensity of the basal reflections, the delamination (dispersibility) of the layers can be defined. The graph of intensity versus 2θ is obtained after the XRD analysis. The basal spacing (d-spacing) of the clay particulates can be calculated from 2θ value of the first peak position. Then interlayer spacing values can be obtained according to Bragg's law.

Organoclays used in this study have one or more peaks at different positions. If the polymer matrix cannot enter into the clay galleries, the position of the peak does not change. However, when the interlayer space (d_{001}) expands, the positions of the peak shifts to the left. In other words, low 2θ values indicate larger interlayer spacing. The shifting to the left of the diffraction peak indicates

an intercalated structure. Moreover, the absence of the diffraction peak means that the clay platelets are completely exfoliated (delaminated) [34].

In this study, the XRD analysis were performed form the angle of 2θ = 1° to the angle of 2θ = 10°. The XRD patterns of organoclays Cloisite® 30B, 15A and 25A in powder form are given in Figure 4.1.1.

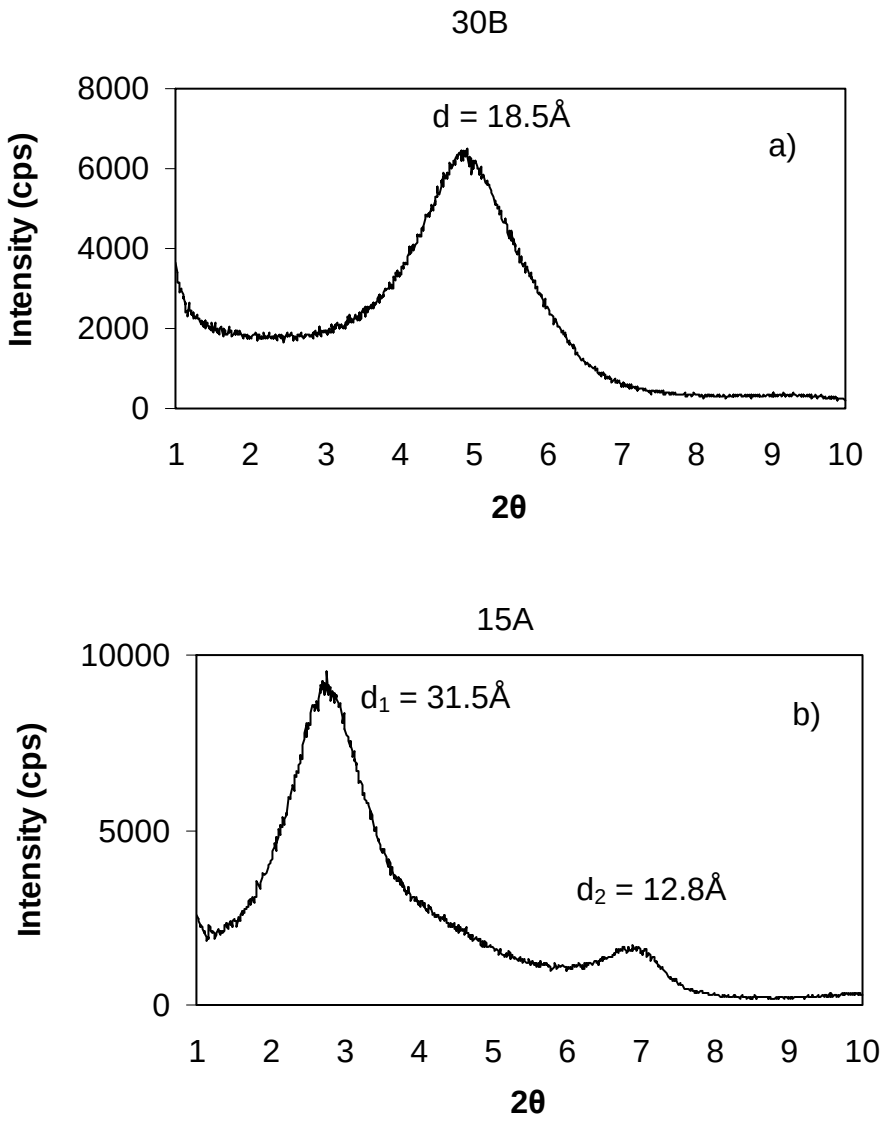

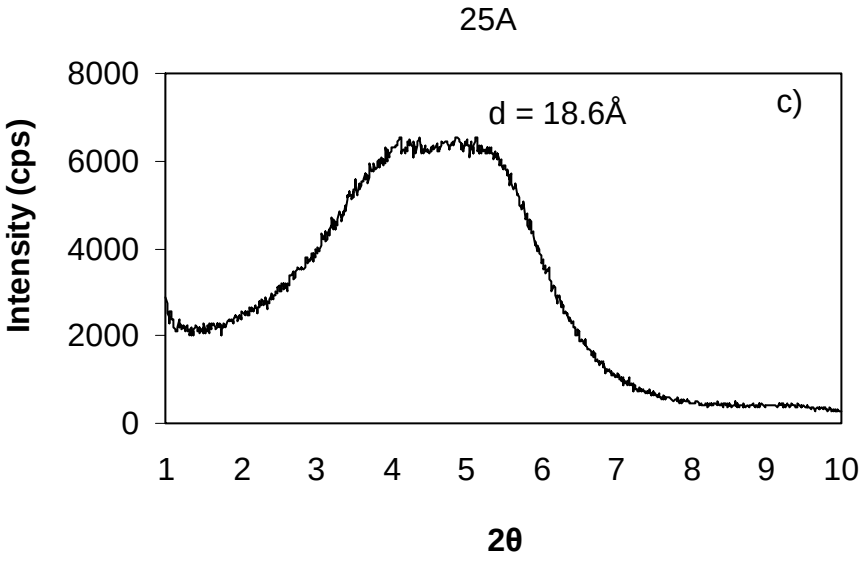

Figure 4.1.1. X-ray diffraction patterns of organoclays Cloisite® 30B (a), 15A(b) and 25A (c).

Figure 4.1.1.a shows the result of XRD pattern of Cloisite® 30B and the characteristic diffraction peak at 4.77° corresponding to the 001 plane diffraction. The interlayer spacing of Cloisite® 30B is calculated as 18.5 Å. Figure 4.1.b and c show the result of XRD patterns of Cloisite® 15A and Cloisite® 25A, respectively. For Cloisite® 15A, the interlayer spacing is calculated as d_{001} = 31.5 Å since the characteristic diffraction peak is at 2.8°. As for Cloisite® 25A, d is equal to the 18.6 Å at 2θ = 4.74°.

XRD diffractogram of Cloisite® 15A organoclay shows two diffraction peaks. The second peak can result from a second silicate layer if 2θ is about double the value of the first characteristic peak of the clay. However, as observed here this is not the case. The second peak (d_2) corresponds to 12.8 Å, which is the d-spacing of unmodified Na^+ montmorillonite according to Shouthern Clay. Thus, it corresponds the clay which is not modified by the quaternary ammonium salt.

In order to compare the result of the XRD analysis more accurately, XRD patterns are drawn for all samples. Figure 4.1.2 demonstrates the XRD patterns of pure Cloisite® 30B, the binary mixture of PP/ Cloisite® 30B, the ternary mixtures of PP/ Cloisite® 30B/Lotader® 2210 (E-nBA-MAH), PP/ Cloisite® 30B/Lotader® 8900 (E-MA-GMA), and PP/ Cloisite® 30B/Lotader® 8840 (E-GMA).

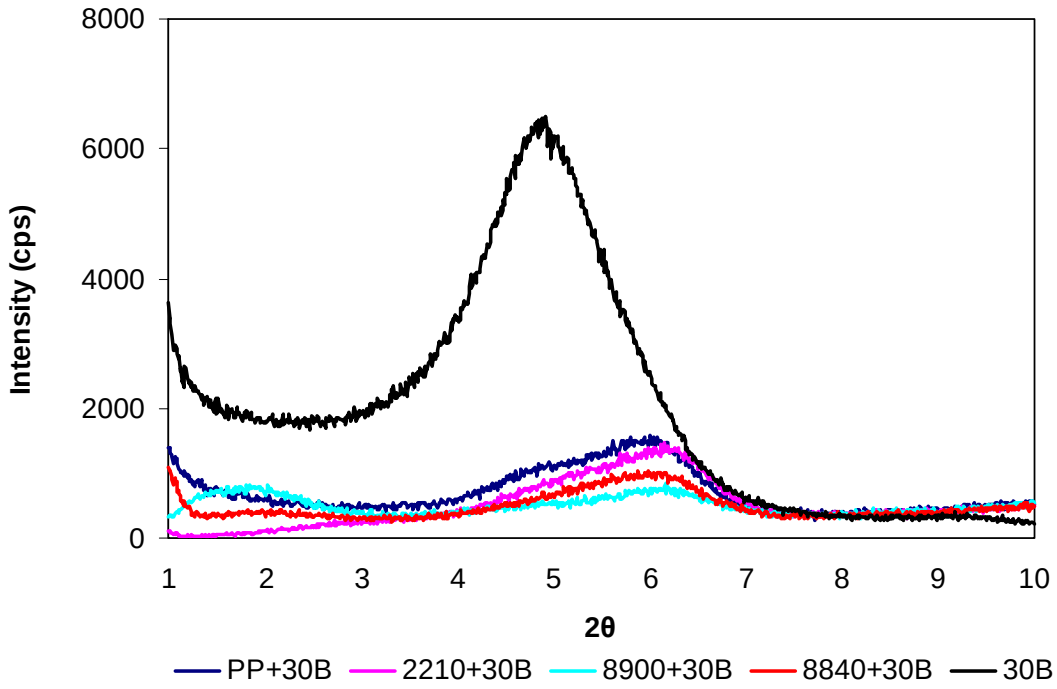

Figure 4.1.2. XRD patterns of PP composites containing Cloisite® 30B.

Table 4.1.1. 2θ and d-spacing data of samples containing Cloisite® 30B

	2θ(°)	**d (Å)**
Cloisite® 30B (in powder form)	4.8	18.5
PP+Cloisite® 30B	6.0	14.7
PP+Cloisite® 30B +2210 (E-nBA-MAH)	6.2	14.3
PP+Cloisite® 30B +8900(E-MA-GMA)	6.2	14.3
PP+Cloisite® 30B +8840(E-GMA)	5.9	15.0

In Figure 4.1.2, there is a shift in the peak angle 2θ to larger values (shifting to the right) for the organoclay Cloisite® 30B. This shows that the polymer matrix could not enter into the interlayer spacing. The d-spacing of the Cloisite® 30B became smaller which is seen in Table 4.1.1. Unfortunately, the production of nanocomposites with Cloisite® 30B is not successful. The silicate layers of the organoclay Cloisite® 30B did not separate from each other, so that the composites that were produced with Cloisite® 30B and three types of compatibilizers can be called as microcomposites. The reason of this observation can be that compatibilizers Lotader® 2210, 8900 and 8840 may not play an adequate compatibilizer role due to the very high polar characteristic of 30B [18]. Therefore, these compatibilizers cannot interact intimately with 30B. The d-spacing decreases probably due to the pressure applied during injection molding since pure Cloisite® 30B is in powder form.

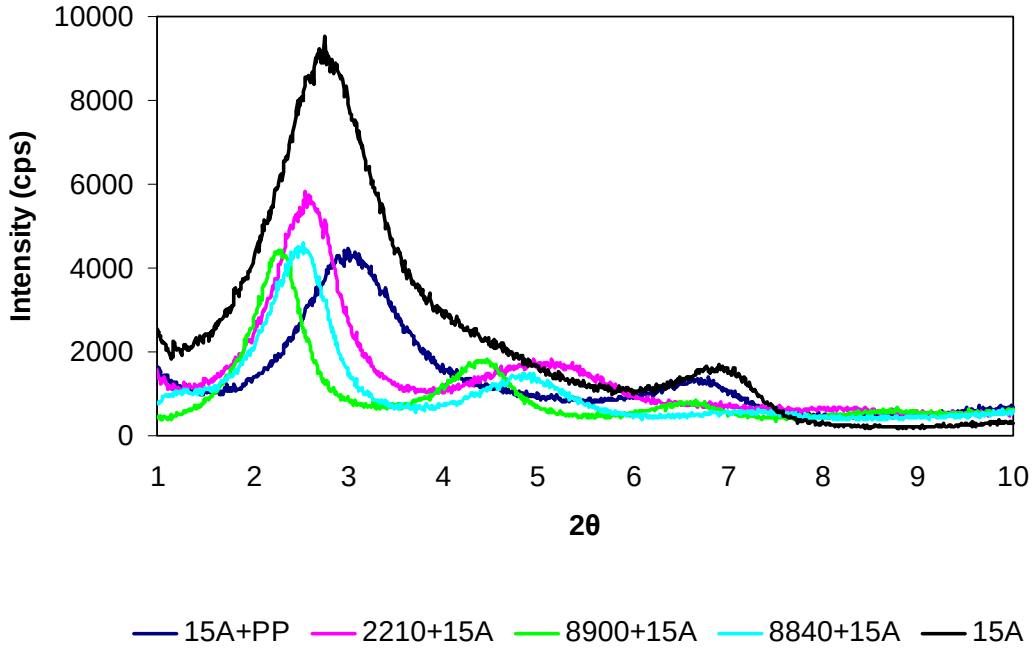

Figure 4.1.3. XRD patterns of PP composites containing Cloisite® 15A.

Figure 4.1.3 shows the XRD profiles of Cloisite® 15A, the binary mixture of PP/ Cloisite® 15A and the ternary mixture of PP/ Cloisite® 15A/Lotaders® 2210, 8900 and 8840. Cloisite® 15A has a major reflections at approximately 2θ = 2.8° associated with a d-spacing (d_1) of 31.5 Å which is shown in Table 4.1.2. The characteristic peak of Cloisite® 15A shifts to the right or larger angle when mixed with the PP without compatibilizer. This could also be due to the high injection pressure applied during molding. The blend of PP/ Cloisite® 15A has a peak at about 2θ = 3.01°, which corresponds to a d-spacing of 29.3 Å. Since this blend does not have any compatibilizer, the interlayer spacing of Cloisite® 15A decreases. Although, PP and Cloisite® 15A are both nonpolar, apparently PP molecules can not enter between the silicate layers in this process.

Table 4.1.2. 2θ and d-spacing data of samples containing Cloisite® 15A

	2θ(°)	**d_1 (Å)**	**d_2 (Å)**	**d_3 (Å)**
Cloisite® 15A (in powder form)	2.8	31.5	12.8	-
PP+Cloisite® 15A	3.0	29.3	13.3	-
PP+Cloisite® 15A +2210 (E-nBA-MAH)	2.6	34.5	17.1	-
PP+Cloisite® 15A +8900 (E-MA-GMA)	2.3	38.7	19.7	13.3
PP+Cloisite® 15A +8840 (E-GMA)	2.5	34.9	18.0	-

On the other hand, all of the elastomers are more polar than PP. Also, all of the elastomers have lower viscosity (higher MFI) than PP as analyzed later. Thus, it is thought that the elastomers may diffuse into the interlayer spacing more easily than PP chains. Once, the d-spacing of the clay increases due to this diffusion, the PP chains may then enter in between the silicate layers, especially in the ease of nonpolar clays such as Cloisite® 15A and Cloisite® 25A.

The d-spacing data for nanocomposites containing Cloisite® 15A are calculated by using Bragg's Equation from the diffraction peaks in the Figure 4.1.3. This peaks are denoted as d_1 , d_2 and d_3 starting from left to right. The observation of second diffraction peaks in the nanocomposites containing Cloisite® 15A may be due to the presence of unmodified clay portions in the structure, since it is close to the peak of unmodified Na^+ montmorillonite, which is 12.8 Å.

For ternary mixture of PP/Cloisite® 15A/Lotader® 2210 the characteristic peak is observed at $2\theta = 2.56°$ and the interlayer spacing is d = 34.47 Å (Table 4.1.2). The increase in the d-spacing support the mechanism outlined. The increase of the interlayer spacing is the 9.5%, and the structure of the nanocomposite is intercalated.

Similarly, the ternary nanocomposites of PP/Cloisite® 15A/Lotader® 8900 have an intercalated structure with an increase of 22.9% in the d-spacing. In this case the interlayer spacing is 38.7 Å with the reflection at approximately $2\theta = 2.28°$. The separation of the silicate layers is the maximum for Lotader® 8900 (E-MA-GMA) with respect to other elastomers used in this study.

As for the ternary nanocomposite of PP/Cloisite® 15A/Lotader® 8840, the angle 2θ is almost 2.53 ° and the d-spacing is 34.88 Å from Bragg's law corresponding to an increase of 10.8%. As a result, it can be said that Lotader® 8840 also provides compatibility between the polypropylene matrix and the organoclay Cloisite® 15A.

The second peak in the nanocomposites refer to the intercalated form of d_2 peak in Cloisite® 15A powder. In other words, polymer chains enter the interlayer spacing of unmodified sections and expand these interlayers.

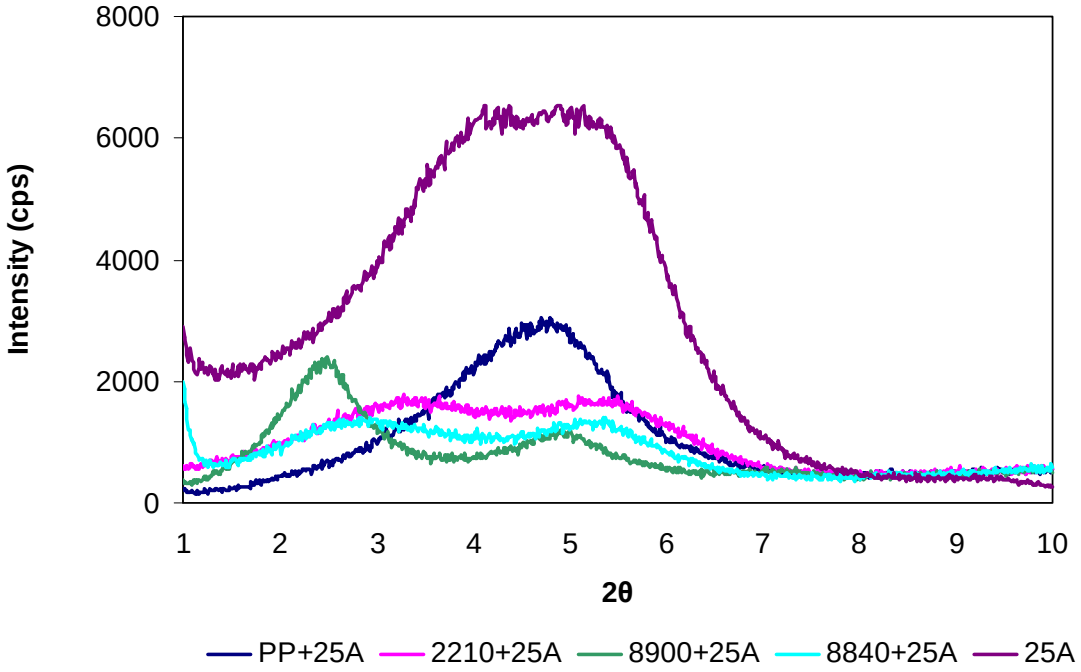

Figure 4.1.4. XRD patterns of PP composites containing Cloisite® 25A

Table 4.1.3. 2θ and d-spacing data of samples containing Cloisite® 25A

	2θ(°)	**d_1 (Å)**	**d_2 (Å)**
Cloisite® 25A (in powder form)	4.8	18.8	-
PP+Cloisite® 25A	4.7	18.4	-
PP+Cloisite® 25A +2210 (E-nBA-MAH)	3.3	26.9	16.1
PP+Cloisite® 25A +8900 (E-MA-GMA)	2.5	35.4	17.6
PP+Cloisite® 25A +8840 (E-GMA)	2.9	30.0	16.5

The XRD patterns of composites containing the organoclay of Cloisite® 25A is shown in Figure 4.1.4. Cloisite® 25A shows a diffraction peak at 2θ = 4.7°, which corresponds to an interlayer spacing of 18.8 Å. In the absence of compatibilizer, binary mixture of PP/Cloisite® 25A has a diffraction peak at 2θ =

4.79° associated with the values of d-spacing of 18.4 Å. The d-spacing of Cloisite® 25A gets slightly smaller in the binary mixture of PP/Cloisite® 25A. The high injection pressures applied may have caused the decrease in the d-spacing. The diffraction peak of the ternary nanocomposite of PP/Cloisite® 25A/Lotader® 2210 gives 2θ = 3.28° and the interlayer spacing of d_1 = 26.9 Å indicating an increase of 43.1% in the interlayer spacing. With the aid of compatibilizer the clay aggregates are broken down into smaller stacks and intercalation with the mechanism outlined earlier occurred [35].

In the ternary nanocomposite of PP/Cloisite® 25A/Lotader® 8900, the maximum increase in the clay interlayers is observed with respect to other ternary systems shown in Figure 4.1.4. It gives the reflection peak at 2θ = 2.49° corresponding to gallery distance of d_1 = 35.4 Å. The increase in the d-spacing is the 88.3 % indicating high level of intercalation. It also shows a peak at d_2=17.6 Å. This may be due to the secondary peak corresponding to n=2 in Bragg' s equation since $2d_2$ is closed to d_1.

The ternary nanocomposite of PP/Cloisite® 25A/Lotader® 8840 has the diffraction peak at 2θ = 2.9° with d-spacing of d = 30.0 Å indicating an increase of 59.6%. Figure 4.1.4 shows that this ternary nanocomposite as well as PP/Cloisite® 25A/Lotader® 8840 show some exfoliation since the intensity of the peaks gets smaller.

The presence of second diffraction peaks (d_2) in the ternary nanocomposites containing 25A may have resulted the secondary reflections as discussed before, since there is no secondary peak in Cloisite® 25A and also $2d_2$ is close to d_1.

The nanocomposites, produced with Cloisite® 15A/Lotader® 8900 and Cloisite® 25A/Lotader® 8900 which gave the maximum increase in the interlayer spacing with respect to other ternary systems produced in this study are chosen in order to investigate the effect of addition order of components on the structure. Figure 4.1.5 shows the XRD patterns of nanocomposites produced with polypropylene, Lotader® 8900, and Cloisite® 15A are represented with the letters of P, E, C1, respectively.

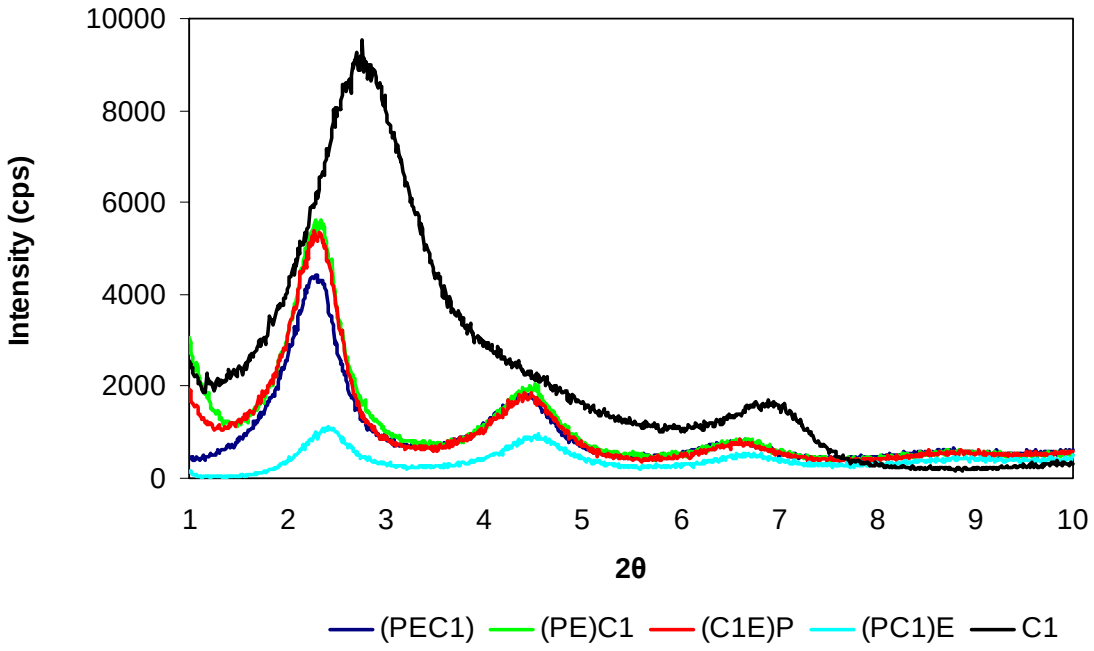

Figure 4.1.5. XRD patterns of nanocomposites with different mixing order of components P, E and C1.

As it is seen in Figure 4.1.5 and Table 4.1.4, there is no significant difference between the (PEC1), (PE)C1 and (C1E)P. The characteristic diffraction peak of Cloisite® 15A shifts to lower angle for these nanocomposites. In Figure 4.1.5 reflections for d_2 and d_3 are also seen. These values are close to reflections that

would be obtained by using Bragg's Law with n=2 and n=3. The elastomer 8900 has GMA functional group providing compatibility between the elastomer and clay surface, and enhance the intercalation of the polymer matrix. Exfoliated structures cannot be achieved by changing the mixing order of P, E, C1 in these nanocomposites.

Table 4.1.4. 2θ and d-spacing data of samples containing Cloisite® 15A processed by different mixing orders

	2θ(°)	**d_1 (Å)**	**d_2 (Å)**	**d_3 (Å)**
Cloisite® 15A (in powder form)	2.8	31.5	12.8	-
PP+Cloisite® 15A +8900(E-MA-GMA)	2.3	38.7	19.7	13.3
(PP+8900)+15A (PE)C1	2.3	38.7	19.5	13.1
(15A+8900)+PP (C1E)P	2.3	38.9	19.7	13.4
(PP+15A)+8900 (PC1)E	2.4	36.6	19.4	13.1

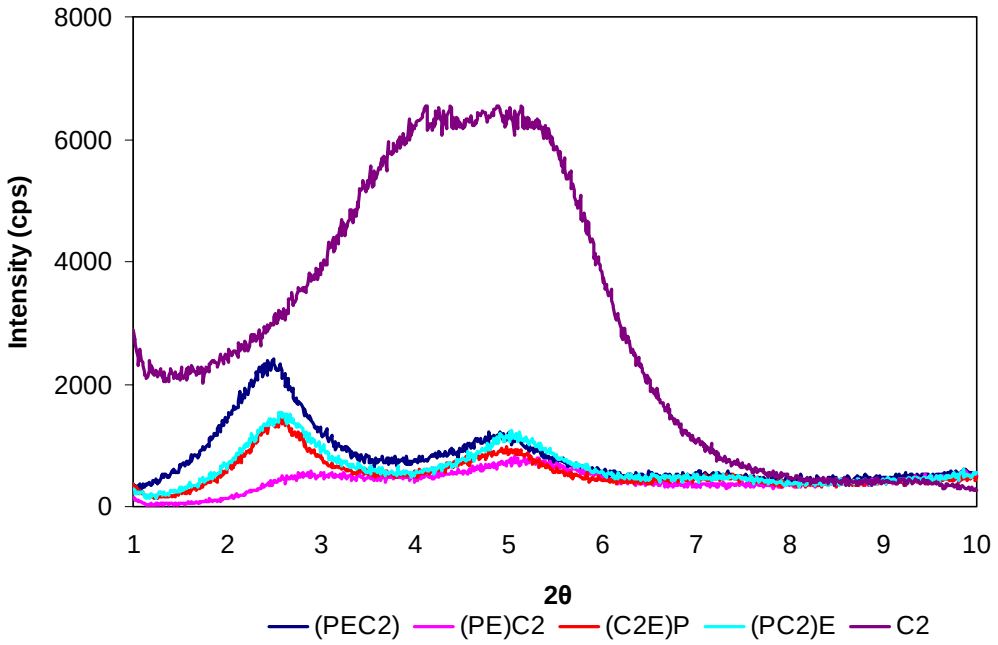

Figure 4.1.6. XRD patterns of nanocomposites according to mixing order of components P, E and C2.

Since the nanocomposite of PP/Cloisite® 25A/Lotader® 8900 gave the maximum increase in the interlayer distance, the mixing orders of these components were changed. The letters P, E and C2 represent polypropylene, Lotader® 8900 and Cloisite® 25A, respectively. Figure 4.1.6 shows the XRD patterns of nanocomposites with different mixing orders of components P, E and C2 and Table 4.1.5 shows the data of d-spacings. The nanocomposites processed with (PEC2), (C2E)P and (PC2)E mixing orders have intercalated structures. However, the structure of (PE)C2 nanocomposite approach exfoliation implied by the absence of any distinct diffraction peak. In this mixing order PP and elastomer were extruded first, followed by the addition of clay in the second extrusion.

The peaks obtained as d_2 could again be close to the secondary reflection that would be obtained with n=2.

Table 4.1.5. 2θ and d-spacing data of samples containing Cloisite® 25A processed by different mixing orders

	2θ(°)	**d_1 (Å)**	**d_2 (Å)**
Cloisite® 25A (in powder form)	4.8	18.8	-
PP+Cloisite® 25A +8900(E-MA-GMA)	2.5	35.4	17.6
(PP+8900)+25A (PE)C2	2.9	30.5	16.2
(25A+8900)+PP (C2E)P	2.6	34.6	17.4
(PP+25A)+8900 (PC2)E	2.6	34.2	17.5

4.1.2. Scanning Electron Microscopy (SEM)

In order to investigate the morphology of the samples that were produced in this study, scanning electron microscopy analysis is performed on fractured surfaces. SEM analysis is also carried out to determine the distribution of elastomer domains in polypropylene matrix, since this factor is a very important parameter in toughening mechanism. Neat PP and the mixtures of PP/compatibilizer, PP/organoclay, and PP/compatibilizer/organoclay were produced with extrusion by twin screw extruder, followed by injection molding. The fractured surfaces were obtained by breaking the samples with the impact test machine. In this section, SEM images are shown at magnifications of x250 and x3000 in order to observe the details.

The fractured surfaces of neat PP extruded twice are shown in Figure 4.1.7. The surface of continuous PP matrix is featureless and smooth implying little energy is dissipated during the impact processes [61]. Also, few crack lines, indicating low impact strength, can easily be seen.

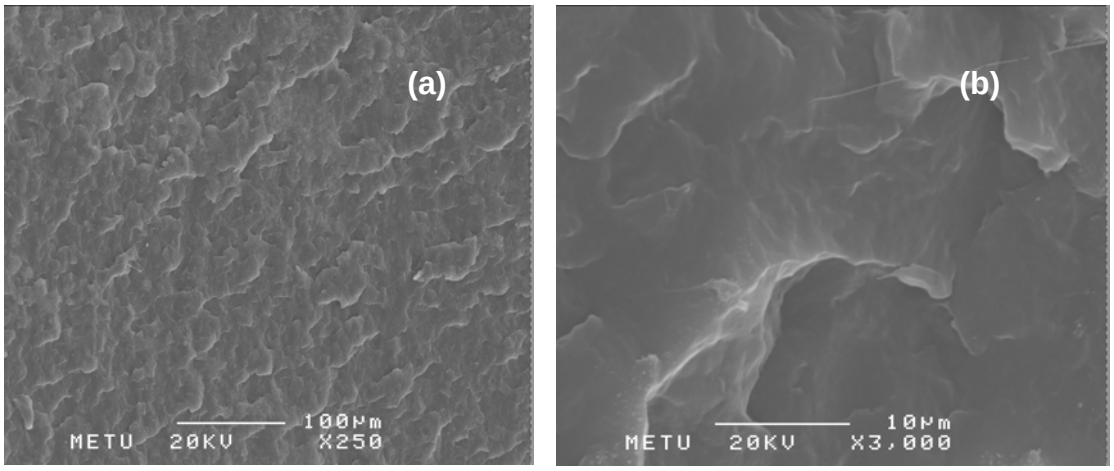

Figure 4.1.7. SEM micrographs of pure Polypropylene (PP) (a) x250 (b) x3000

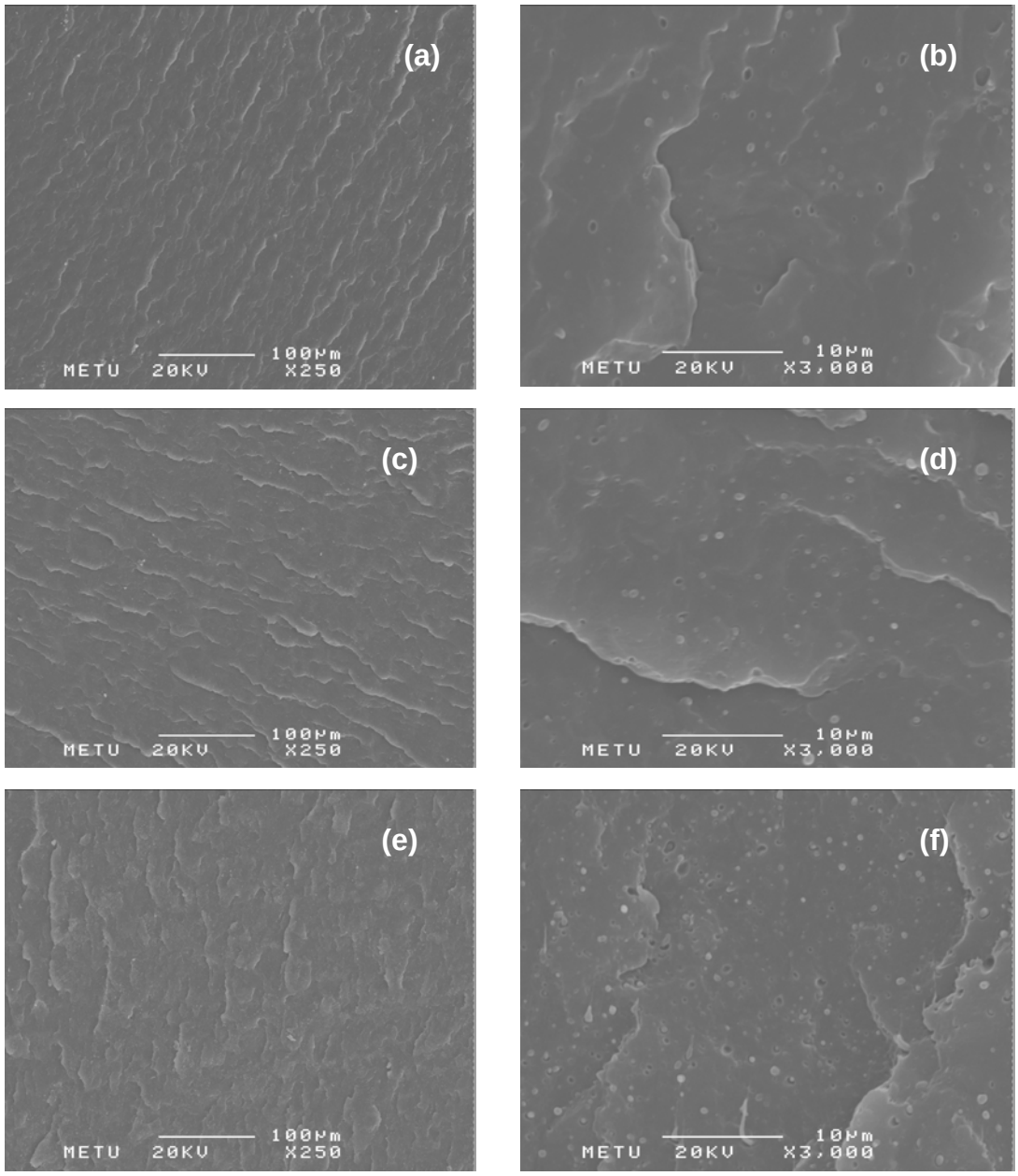

Figure 4.1.8. SEM micrographs of PP/Lotader® 2210 (E-nBA-MAH) blends with following contents of 2210 (a) 5 wt% at x250, (b) 5 wt% at x3000, (c) 10 wt% at x250, (d) 10 wt% at x3000, (e) 15 wt% at x250, (f) 15 wt% at x3000.

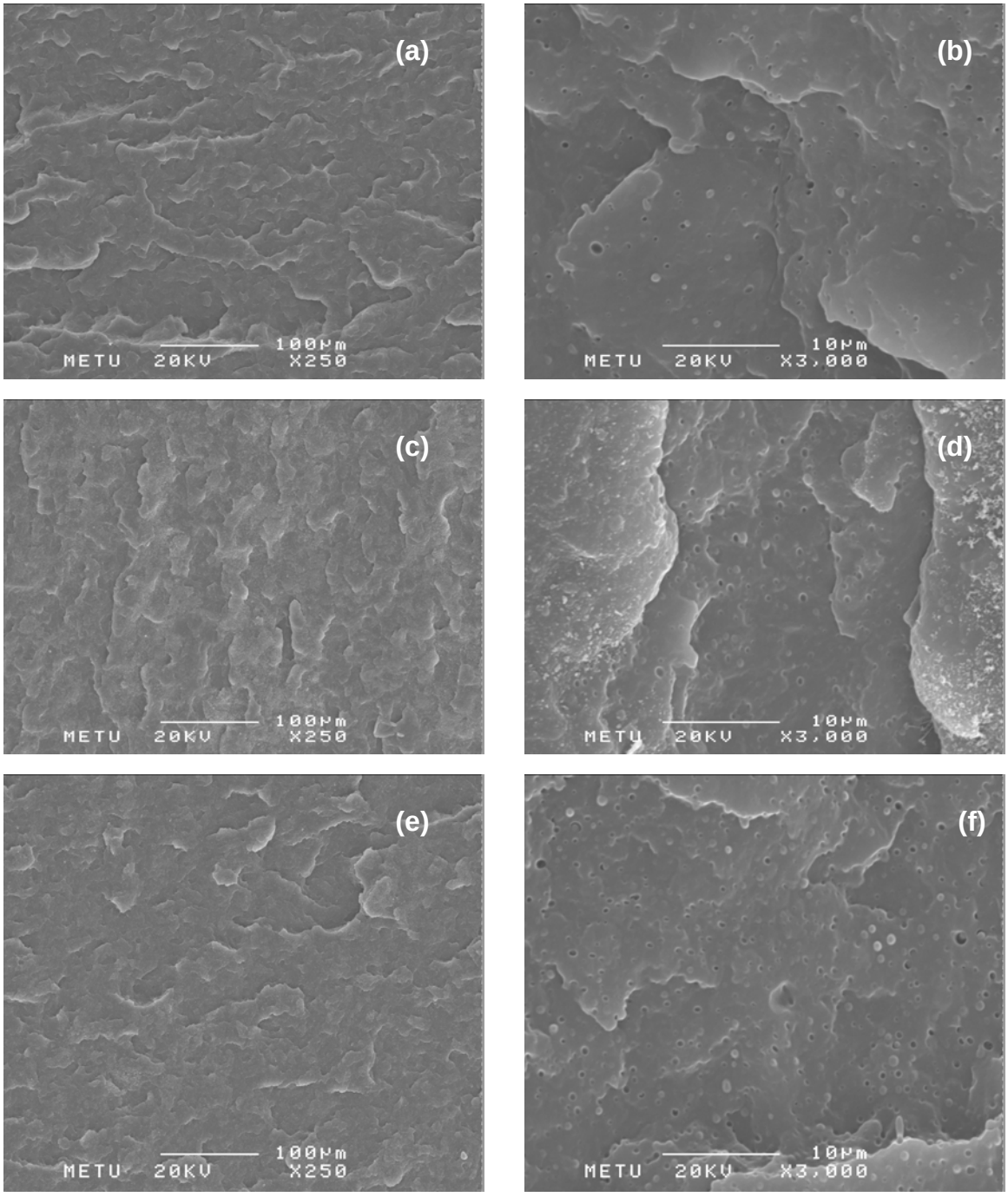

Figure 4.1.9. SEM micrographs of PP/Lotader® 8900 (E-MA-GMA) composites with following content of 8900 (a) 5 wt% at 250, (b) 5 wt% at 3000, (c) 10 wt% at 250, (d) 10 wt% at 3000, (e) 15 wt% at 250, (f) 15 wt% at x3000.

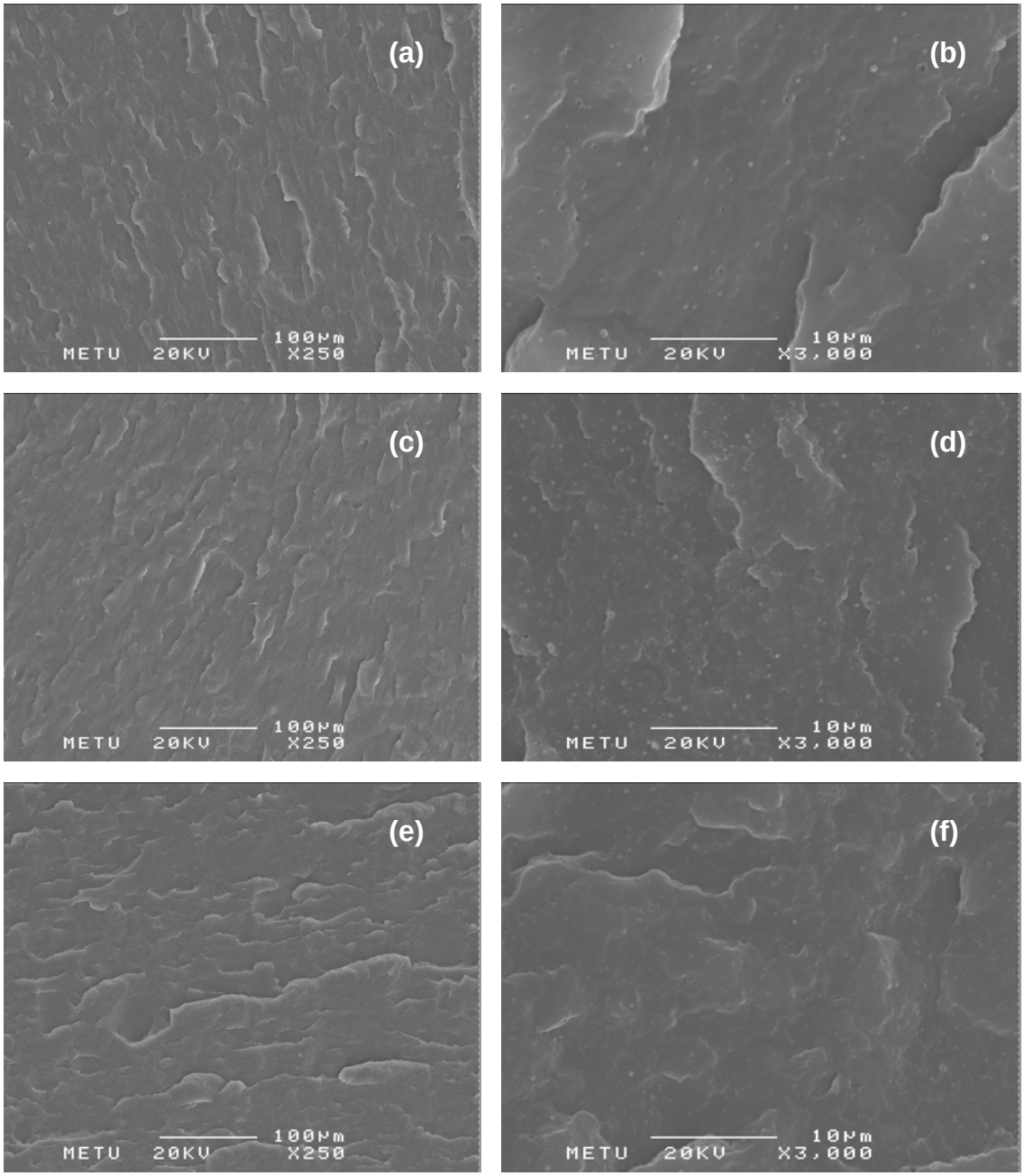

Figure 4.1.10. SEM micrographs of PP/Lotader® 8840 (E-GMA) composites with following content of 8840 (a) 5 wt% at x250, (b) 5 wt% at x3000, (c) 10 wt% at x250, (d) 10 wt% at x3000, (e) 15 wt% at x250, (f) 15 wt% at x3000.

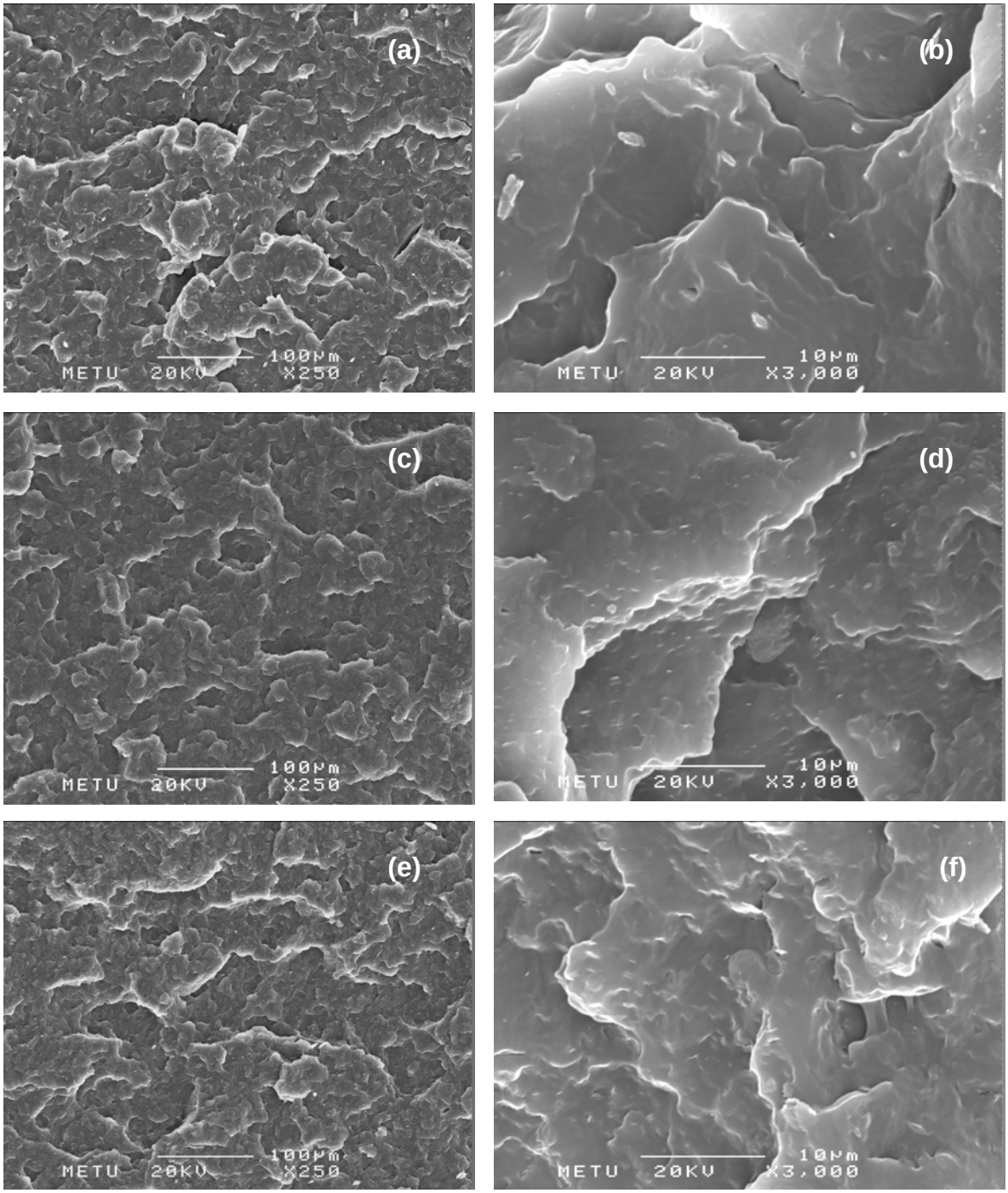

Figure 4.1.11. SEM micrographs of PP/Clay composites containing (a) Cloisite® 30B at x250, (b) Cloisite® 30B at x3000, (c) Cloisite® 15A at x250, (d) Cloisite® 15A at x3000, (e) Cloisite® 25A at x250, (f) Cloisite® 25A at x3000.

Figures 4.1.8-4.1.10 show the micrographs of PP/elastomer blends with concentrations of 5, 10 and 15 wt % elastomer but no organoclay at magnifications of x250 and x3000, respectively. It is clear that the featureless structure of neat PP disappears when melt blended with elastomeric material. There are two phases in the micrograms: particle-in-matrix morphology. Some spherical microvoids , called as domains (caused by the pull-out of elastomeric particles), are seen, and they dispersed throughout the matrix. The factors affecting the dispersion of elastomeric domains in the PP matrix are melt viscosity of the components, shear stresses and rate, the mobility of the interphase, and the surface tension [36]. As expected, when the elastomer concentration increase from 5 wt % to 15 wt %, the number of the domains increase.

In Figure 4.1.9, which shows SEM micrographs of PP/Lotader® 8900 (E-MA-GMA) blend, the micrograph containing 5 wt % elastomers is smoother than those of the blends containing 10 and 15 wt%. Also, the dispersion of the elastomer domains are more homogeneous in the blends containing 5 wt % of elastomer indicating higher compatibility at this concentration. This may enhance the mechanical properties. In addition, the blends containing Lotader® 8900 (E-MA-GMA) have well dispersed domains in comparison to the blends containing Lotader® 2210 (E-nBA-MAH) and Lotader® 8840 (E-GMA) for all compositions. This may indicate that Lotader® 8900 (E-MA-GMA) is more compatible with PP matrix than the others.

Figure 4.1.11 shows the micrographs of samples containing 2 wt % organoclays Cloisite® 30B, 15A and 25A, but no elastomer. It is observed that crack lines go through the surface structure and the particles of clay are dispersed in PP matrix. Surface roughness indicates that cracks progressed along a more

tortuous path. This increases the fracture surface area and the toughness, tensile strength and modulus with respect to neat PP.

SEM observation showed that the clays were dispersed into the PP matrix in the form of large and small aggregates. It is very difficult to estimate the size of aggregates owing to their non-isometric sizes and dispersion in the matrix randomly. The size of these aggregates strongly depend on the orientation of the particles. However, the fracture mode of samples and the dispersion quality of clays, such as aggregate concentration can be observed [62].

There are relatively large clay agglomerates in the continuous PP matrix in PP/Cloisite® 30B composites when compared with the composites of PP/Cloisite® 15A and PP/Cloisite® 25A as shown in Figure 4.1.11. These would be poor interfacial bonding between the matrix and Cloisite® 30B, since polar Cloisite® 30B is the least compatible with PP as analyzed also with XRD. However, in PP/Cloisite® 15A and PP/Cloisite® 25A composites, the size of nanoclay aggregates is reduced significantly. This means that the dispersion of these organoclays is improved [62]. This observation is also supported by tensile tests, analyzed later. The tensile strength and elongation at break values of PP/Cloisite® 15A and PP/Cloisite® 25A composites are higher than PP/Cloisite® 30B composite.

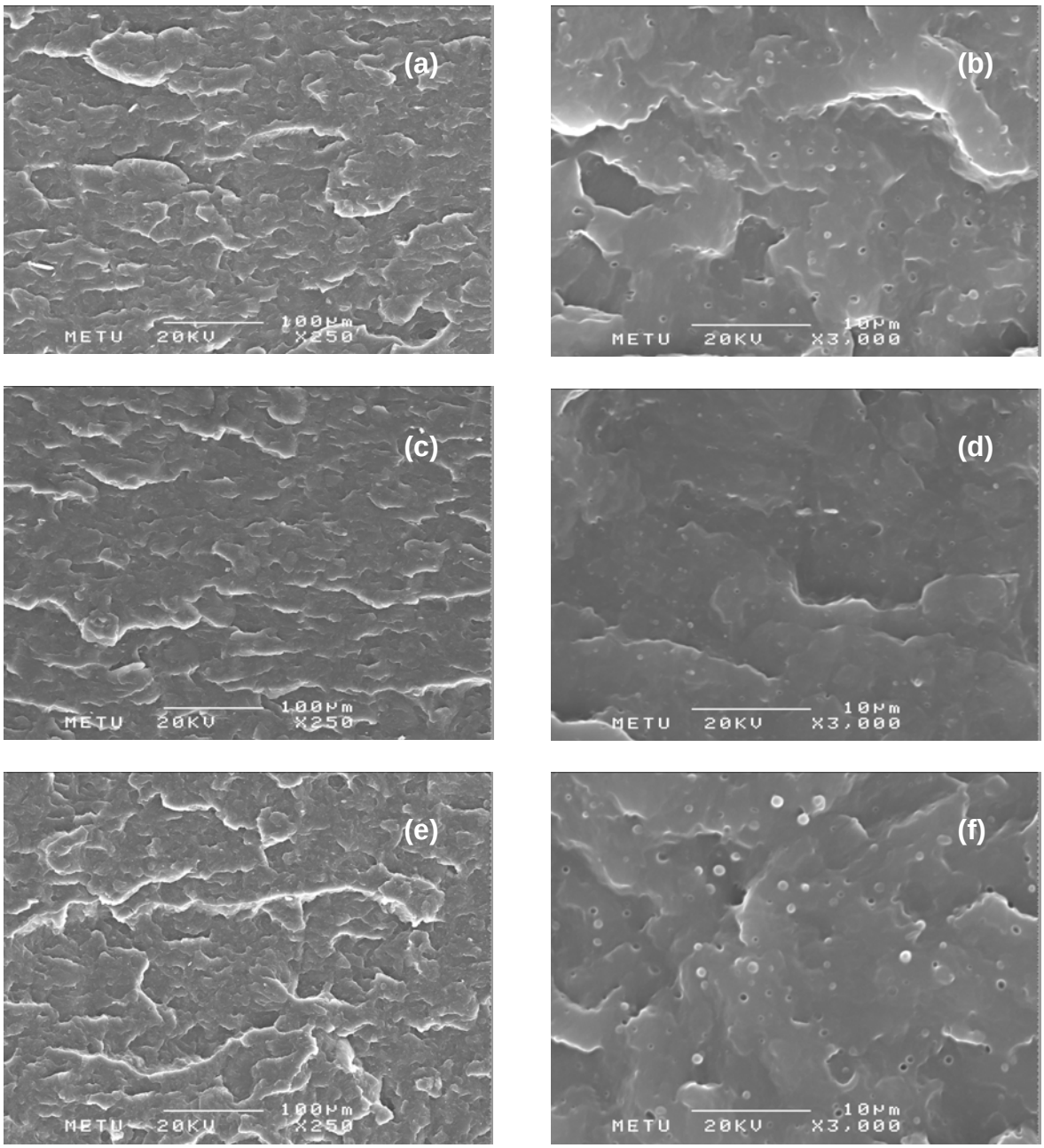

Figure 4.1.12. SEM micrographs of ternary nanocomposites of PP/2 wt% Cloisite® 30B/5 wt% compatibilizer (a) Lotader® 2210 at x 250, (b) Lotader® 2210 at x3000, (c) Lotader® 8900 at x250, (d)Lotader® 8900 at x3000, (e) Lotader® 8840 at x250 (f) Lotader® 8840 at x3000.

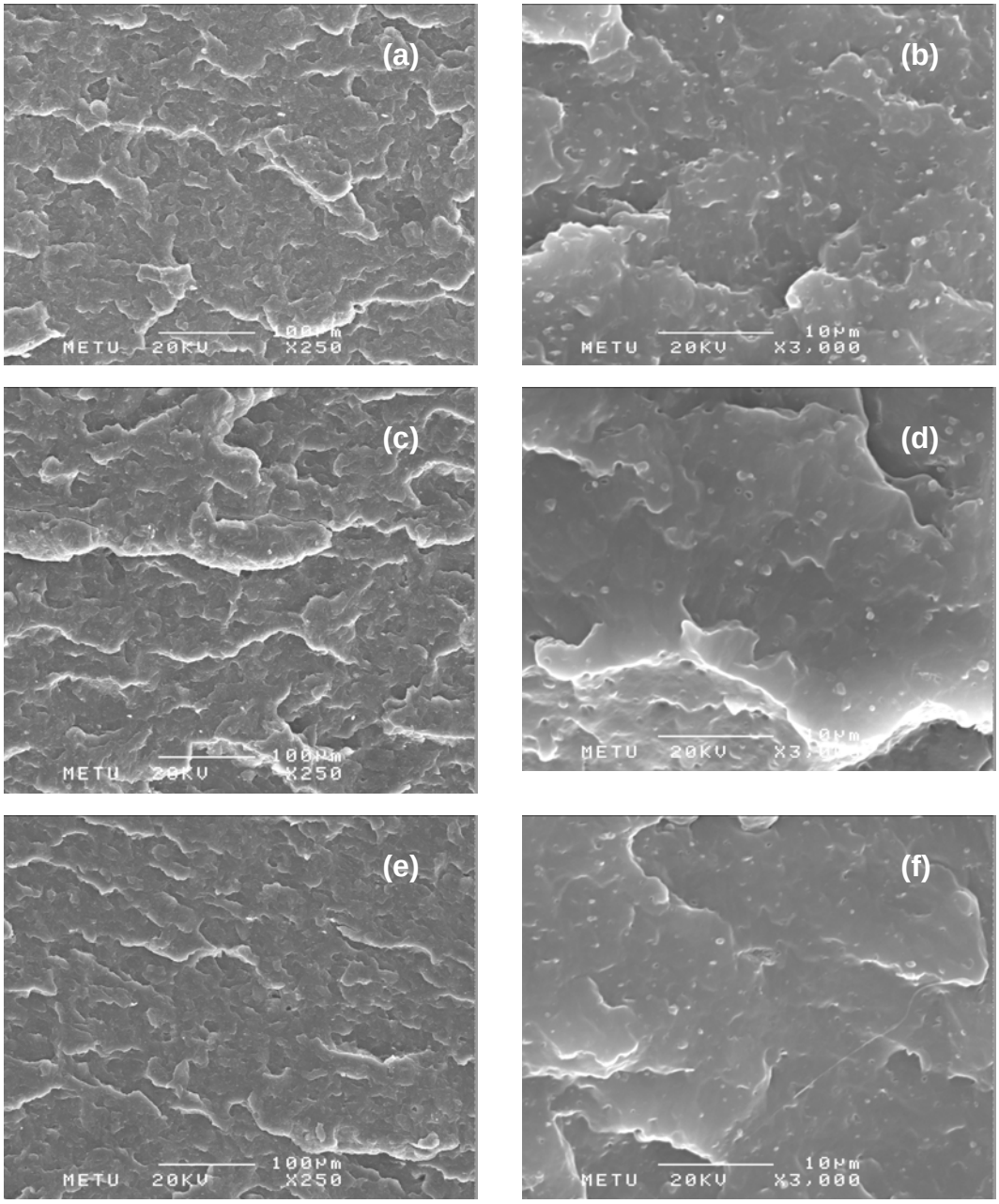

Figure 4.1.13. SEM micrographs of ternary nanocomposites of PP/2 wt% Cloisite® 15A/5 wt% compatibilizer (a) Lotader® 2210 at x250, (b) Lotader® 2210 at x3000, (c) Lotader® 8900 at x250, (d) Lotader® 8900 at x3000, (e) Lotader® 8840 at x250, (f) Lotader® 8840 at x3000.

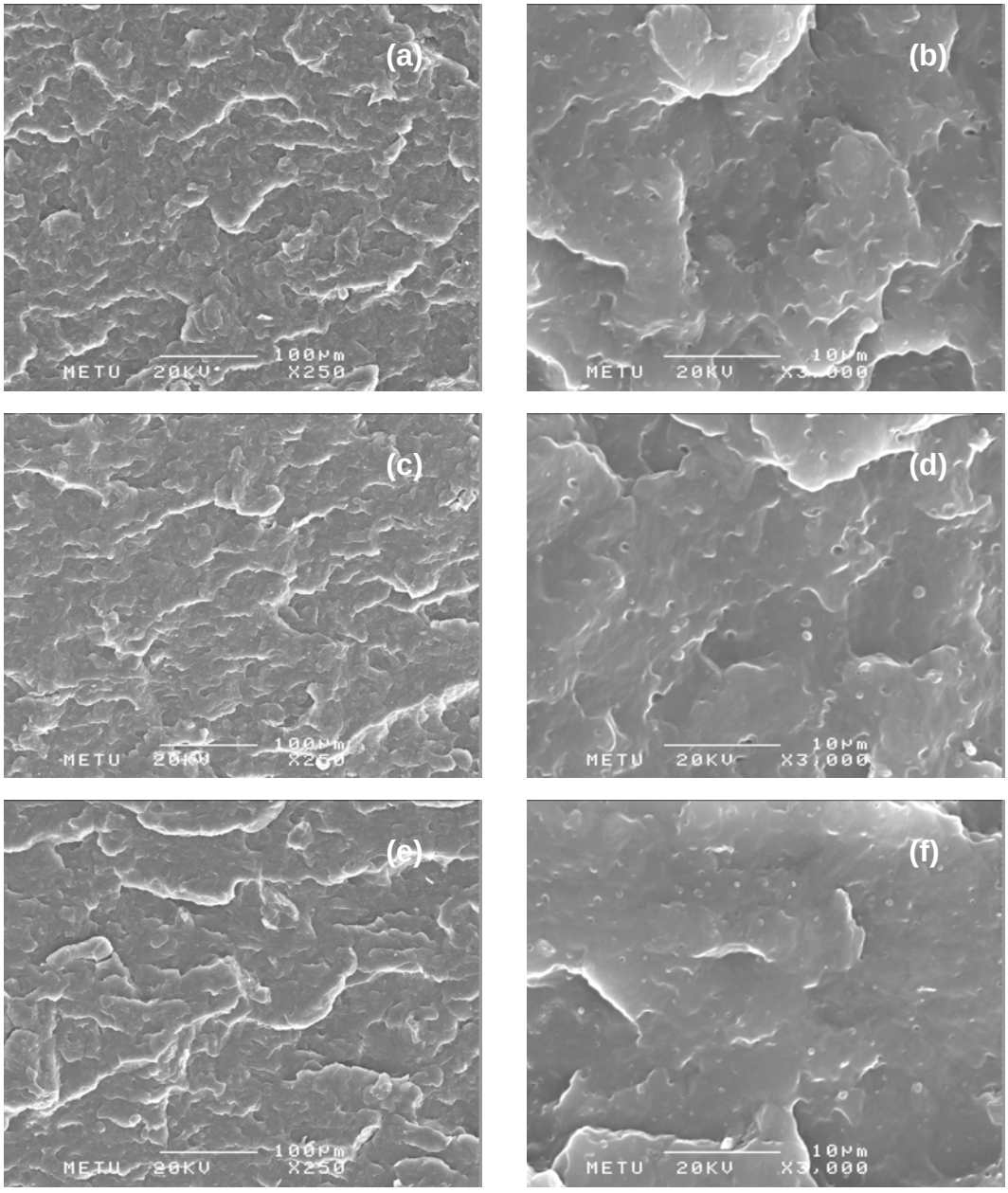

Figure 4.1.14. SEM micrographs of ternary nanocomposites of PP/2 wt% Cloisite® 25A/5 wt% compatibilizer (a) Lotader® 2210 at x250, (b) Lotader® 2210 at x3000, (c) Lotader® 8900 at x250, (d) Lotader® 8900 at x3000, (e) Lotader® 8840 at x250, (f) Lotader® 8840 at x3000.

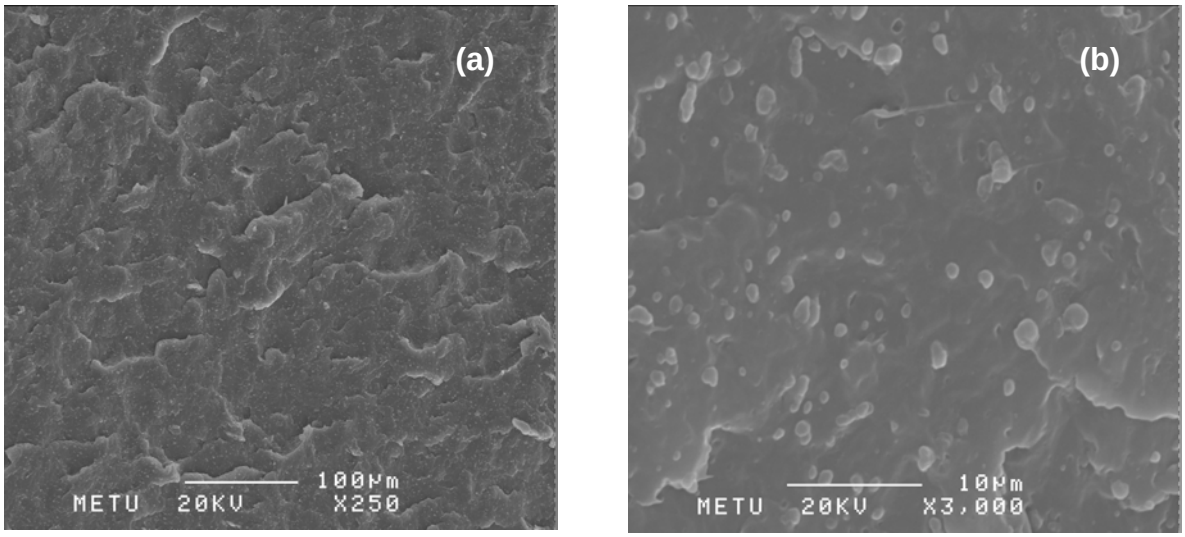

Figure 4.1.15. SEM micrograph of Mixing sequence of (PP+8900)+15A or (PE)C1 (a) x250, (b) x3000.

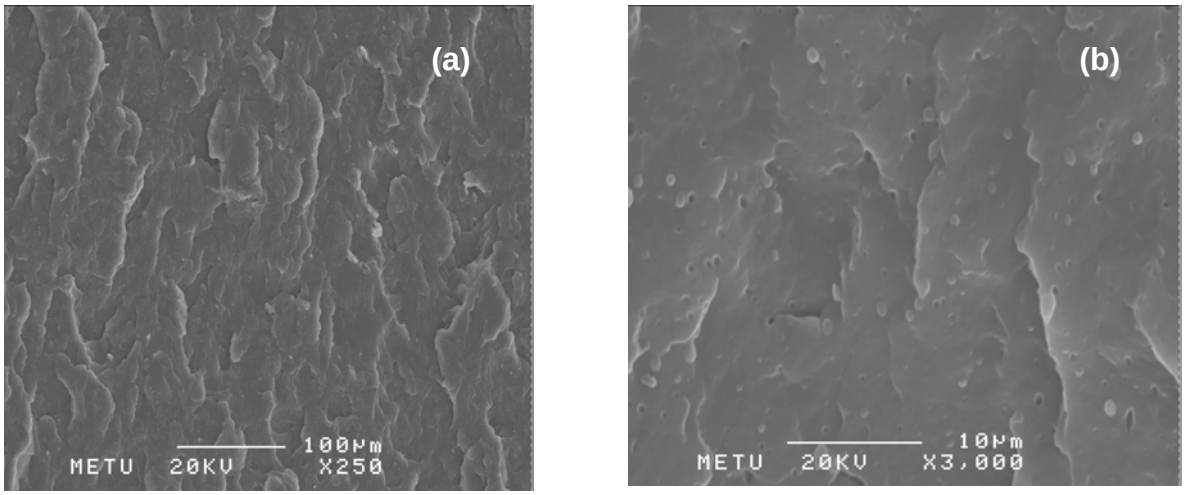

Figure 4.1.16. SEM micrograph of Mixing sequence of (PP+8900)+25A or (PE)C2 (a) x250, (b) x3000.

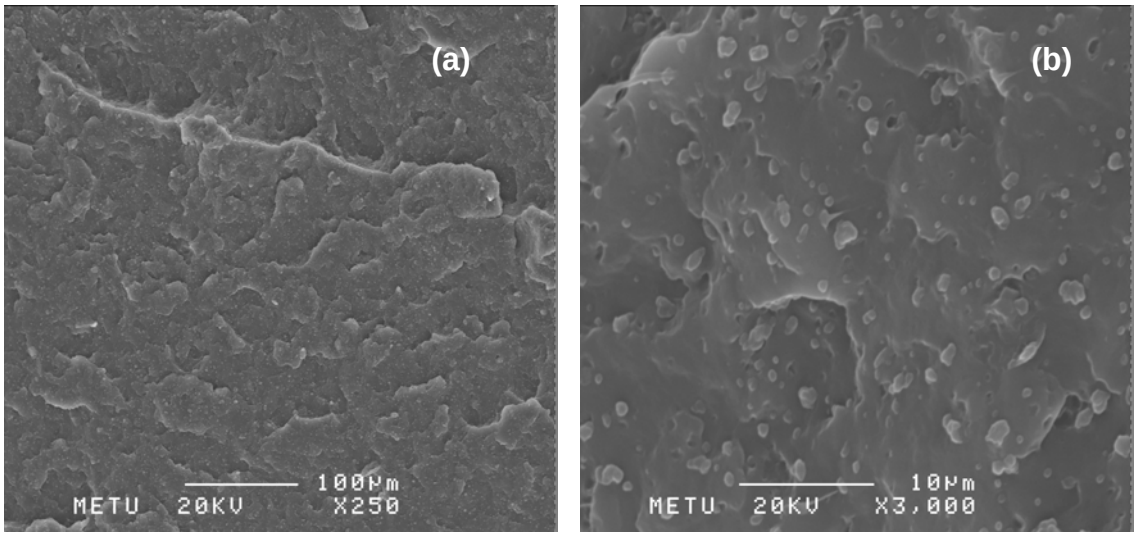

Figure 4.1.17. SEM micrograph of Mixing sequence of (15A+8900)+PP or (C1E)P (a) x250, (b) x3000.

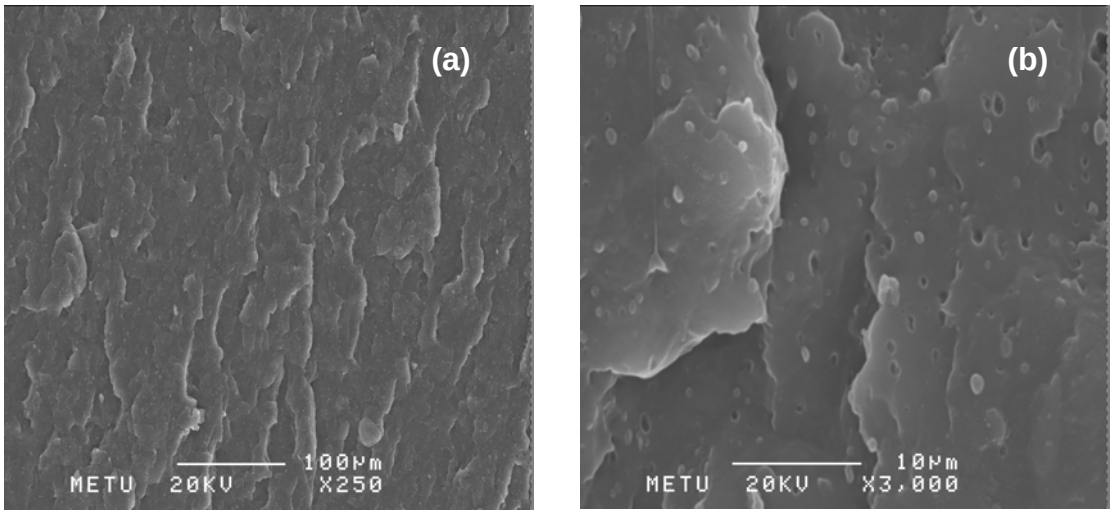

Figure 4.1.18. SEM micrograph of Mixing sequence of (25A+8900)+PP or (C2E)P (a) x250, (b) x3000.

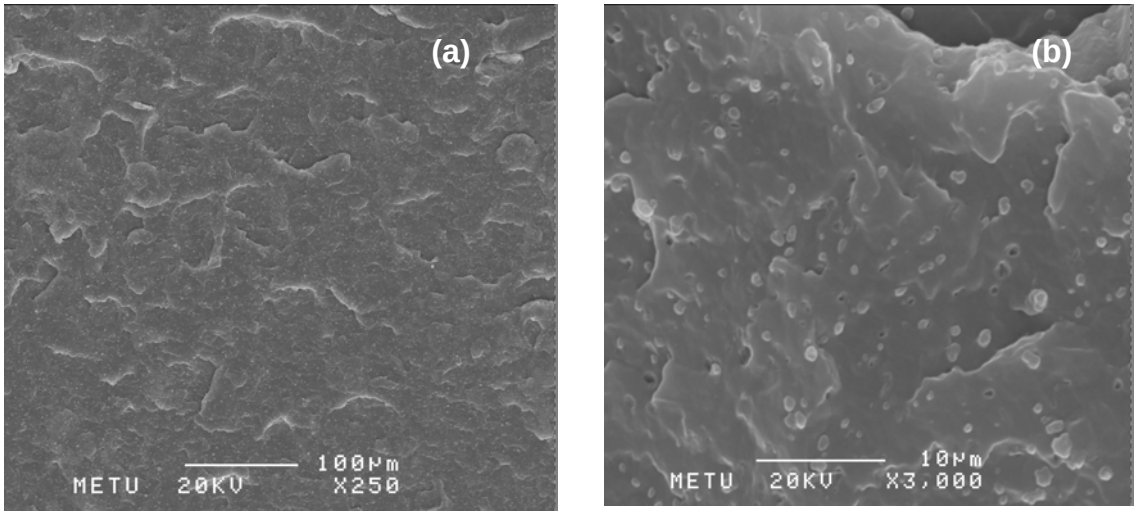

Figure 4.1.19. SEM micrograph of Mixing sequence of (PP+15A)+8900 or (PC1)E (a) x250, (b) x3000.

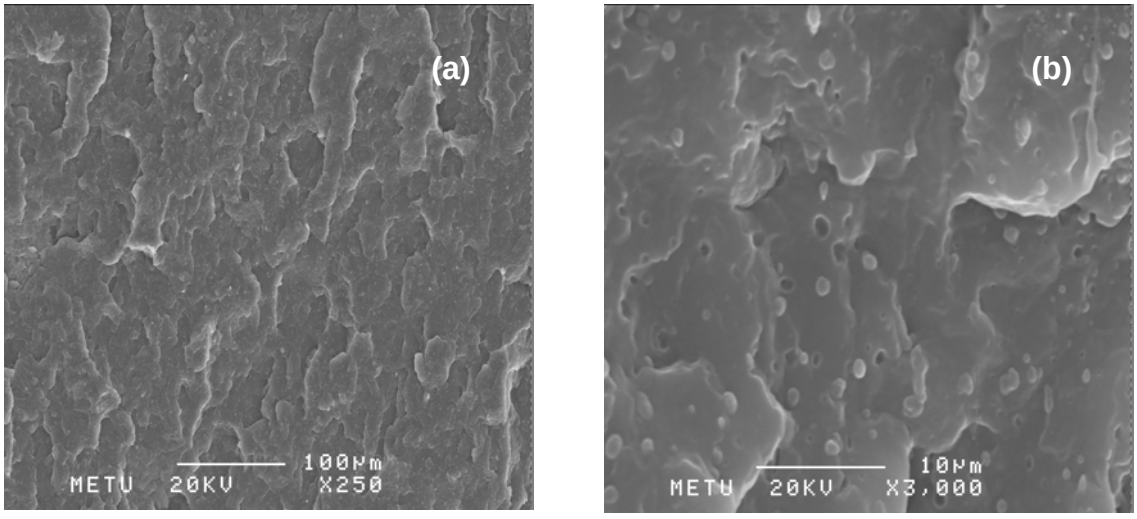

Figure 4.1.20. SEM micrograph of Mixing sequence of (PP+25A)+8900 or (PC2)E (a) x250, (b) x3000.

Figure 4.1.12, 4.1.13 and 4.1.14 are SEM micrographs of the fractured surfaces of ternary PP/organoclay/compatibilizer nanocomposites containing 2 weight percent organoclay and 5 weight percent compatibilizer prepared by feeding all materials to the extruder simultaneously in the first run.

Figures 4.1.12 (a) and (b) are the micrographs of PP/Cloisite® 30B/Lotader 2210 (E-nBA-MAH) nanocomposites at magnifications of x250 and x3000, respectively. Figures 4.1.12 (c) and (d) are the micrographs of PP/Cloisite® 30B/Lotader® AX8900 (E-MA-GMA) nanocomposites at magnifications of x250 and x3000, respectively. Elastomer domains and crack propagation lines can be observed in the fractured surface.

SEM micrographs of fractured surface of ternary compositions of PP/Cloisite® 30B/Lotader® AX8840 (E-GMA) are shown in Figures 4.1.12. (e) and (f). Agglomerates of clay particles are present on the surfaces while elastomer domains get smaller in this case. This agglomeration of clay particles would decrease the mechanical properties.

Figure 4.1.13 and 4.1.14 show the SEM micrographs of ternary nanocomposites of PP/Cloisite® 15A/compatibilizers and PP/Cloisite® 25A/compatibilizers, respectively. The micrographs at magnifications of x250 do not exhibit significant differences for all compositions. However, when the micrographs at magnifications of x3000 are examined, ternary nanocomposites that have Lotader® 2210 and Lotader® 8900 as compatibilizers have larger domain sizes.

Figures 4.1.15 through 4.1.20 show the SEM micrographs of ternary nanocomposites prepared by different mixing orders. The fractured surfaces at magnifications of x250, do not obvious differences in the structures. In the

mixing sequences of (PP+8900)+15A i.e. (PE)C1 and (PP+8900)+25A i.e. (PE)C2 elastomer domains cannot observed at magnifications of x3000, and there are clay agglomerates in the structures. However, in the mixing sequence of (15A+8900)+PP i.e. (C1E)P, (25A+8900)+PP i.e. (C2E)P, (PP+15A)+8900 i.e. (PC1)E and (PP+25A)+8900 i.e. (PC2)E both the elastomer domains and clay particulates can be observed.

4.1.3 TEM Analysis

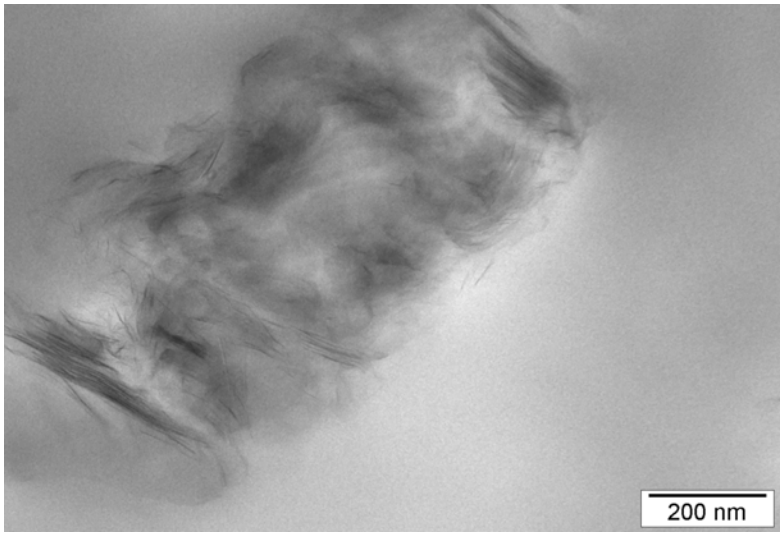

Figure 4.1.21. TEM micrograph of PP/2 wt% Cloisite® 25A/5 wt%Lotader® 8900 E-MA-GMA nanocomposite processed by (PEC2) mixing sequence.

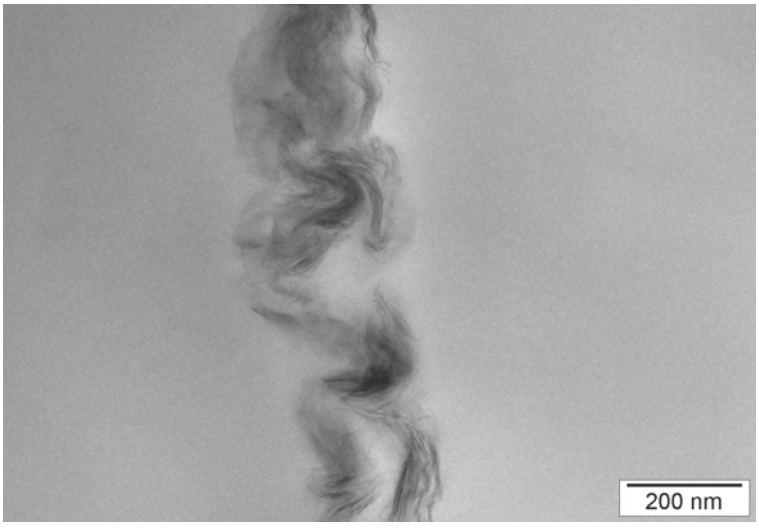

Figure 4.1.22. TEM micrograph of PP/2 wt% Cloisite® 25A/5 wt% Lotader® 8900 E-MA-GMA nanocomposite processed by (PE)C2 mixing sequence.

TEM analysis were performed for two ternary nanocomposites of PP/Cloisite® 25A/Lotader® 8900 (E-MA-GMA) processed by different mixing sequences.

Figure 4.1.21 shows the TEM micrograph of PP/Cloisite® 25A/Lotader® 8900 (E-MA-GMA) ternary nanocomposites processed by (PEC2) mixing sequences. The dark lines represent the clay layers whose average thicknesses are just a few nanometers. This mixing sequence, in which PP, elastomer and organoclay are fed to the system simultaneously, has an intercalated structure according to Figure 4.1.21. The XRD results show that characteristic clay diffraction peak for Cloisite® 25A is shifted to lower 2θ angles indicating intercalation and the increase in the d-spacing is the highest for this ternary nanocomposite. According to the tensile test, analyzed later, (PEC2) ternary nanocomposite also gives the highest Young's modulus due to the three-way interaction.

Figure 4.1.22 shows the TEM micrographs of PP/Cloisite® 25A/Lotader® 8900 (E-MA-GMA) ternary nanocomposite processed by (PE)C2 mixing sequences in which PP and elastomer are mixed prior to organoclay. In this micrograph there are individual clay layers which indicate an intercalated structure. Similar information is also obtained from the XRD result. On the other hand, the dark areas indicate that the clay platelets are poorly dispersed as aggregates in the continuous PP phase. According to the tensile test, the mixing order (PE)C2 gives the lowest Young's modulus. Mixing organoclay with polypropylene or elastomer in the second extrusion run, only once, may hinder its dispersion in the PP matrix.

4.2. Thermal Analysis

4.2.1. Differential Scanning Analysis (DSC)

Crystallization behavior of neat PP, PP/elastomer blends, PP/organoclay nanocomposites and PP/organoclay/elastomer nanocomposites are obtained from DSC experiments. The values of melting and crystallization temperature; heat of fusion and crystallinity of samples that are obtained in this study are shown in Table 4.2.1 for blends of PP and elastomers and in Table 2.2.2 for the nanocomposites. The percent crystallinity of the polypropylene phase is calculated as the ratio of the heat of fusion of the sample (ΔH_f), divided by the weight fraction of polypropylene in the nanocomposite and the heat of fusion of the pure crystalline form of polypropylene (ΔH_f^o). The ΔH_f^o value for polypropylene matrix is taken as 209 J/g [38]. DSC thermograms of all samples are given in Appendix A, from A.1 through A.29.

Since the glass transition temperature of PP are below the room temperature, Tg is not detected with analysis of DSC. According to the data sheets, the melting points of elastomers E-nBA-MAH, E-MA-GMA and E-GMA are given as 107°C, 60°C and 105°C. respectively.

All materials exhibited a single melting endotherm and approximately constant melting temperature (≈165°C). When a compatibilizer is added to the nanocomposites, the crystallization behavior tends to be similar to that of neat PP, except for addition 5 wt% 2210 into PP or mixture of PP+25A. In the nanocomposite of PP+25A+2210 which is produced by the sequence of (PEC2);

the nucleating effect of compatibilizer Lotader® 2210 (E-nBA-MAH) can be observed. PP+2210 also exhibits a higher crystallinity in comparison to other materials. Thus, elastomer 2210 (E-nBA-MAH) act as nucleating agent at low contents, but decreases crystallinity at high contents.

The presence of clay shown in Table 4.2.2 did not seem to influence the crystallinity significantly. This may be the result of well-dispersed clay in the polymer matrix [38]. The clay content is 2 wt% and the elastomer content is 5 wt% in Table 4.2.2.

Table 4.2.1 Melting temperatures and % crystallinities in PP/elastomer polymer blends

Sample	Tm (°C)	PP wt%	ΔH(j/g)	Xc (%)
PP	165.8	100	76.13	36.43
PP+5% 2210 (E-nBA-MAH)	165.2	95	83.14	41.87
PP+10%2210(E-nBA-MAH)	165.8	90	70.27	37.36
PP+15%2210(E-nBA-MAH)	165.3	85	52.57	29.59
PP+5%8900(E-MA-GMA)	165.9	95	66.20	33.34
PP+10%8900(E-MA-GMA)	165.4	90	78.93	41.96
PP+15%8900(E-MA-GMA)	165.4	85	61.75	34.76
PP+5%8840(E-GMA)	165.6	95	69.05	34.78
PP+10%8840(E-GMA	165.0	90	66.09	35.14
PP+15%8840(E-GMA)	165.4	85	64.05	36.05

Nanocomposites prepared by different mixing orders also do not exhibit significant differences in T_m and crystallinity.

Table 4.2.2. The results of DSC analysis

Sample	Tc (°C)	PP wt%	Tm (°C)	ΔH (j/g)	Xc (%)
PP	156.0	100	165.8	76.1	36.4
PP+2210	156.0	95	165.2	83.1	41.9
PP+8900	156.2	95	165.9	66.2	33.3
PP+8840	154.7	95	165.6	69.1	34.8
PP+30B	156.1	98	166.0	72.1	35.2
PP+30B+2210	154.6	93	164.7	68.0	35.0
PP+30B+8900	155.0	93	165.0	70.2	36.1
PP+30B+8840	154.0	93	164.6	65.3	33.6
PP+15A	154.7	98	165.1	71.2	34.8
PP+15A+2210	154.2	93	165.3	65.5	33.7
PP+15A+8900	154.9	93	164.5	66.5	34.2
PP+15A+8840	154.4	93	164.9	63.4	32.6
PP+25A	155.0	98	165.4	70.2	34.3
PP+25A+2210	154.8	93	165.0	86.2	44.4
PP+25A+8900	153.9	93	164.8	67.7	34.8
PP+25A+8840	154.5	93	165.2	70.3	36.2
(PE)C1	155.4	93	165.9	69.4	35.7
(PE)C2	155.5	93	165.9	67.3	34.6
(C1E)P	155.5	93	165.3	68.8	35.4
(C2E)P	157.7	93	167.2	69.8	35.9
(PC1)E	154.9	93	165.6	70.2	36.1
(PC2)E	154.9	93	165.8	71.5	36.8

4.3. Flow Characteristics

Melt flow index (MFI) is a measure of flow which is inversely related to melt viscosity. Melt viscosity can be defined as a measure of tendency of melted materials to flow [16]. In this study, MFI measurements were carried out under a specified load of 2.16 kg and specified temperature of 230°C in order to understand the flow behavior of the samples and make comments about melt viscosities.

Table 4.3.1, shows the MFI values of materials used in this study. When pure PP is extruded twice, the value of MFI increase owing to decrease of viscosity and thermomechanical degradation of PP.

Table 4.3.1. MFI values of pure materials

Material	**MFI (g/10 min)**
PP (not extruded)	4.00
Pure PP (twice extruded)	4.96
Lotader® 2210 (E-nBA-MAH)	17.01
Lotader® 8900 (E-MA-GMA)	15.62
Lotader® 8840 (E-GMA)	14.21

Since the MFI values of compatibilizers are much higher than the MFI value of pure PP, the MFI values of the blends increases with addition of compatibilizers. As it is shown in Table 4.3.2. , the MFI increases with increasing concentration of the elastomers that decreases the viscosity in the structure.

In Table 4.3.3, the MFI values of PP/organoclay composites can be seen. When organoclay is added into the system the viscosity of the polymer melt increases (MFI decreases) due to the dispersion of clay layers.

Table 4.3.2. MFI values of PP and elastomer blends

Sample	PP (wt %)	MFI (g/10min)
PP	100	4.95
PP+2210	95	5.28
PP+2210	90	4.98
PP+2210	85	5.98
PP+8900	95	5.42
PP+8900	90	5.73
PP+8900	85	6.73
PP+8840	95	5.19
PP+8840	90	5.71
PP+8840	85	6.23

Table 4.3.3. MFI values of PP and organoclay values

Sample	Organoclay wt %	MFI g/10min
PP	0	4.95
PP+30B	2	4.24
PP+15A	2	4.68
PP+25A	2	4.31

Table 4.3.4. shows the MFI values of ternary nanocomposites. In general, the MFI values of ternary nanocomposites are lower than the MFI value of pure PP which means higher melt viscosity. This shows that the effect of organoclay is more dominant than the effect of compatibilizer except for the ternary nanocomposites with Lotader® 2210 (E-nBA-MAH) with organoclays 15A and 25A. The elastomer Lotader® 2210 has much higher MFI value than other elastomers, thus the MFI of the ternary nanocomposites with these materials are higher in comparison to other ternary nanocomposites.

Table 4.3.4. MFI values of ternary PP/compatibilizer/organoclay nanocomposites

Sample	**Compatibilizer (wt %)**	**Organoclay (wt %)**	**MFI (g/10min)**
PP	0	0	4.95
30B+2210	5	2	4.86
30B+8900	5	2	4.93
30B+8840	5	2	4.75
15A+2210	5	2	5.17
15A+8900	5	2	4.38
15A+8840	5	2	4.50
25A+2210	5	2	5.52
25A+8900	5	2	4.80
25A+8840	5	2	4.83

These results indicate better dispersion of organoclays in the presence of compatibilizers Lotader® AX8900 and Lotader® AX8840 as also supported by XRD results.

Table 4.3.5. MFI values of ternary PP/compatibilizer nanocomposites produced by different mixing orders

Sample	Organoclay (wt %)	Compatibilizer (wt %)	MFI (g/10min)
(PEC1)*	2	5	4.38
(PE)C1	2	5	4.83
(C1E)P	2	5	4.95
(PC1)E	2	5	4.69
(PEC2)**	2	5	4.80
(PE)C2	2	5	5.04
(C2E)P	2	5	5.35
(PC2)E	2	5	5.08

* the letters P, E and C1 represent polypropylene, Lotader® AX8900 and Cloisite® 15A, respectively.

** the letter C2 represents Cloisite® 25A.

Table 4.3.5 shows that the effect of changing the mixing order on MFI is not significant.

4.4. Mechanical Analysis

Tensile tests, flexural tests and notched Charpy impact tests were carried out in order to analyze the mechanical properties of injection molded specimens. The effect of compatibilizer type, organoclay type and mixing order of materials on the mechanical properties are investigated in this section.

4.4.1. Tensile Properties

The tensile strength, tensile modulus and tensile strain at break values were determined from the tensile tests. The values of tensile strength and tensile strain at break were read directly from the stress-strain curves, whereas the values of Young's modulus (tensile modulus) were calculated as the slope of stress-strain plots.

Polypropylene shows ductile behavior which means that the stress achieves a maximum called a yield stress at a specific strain. After yielding, PP chains are stretched in direction of load that is called orientation hardening. The values of tensile strength, tensile modulus and tensile strain at break of neat twice extruded PP were determined as 51 MPa, 711 MPa and 289 %, respectively. High value of percentage strain at break shows the effect of orientation hardening behavior.

Tensile properties such as tensile strength, tensile modulus and tensile strain at break of all binary and ternary mixtures produced in this study are shown in Figures 4.4.1 through 4.4.21. The numerical results are given in Appendix B.

At the beginning of the study, the blends of PP/compatibilizer were produced with different compositions of 5, 10 and 15% in order to decide the best composition of compatibilizer during production of nanocomposites. Figures 4.4.1-4.4.3 show the effects of E-BA-MAH elastomer content on tensile properties.

The tensile strength values first increases, but then decreases with the elastomer content owing to the dilution effect of elastomer.

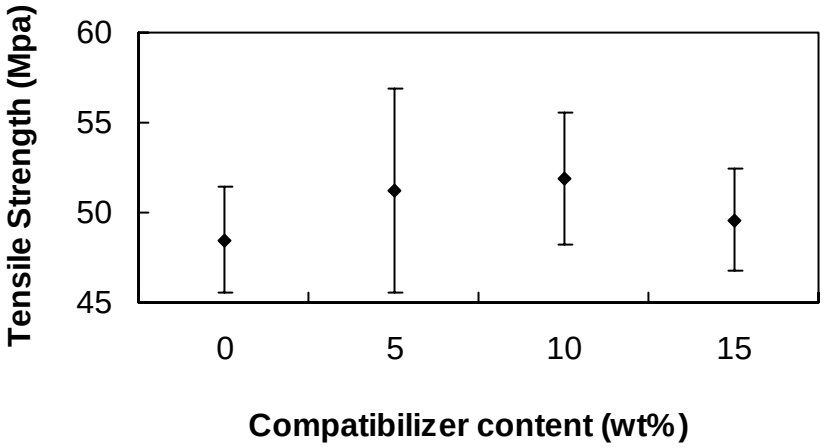

Figure 4.4.1. Effect of compatibilizer content on tensile strength of PP/Lotader® 2210 (E-nBA-MAH) blend.

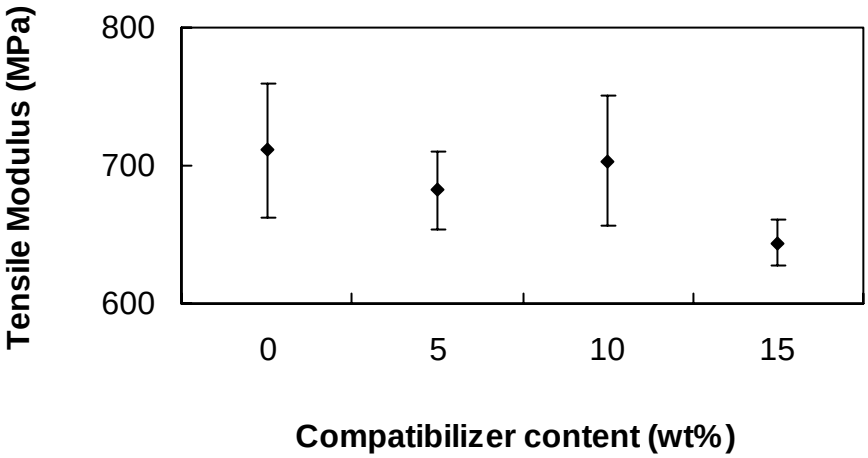

Figure 4.4.2. Effect of compatibilizer content on tensile modulus of PP/Lotader® 2210 (E-nBA-MAH) blend.

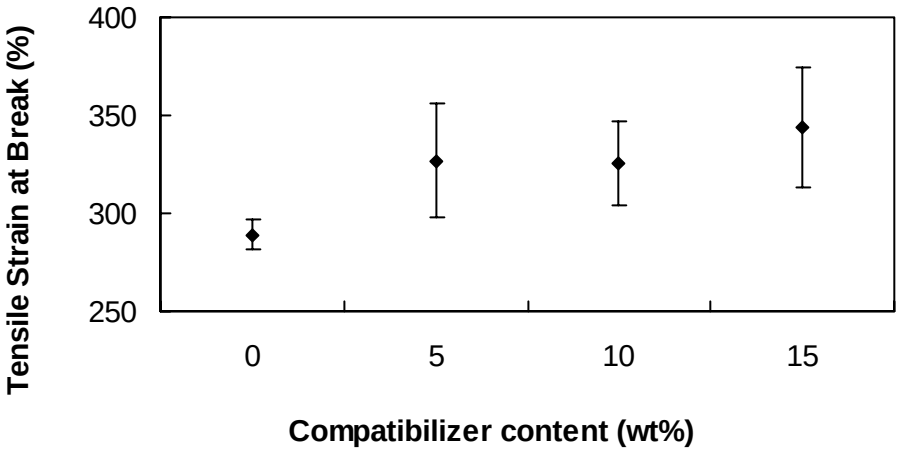

Figure 4.4.3. Effect of compatibilizer content on tensile strain at break of PP/Lotader® 2210 (E-nBA-MAH) blend.

According to DSC data in Table 4.2.1 it is observed that in general % crystallinity decreased with the increase in elastomer content. In PP/E-nBA-MAH blend containing 5 wt %, crystallinity increase with respect to neat PP. This brings increase in tensile strength. When elastomer content increases further, decrease in crystallinity is observed in Table 4.2.1. A decrease in crystallinity brings about decrease in tensile strength and in modulus, however, it increases elongation at break.

Experimental results indicate that in the PP/E-BA-MAH blends, Young's Modulus values are very close to each other in 5 wt % and 10 wt % elastomer containing samples. However, modulus decreases for 15 wt % elastomer containing blend.

It is obvious that % elongation at break increases in the presence of elastomer. Increase in elongation is due to the elastomeric character of the compatibilizers.

The dispersed rubber domains act as stress concentrators during extension process. In this stress state, yielding or crazing occurs all around the rubbery domains, as a result, polymer absorbs high amount of energy and may elongate to a greater extent avoiding a highly localized strain process [39].

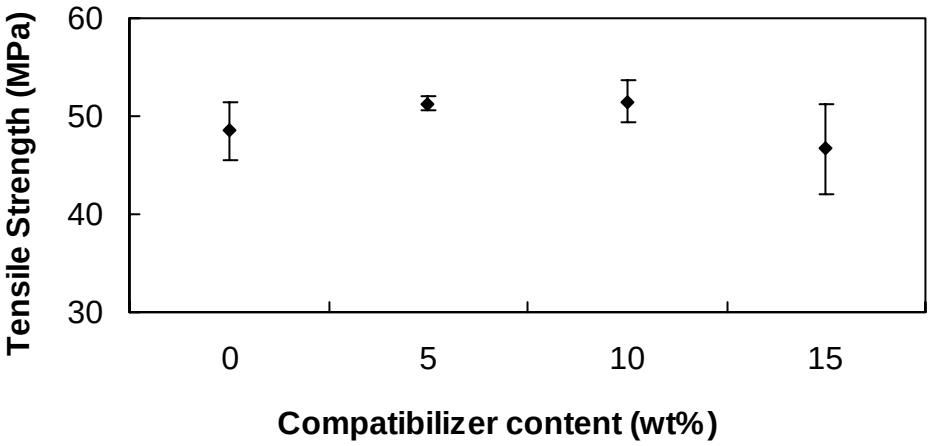

Figure 4.4.4. Effect of compatibilizer content on tensile strength of PP/Lotader® AX8900 (E-MA-GMA) blend.

Figures 4.4.4-4.4.6 show the effects of E-MA-GMA elastomer content on tensile properties. The tensile strength and modulus values first increase, but then decrease with the elastomer content due to the dilution effect of elastomer E-MA-GMA. Decrease in tensile strength and modulus in PP/E-MA-GMA blend containing 15 wt % can be attributed to decrease in crystallinity in this blend.

The decrease in elongation at break for the blend containing 15 wt % elastomer may be attributed to the hindrance of free elastomer particles to cold drawing of the matrix, which may lead to an unstable flow that causes early rupture of the sample [40].

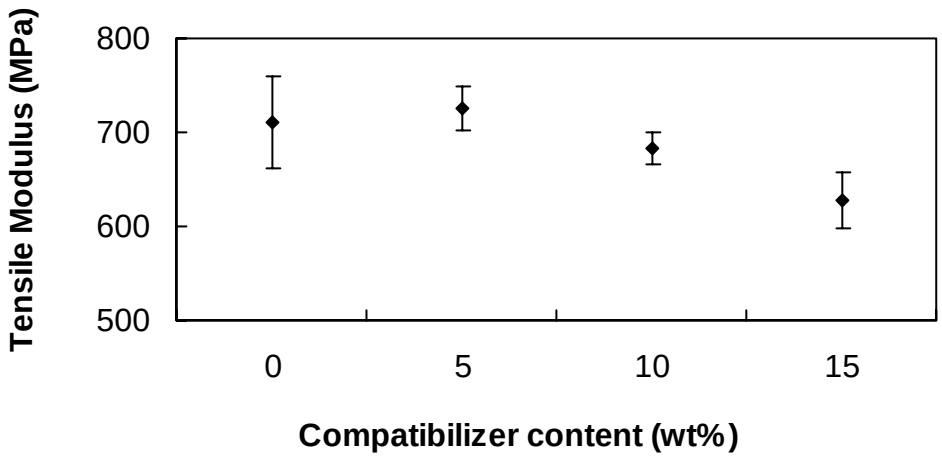

Figure 4.4.5. Effect of compatibilizer content on tensile modulus of PP/Lotader® AX8900 (E-MA-GMA) blend.

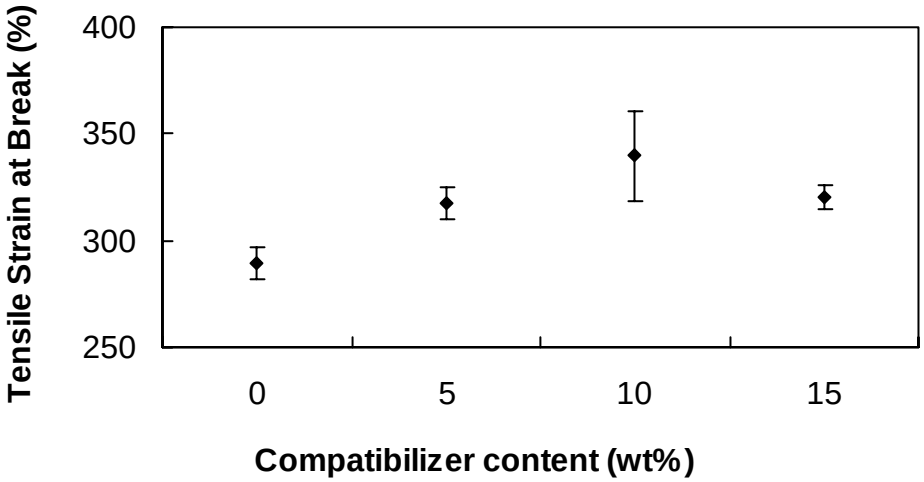

Figure 4.4.6. Effect of compatibilizer content on tensile strain at break of PP/Lotader® AX8900 (E-MA-GMA) blend.

The effects of E-GMA elastomer on the tensile properties of PP are seen in Figures 4.4.7-4.4.9. As discussed before, the values of tensile strength and modulus increase first, then decrease due to the dilution effect of elastomer. In this blend, the crystallinity increases very slightly. Therefore, it may be said that the crystallinity does not effect the tensile properties too much. Increase in elongation is assigned to the elastomeric character of rubber particles. The dispersed rubber particles act as stress concentrators during extension process. Since PP absorbs high amount of energy, it elongates to greater extent by yielding and crazing.

Thus, from the observation of the tensile properties, It can be said that addition of 5 wt % elastomer to PP may have positive effects in increasing in tensile properties as seen from Table 4.4.1.

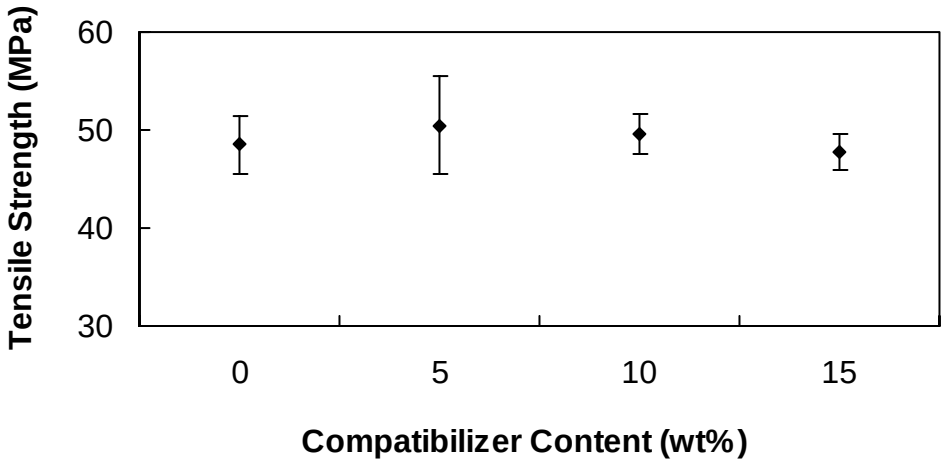

Figure 4.4.7. Effect of compatibilizer content on tensile strength of PP/Lotader® AX8840 (E-GMA) blend.

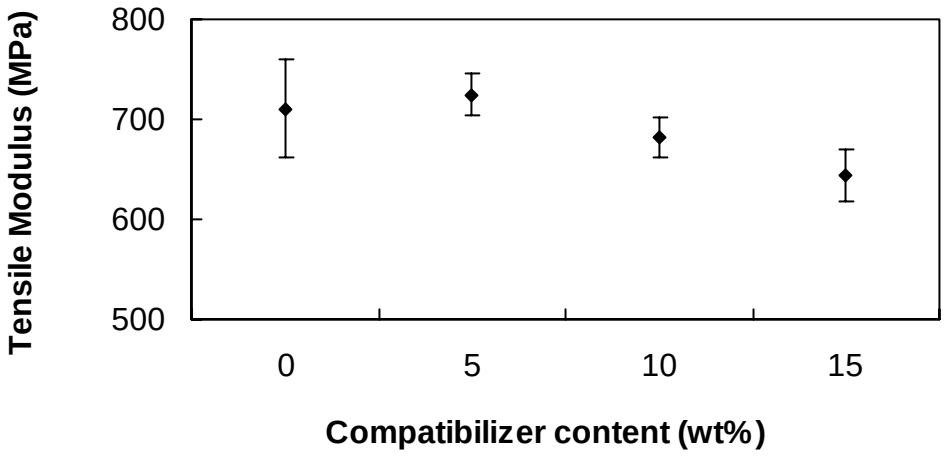

Figure 4.4.8. Effect of compatibilizer content on tensile modulus of PP/Lotader® AX8840 (E-GMA) blend.

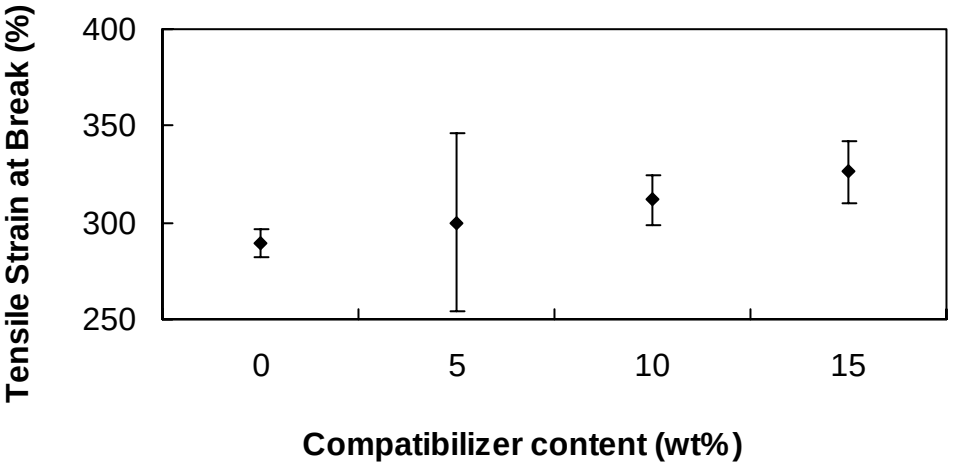

Figure 4.4.9. Effect of compatibilizer content on tensile strain at break of PP/Lotader® AX8840 (E-GMA) blend.

Table 4.4.1. The tensile properties values of PP/elastomer blends containing 5, 10 and 15 wt% elastomer

Samples	Elastomer Content (%)	Tensile Strength (MPa)	Tensile Modulus (MPa)	Strain at Break (%)
PP	0	48.5	711	289
PP/E-nBA/MAH	5	51.2	682	327
PP/E-nBA/MAH	10	51.9	704	325
PP/E-nBA/MAH	15	49.6	644	344
PP/E-MA-GMA	5	51.3	725	317
PP/E-MA-GMA	10	52.5	682	340
PP/E-MA-GMA	15	49.7	628	320
PP/E-GMA	5	50.5	725	300
PP/E-GMA	10	49.5	682	312
PP/E-GMA	15	47.7	644	326

Figures 4.4.10, 4.4.11 and 4.4.12 show the tensile properties of PP/organoclay that has 2 wt% of organoclay. All tensile properties increase by the addition of 2 wt% organoclay with respect to neat PP, although Table 4.1.1 indicates no intercalation in the binary PP/organoclay nanocomposites. The tensile strength values are 50.3 MPa, 51.0 MPa and 51.4 MPa for PP/30B, PP/15A and PP/25A, respectively.

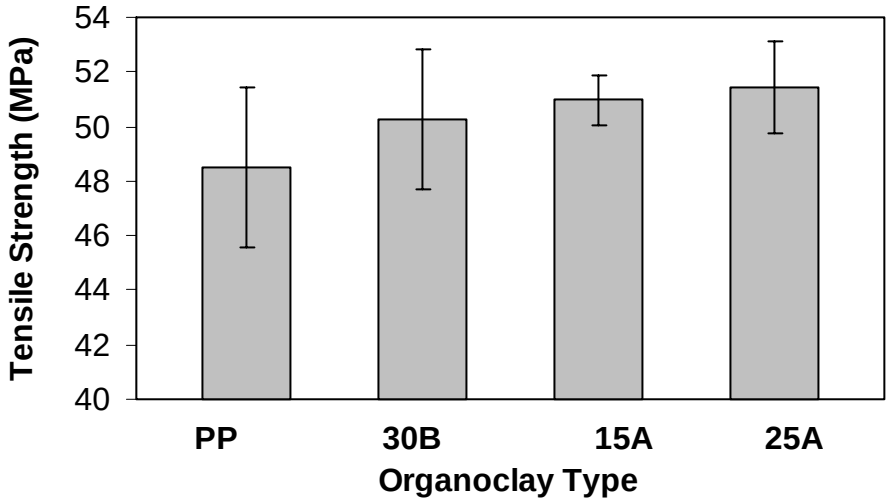

Figure 4.4.10. Tensile strength of PP/organoclay mixtures containing 2 wt% organoclay.

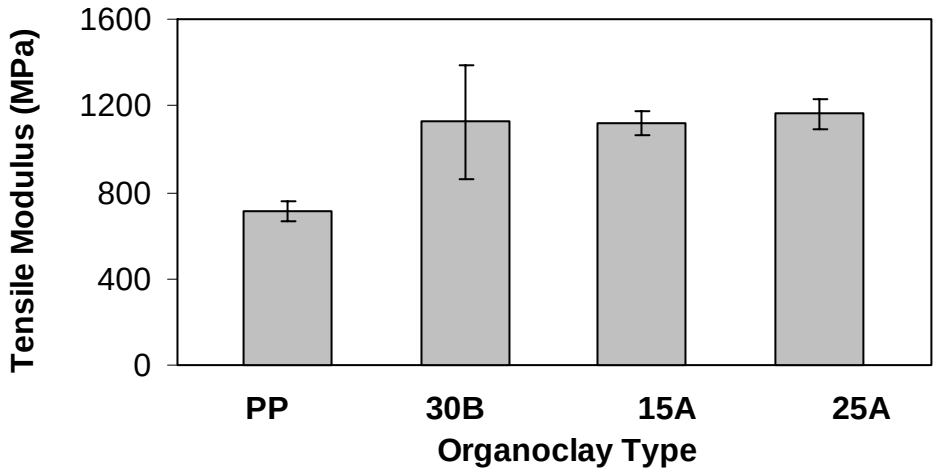

Figure 4.4.11. Tensile modulus of PP/organoclay mixtures containing 2 wt% organoclay.

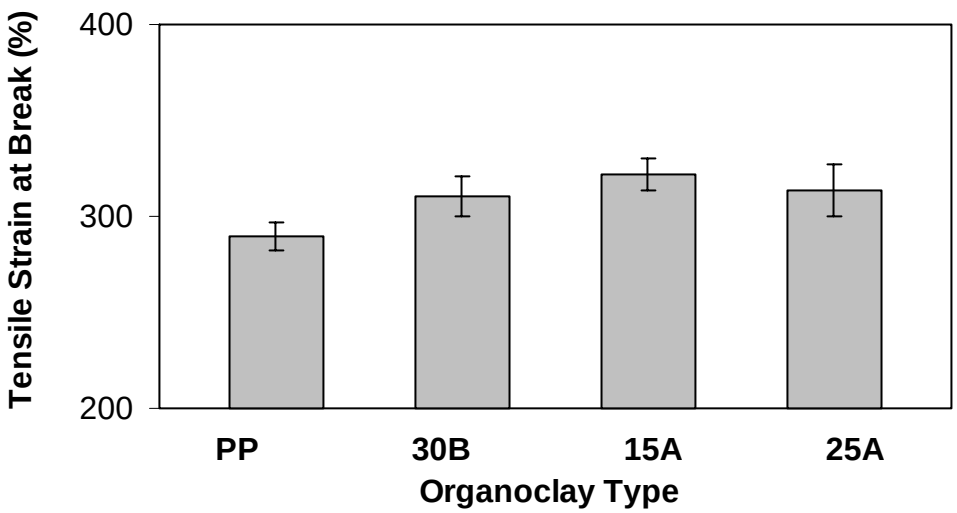

Figure 4.4.12. Tensile strain at break of PP/organoclay mixtures containing 2 wt% organoclay.

When examining the tensile strength, tensile modulus and tensile strain at break results in Figures 4.4.10-4.4.12, there are no remarkable differences among these nanocomposites of PP/organoclay. The interlayer spacing of organoclays in PP/organoclay composites are lower than interlayer spacing of original organoclay as observed by XRD. This implies that all of the PP/organoclay mixtures behave as conventional composites. Also, large clay tactoids are seen in SEM Figures of PP/organoclay mixtures.

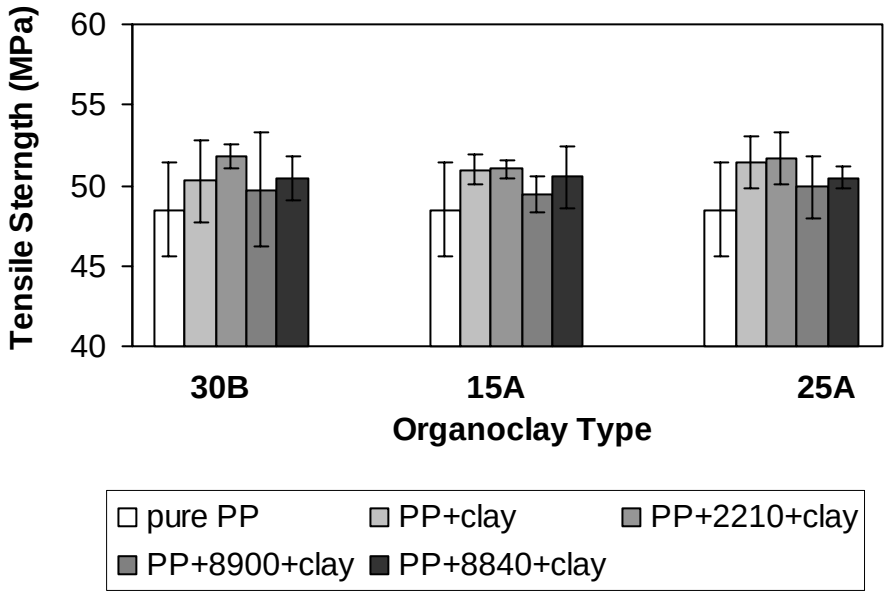

Figure 4.4.13. Tensile strength of ternary PP/compatibilizer/organoclay nanocomposites.

Tensile properties of PP/layered silicate nanocomposites with 2 wt% of organoclay and 5 wt% of compatibilizer are shown in Figures 4.4.13, 4.4.14 and 4.4.15. The first two bars represent tensile properties of pure PP, PP/organoclay mixtures in these Figures. Increase in the tensile strength of nanocomposites is seen in Figure 4.13. Binary PP/organoclay composites have higher tensile strength than does pure PP. From Figure 4.4.13, it is seen that the addition of elastomer decreases the tensile strength of the binary PP/organoclay composites, except for the elastomer Lotader® 2210 (E-nBA-MAH) which increases the crystallinity of the matrix.

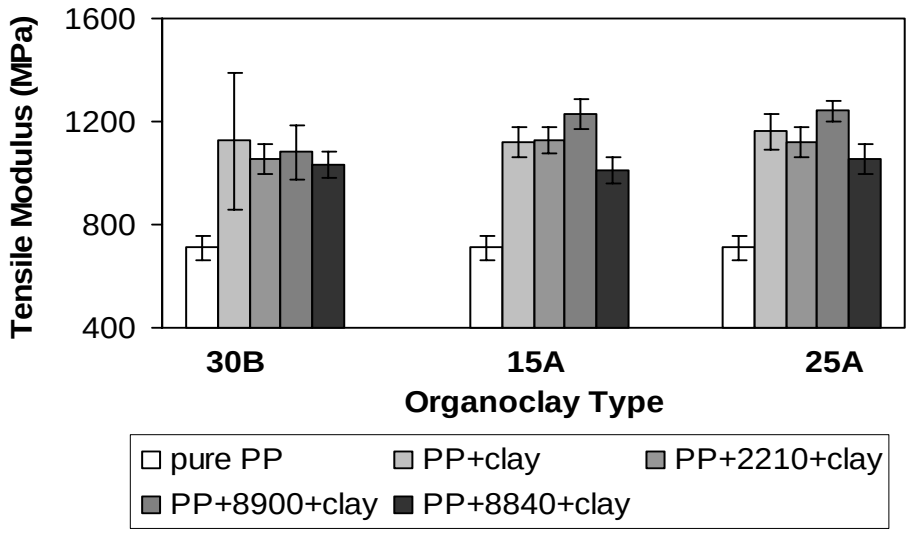

Figure 4.4.14. Tensile modulus of ternary PP/compatibilizer/organoclay nanocomposites.

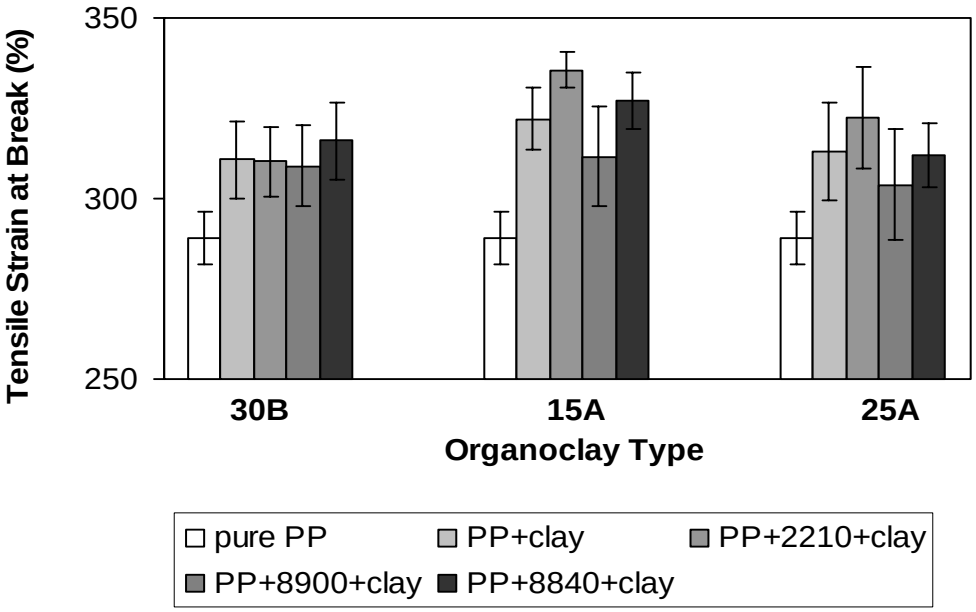

Figure 4.4.15. Tensile strain at break of ternary PP/compatibilizer/organoclay nanocomposites.

Figure 4.4.14 shows tensile modulus (measure of polymer stiffness) of nanocomposites. The tensile modulus values increase significantly with the addition of organoclay to polypropylene. On the other hand further addition of elastomer to binary PP/organoclay composites decrease the tensile modulus except for PP/Cloisite® 15A/Lotader® 8900 (E-MA-GMA) and PP/Cloisite® 25A/Lotader® 8900 (E-MA-GMA) ternary systems. Also, the tensile modulus of ternary nanocomposites containing organoclay 30B are the lowest when compared with the nanocomposites containing organoclays 15A and 25A. This result is also supported by XRD's. The modulus of the nanocomposites PP/25A/8900 (E-MA-GMA) is the highest with respect to other nanocomposites produced in this study. Similarly, the increase in the d-spacing of the 25A in PP/25A/8900 (E-MA-GMA) nanocomposites is the highest compared to the increase in d-spacings of other organoclays used in this study. These results support each other. The reason for this improvement in tensile modulus can be considered as intercalation of the silicate layers in the presence of compatibilizer. Therefore, the effect of addition order is studied in PP/Cloisite® 15A/Lotader® 8900 (E-MA-GMA) and PP/Cloisite® 25A/Lotader® 8900 (E-MA-GMA) ternary systems.

Figure 4.4.15 shows the tensile strain at break values of nanocomposites. Addition of 2 wt% clay alone or with 5 wt% elastomer increases the elongation at break of nanocomposites.

Two different compositions were prepared in order to investigate the effect of mixing order on tensile properties of nanocomposites. They are ternary mixing sequence of PP/E-MA-GMA/15A (93/5/2 wt%) and PP/E-MA-GMA/25A (93/5/2 wt%). As discussed before, the interlayer spacing of Cloisite® 15A and Cloisite® 25A exhibited the highest value with the presence of Lotader® 8900 (E-MA-

GMA) according to the XRD results. In addition to that, they showed good tensile properties.

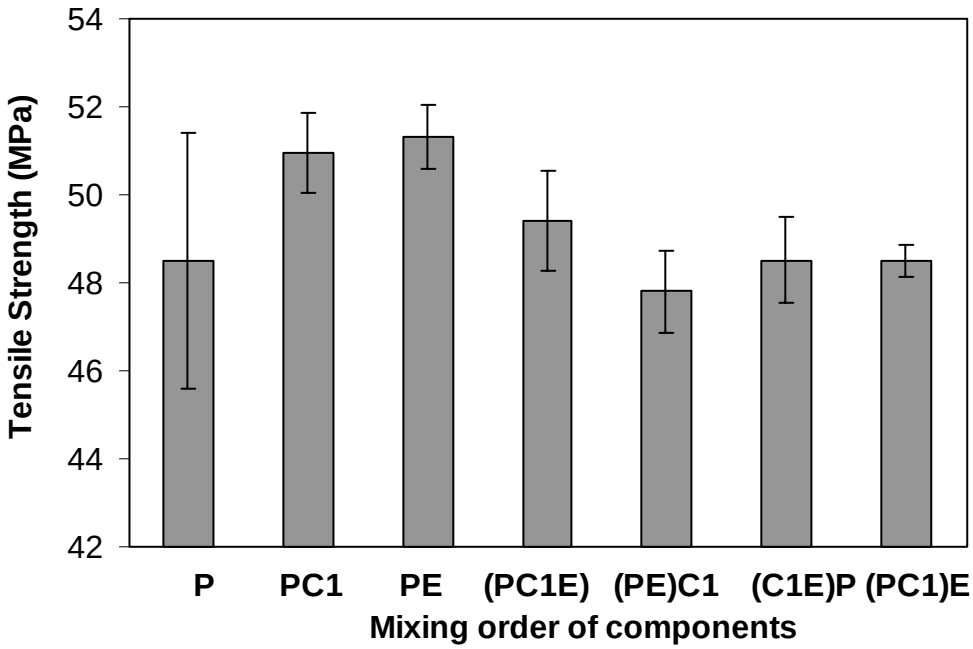

Figure 4.4.16. Effect of mixing order on tensile strength PP/E-MA-GMA/15A nanocomposites containing 5 wt% compatibilizer and 2 wt% organoclay.

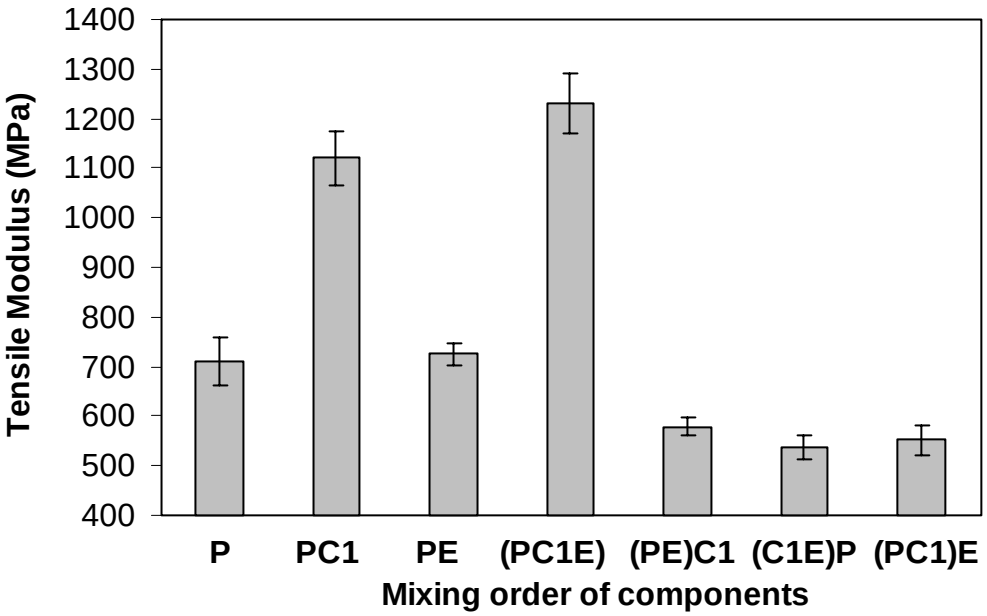

Figure 4.4.17. Effect of mixing order on tensile modulus PP/E-MA-GMA/15A nanocomposites containing 5 wt% compatibilizer and 2 wt% organoclay.

Tensile properties of these nanocomposites are shown from Figures 4.4.16 to 4.4.21. In the graphs, first three bars represent the tensile properties of P (PP), PC (PP/organoclay) and PE (P/E-MA-GMA) respectively, for a better comparison of all materials. Here, the symbol C1 and C2 represent the organoclays 15A and 25A, respectively. Four different mixing sequences were studied to obtain the ternary nanocomposites. They can be shown as:

MO1: (PEC1), (PEC2)
MO2: (PE)C1, (PE)C2
MO3: (C1E)P, (C2E)P
MO4: (PC1)E, (PC2)E

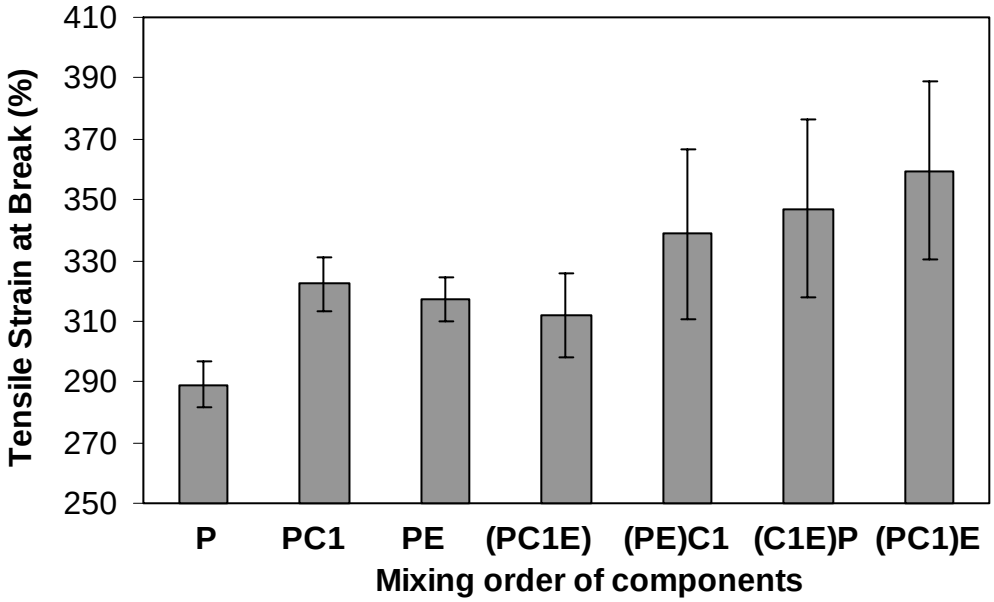

Figure 4.4.18. Effect of mixing order on the tensile strain at break PP/E-MA-GMA/15A nanocomposites containing 5 wt% compatibilizer and 2 wt% organoclay.

The materials shown in parenthesis are compounded in the first extrusion run. The material shown outside the parenthesis is mixed to the system in the second extrusion. Mixing order of (PEC1) and (PEC2) i.e. MO1 is the best mixing sequence according to the tensile strength and modulus. That is to say, when all the materials are fed to the extruder in the first run, the tensile properties are the best in comparison to properties obtained in other mixing sequences. However, the elongation at break behavior of these nanocomposites is smaller. The XRD data in Table 4.4.1 shows that the d-spacing of the nanocomposites mixed by different orders are similar. However, in mixing MO1 all the components under extrusion twice, thus there is a better chance of three-way interaction. In mixing order MO2, PP and compatibilizer were mixed in the first run, organoclay was added to the system in the second run. Thus,

organoclay was exposed to the extrusion process only once. Thus, less shear is applied on the organoclay. Owing to the low interaction of the organoclay and polymer matrix, the nanocomposite prepared by MO2 mixing sequence has poor tensile properties.

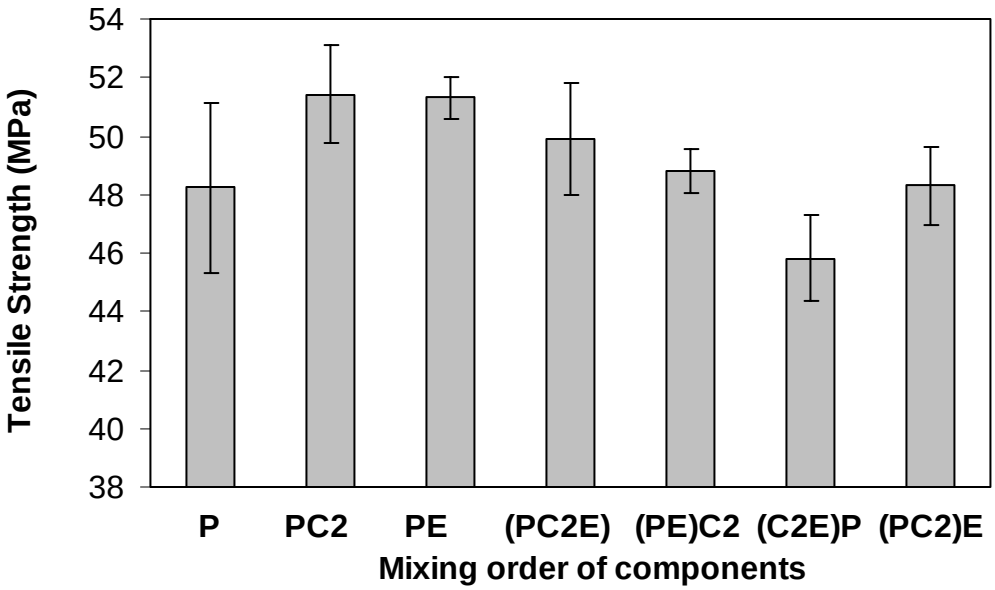

Figure 4.4.19. Effect of mixing order on tensile strength PP/E-MA-GMA/25A nanocomposites containing 5 wt% compatibilizer and 2 wt% organoclay.

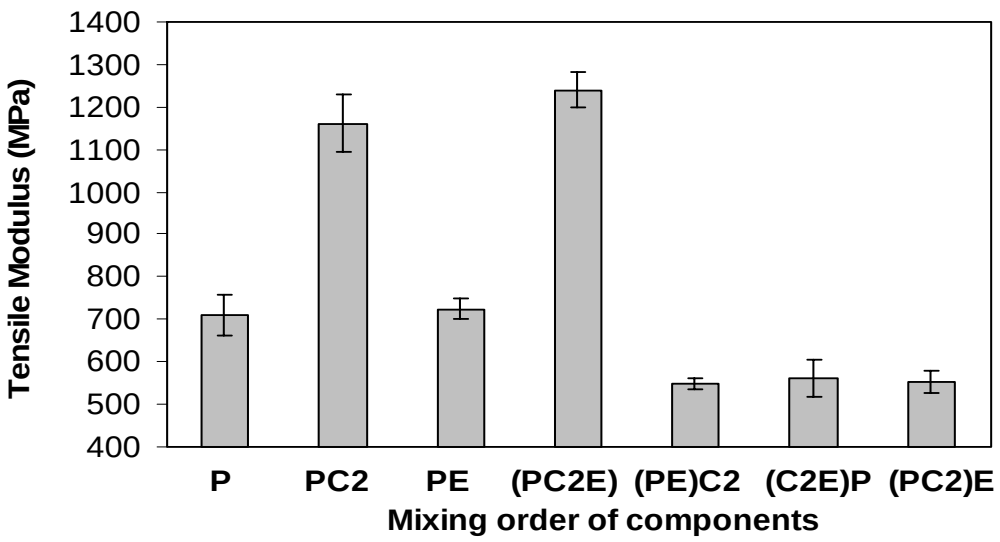

Figure 4.4.20. Effect of mixing order on tensile modulus PP/E-MA-GMA/25A nanocomposites containing 5 wt% compatibilizer and 2 wt% organoclay.

In MO3 mixing order, compatibilizer and organoclay were mixed in the first run of extrusion. In this mixing order, compatibilizer can not apply enough shear for dispersion of clay particulates. When compatibilizer and organoclay were mixed in the first run of extrusion process like MO3, compatibilizer could not apply enough shear for dispersion of clay particulates. The results of MFI supports this situation. The MFI values of compatibilizers are much higher than neat PP.

In MO4 mixing order, organoclay and PP are mixed in the first run, whereas the elastomer is added to the system in the second run. In the absence of compatibilizer in the first run, clay particulates may be dispersed in the polymer matrix in micro-dimensions. In the second run, addition of compatibilizer was unable to open the clay galleries of organoclays which were already dispersed in micro dimensions in the highly viscous PP matrix. Due to the high applied

shear and interactions of all materials with each other during extrusion, the mixing sequence of MO1 (PEC) has the best tensile strength and modulus. It is observed that both 15A and 25A exhibited similar trends in the mixing order studies.

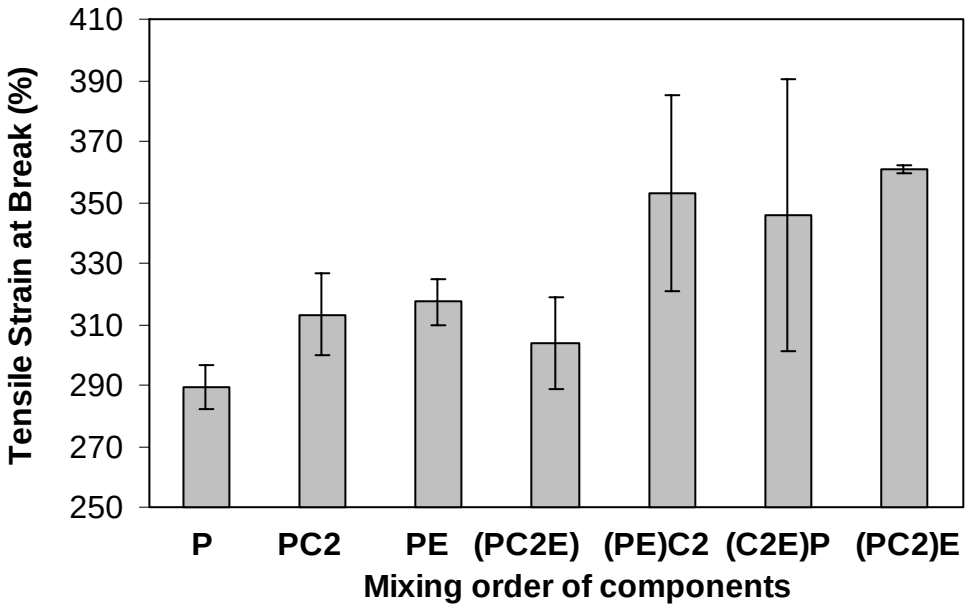

Figure 4.4.21. Effect of mixing order on tensile strain at break PP/E-MA-GMA/25A nanocomposites containing 5 wt% compatibilizer and 2 wt% organoclay.

4.4.2. Flexural Properties

Flexural properties were determined by three point bending according to the standard ISO 178. The values of flexural strength and flexural modulus were calculated from the load versus deflection curve. Flexural tests were performed on five samples in each experimental set. The results are reported as the

average of five samples. Flexural strength was calculated from the point of maximum load and flexural modulus was calculated from the slope of this curve by the equations given in the standard. Figures 4.4.22 through 4.4.35 show the flexural strength and modulus of all the samples.

Flexural test is comprised of tension and compression on the two sides of the sample. When flexural properties are compared with the tensile properties, the tensile strength values are higher than the flexural strength values though the flexural modulus values are higher than the tensile modulus values. However, both flexural strength and flexural modulus values should be higher than the tensile strength and tensile modulus values because of the nature of the flexural test. During a tensile test, the specimens exhibited orientation hardening and elongated to high values. Then, the maximum tensile stress value was at the point of break. Thus, the value of stress at yield was lower than the value of stress at break which is called as the tensile strength values of the specimens. As for the flexural tests, no fracture was observed and the tests were ended manually when the specimen was bent against the wall of the test machine. Thus, the tensile strength values observed are higher than the flexural values.

Figures 4.4.22-4.4.27 show the effect of compatibilizer content on the flexural properties. Addition of compatibilizer decreases both the flexural strength and flexural modulus. Compatibilizers give slightly elastomeric behavior to the neat PP, since they have much lower tensile strength and modulus than the neat PP. Therefore, in general they decrease the mechanical properties like flexural strength and flexural modulus. However, they increase the flexural modulus in some case, as they do for the tensile modulus as well.

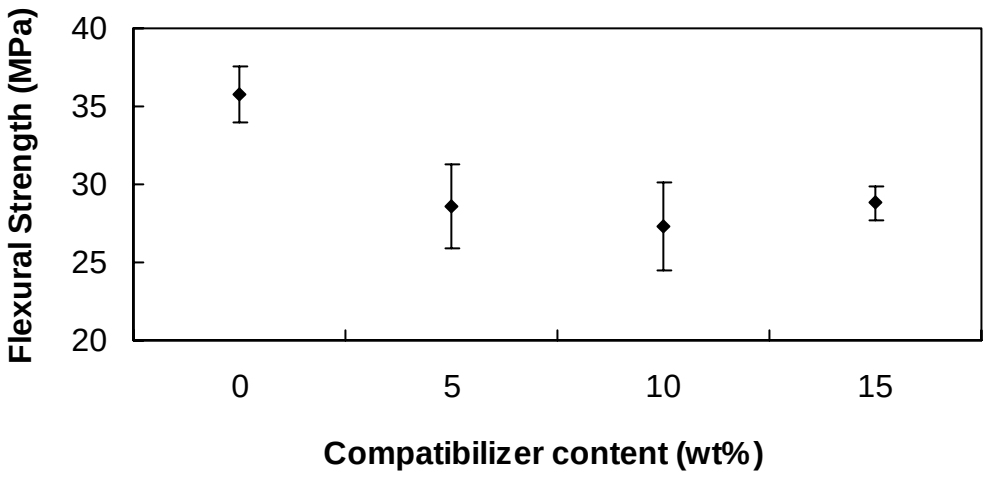

Figure 4.4.22. Effect of compatibilizer content on flexural strength of PP/Lotader® 2210 (E-nBA-MAH) blend.

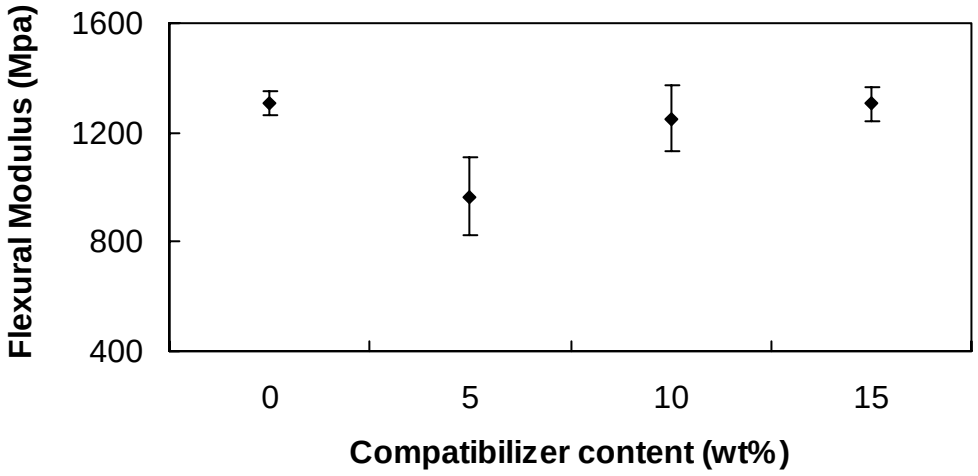

Figure 4.4.23. Effect of compatibilizer content on flexural modulus of PP/Lotader® 2210 (E-nBA-MAH) blend.

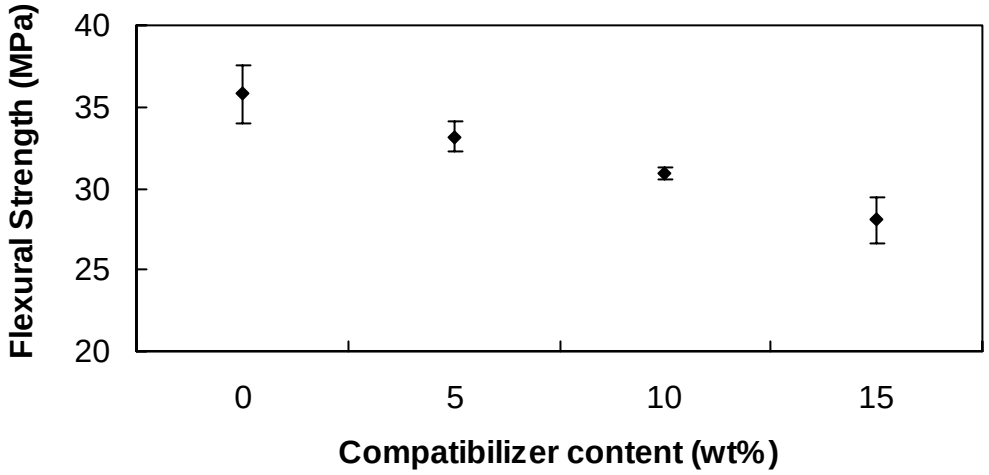

Figure 4.4.24. Effect of compatibilizer content on flexural strength of PP/Lotader® 8900 (E-MA-GMA) blend.

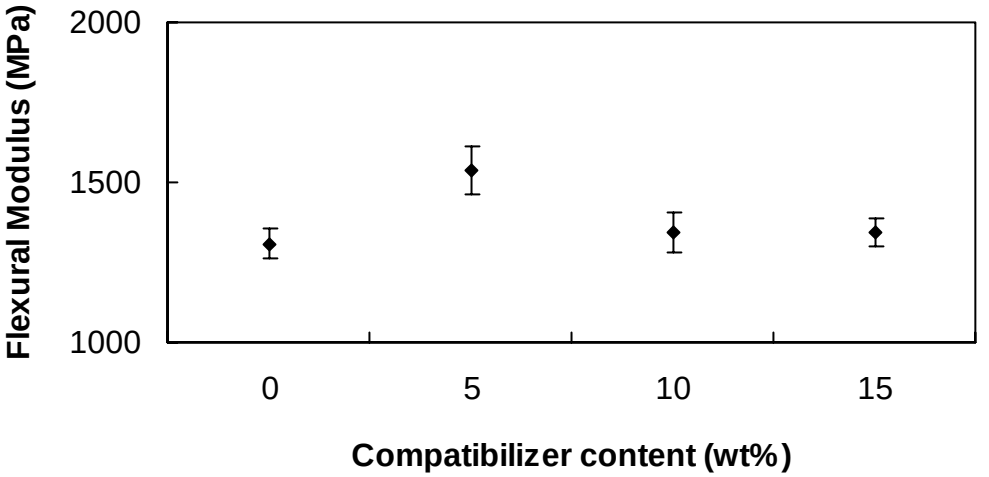

Figure 4.4.25. Effect of compatibilizer content on flexural modulus of PP/Lotader® 8900 (E-MA-GMA) blend.

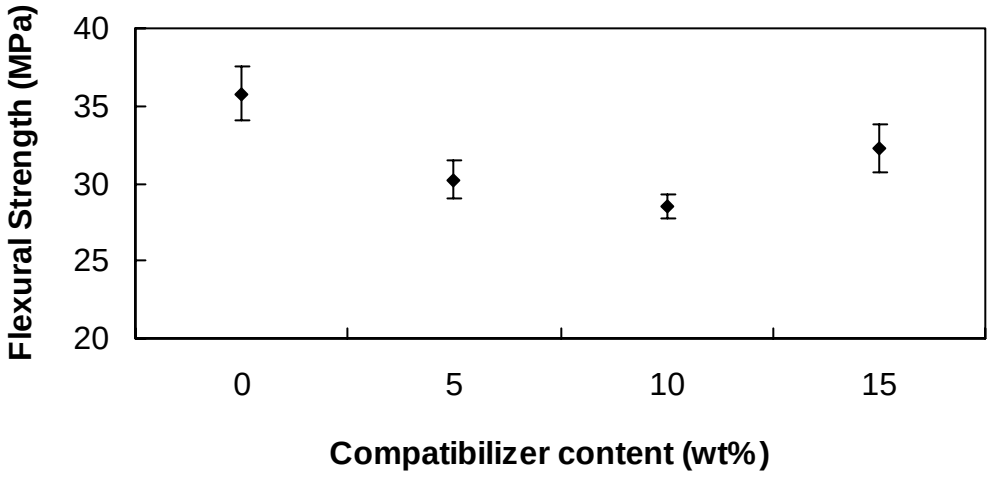

Figure 4.4.26. Effect of compatibilizer content on flexural strength of PP/Lotader® AX8840 (E-GMA) blend.

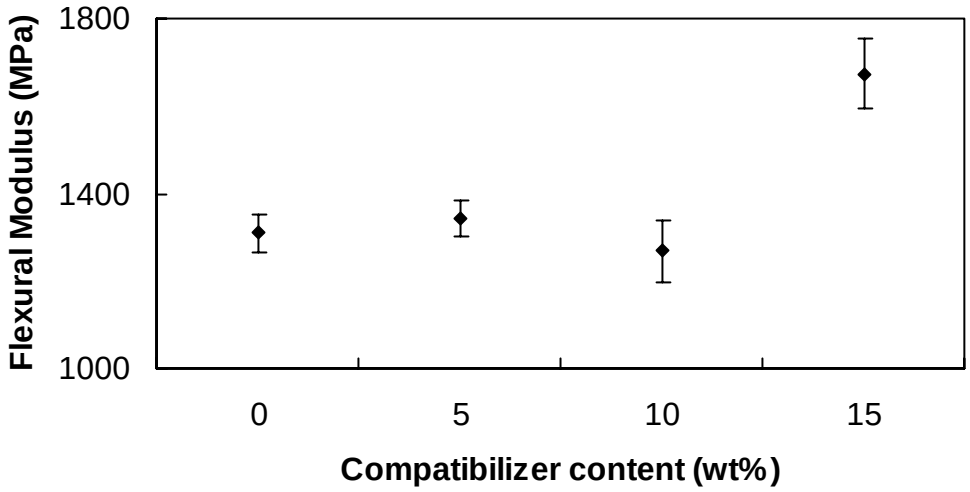

Figure 4.4.27. Effect of compatibilizer content on flexural modulus of PP/Lotader® AX8840 (E-GMA) blend.

The flexural properties of PP/organoclay mixtures containing 2 wt % are shown in Figures 4.4.28 and 4.4.29. Modulus can be defined as a measure of material's stiffness. As it is seen in Figures, addition of clay particles increases the flexural modulus depending on the degree of dispersion of the silicate layers in the PP matrix. Thus, the highest increase in the flexural modulus is seen for PP/15A and PP/25A composites.

Flexural properties of ternary nanocomposites can be seen in Figures 4.4.30 and 4.4.31. Among the ternary nanocomposites, the highest flexural strength and modulus values also belong to PP/E-MA-GMA/15A, and PP/E-MA-GMA/25A nanocomposites (like tensile strength and modulus) owing to the high intercalation observed for these nanocomposites.

The improvements in the flexural strength of ternary nanocomposites of PP/E-MA-GMA/15A and PP/E-MA-GMA/25A are calculated as 8% and 4% respectively, and modulus of ternary nanocomposites of PP/E-MA-GMA/15A and PP/E-MA-GMA/25A increase by 22% and 21% respectively with respect to neat PP.

Figures 4.4.32 through 4.4.35 display the effect of mixing order of materials on flexural properties. The mixing order MO1 is the best among mixing orders investigated, since in this mixing order the three-way interactions are maximized. There is a significant decrease in the flexural properties of other mixing order sequences.

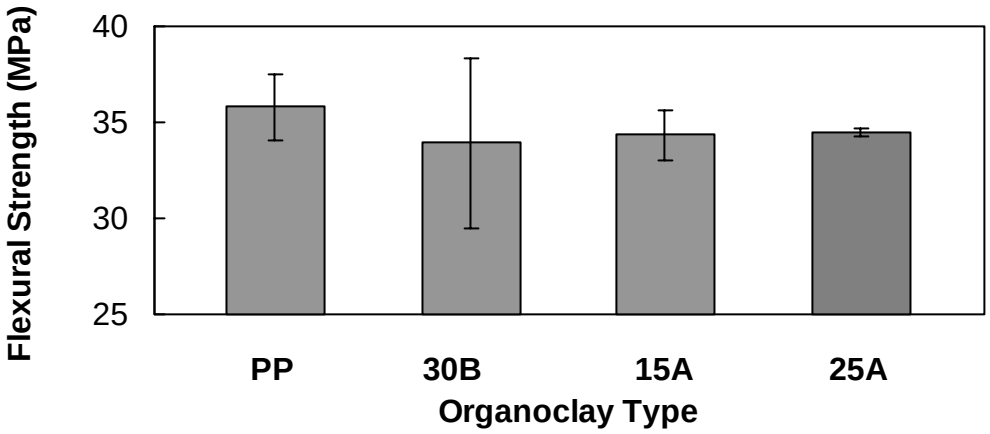

Figure 4.4.28. Flexural strength of PP/organoclay mixtures containing 2 wt% organoclay.

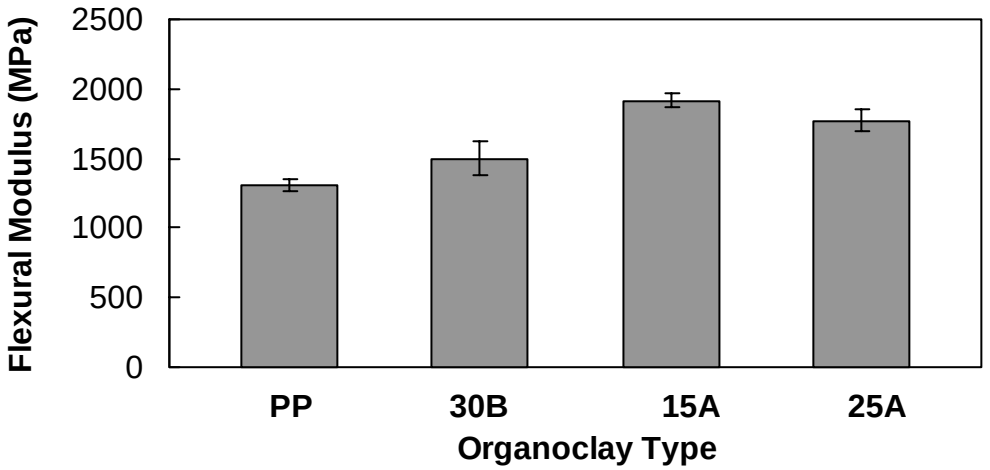

Figure 4.4.29. Flexural modulus of PP/organoclay mixtures containing 2 wt% organoclay.

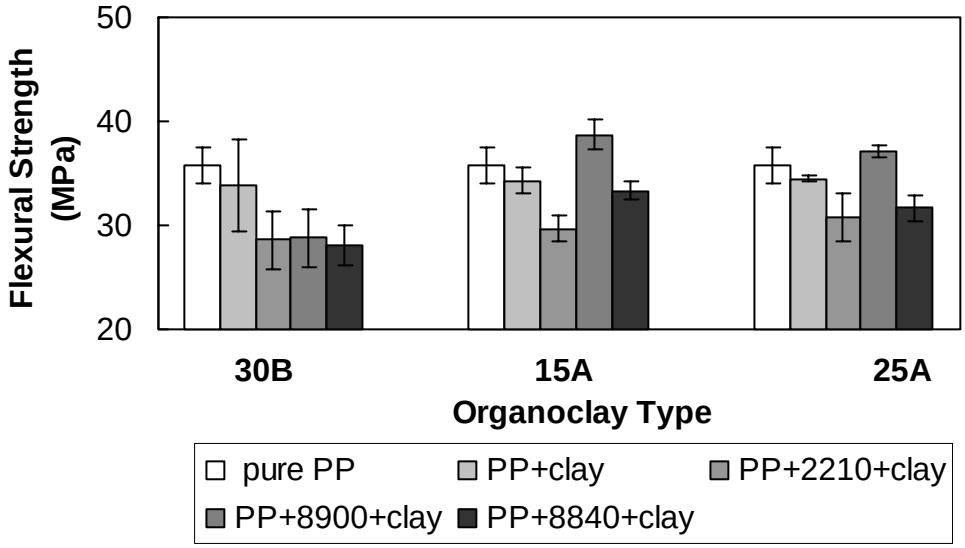

Figure 4.4.30. Flexural strength of ternary PP/compatibilizer/organoclay nanocomposites.

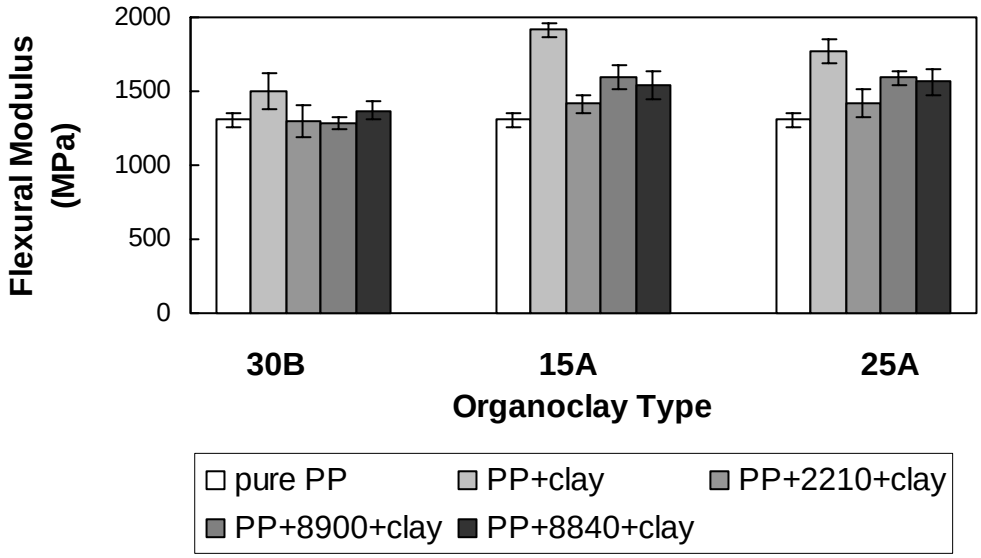

Figure 4.4.31. Flexural modulus of ternary PP/compatibilizer/organoclay nanocomposites.

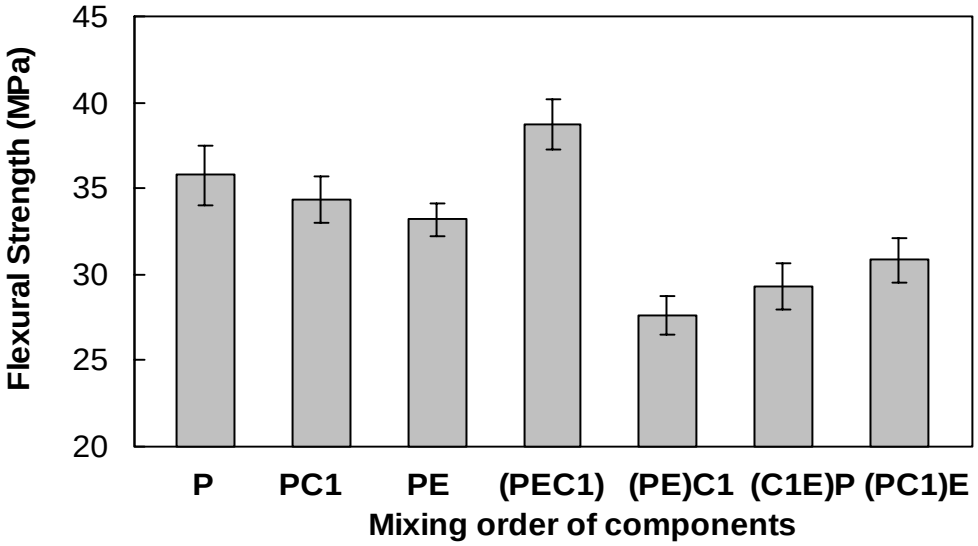

Figure 4.4.32. Effect of mixing order on flexural strength PP/E-MA-GMA/15A nanocomposites containing 5 wt% compatibilizer and 2 wt% organoclay.

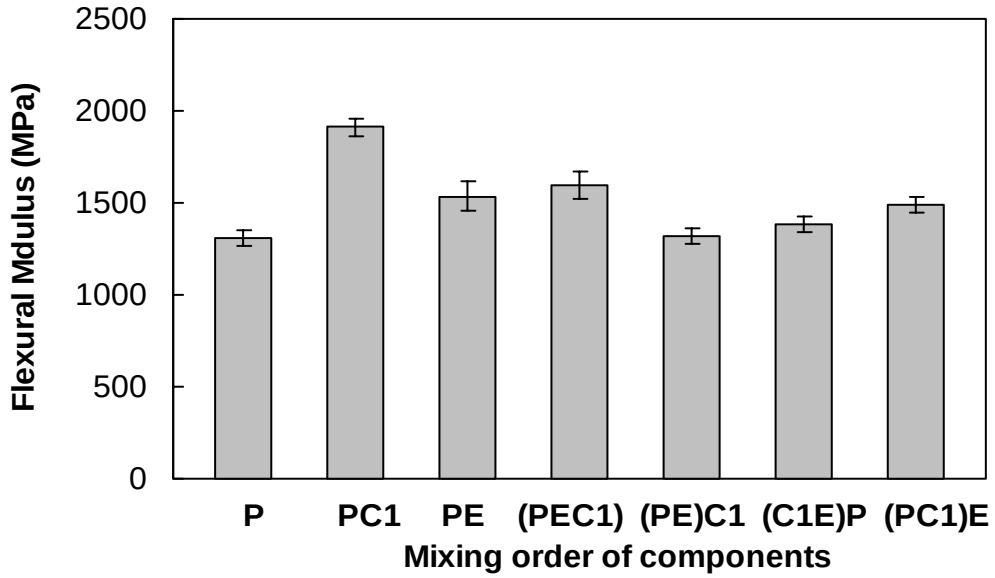

Figure 4.4.33. Effect of mixing order on flexural modulus PP/E-MA-GMA/15A nanocomposites containing 5 wt% compatibilizer and 2 wt% organoclay.

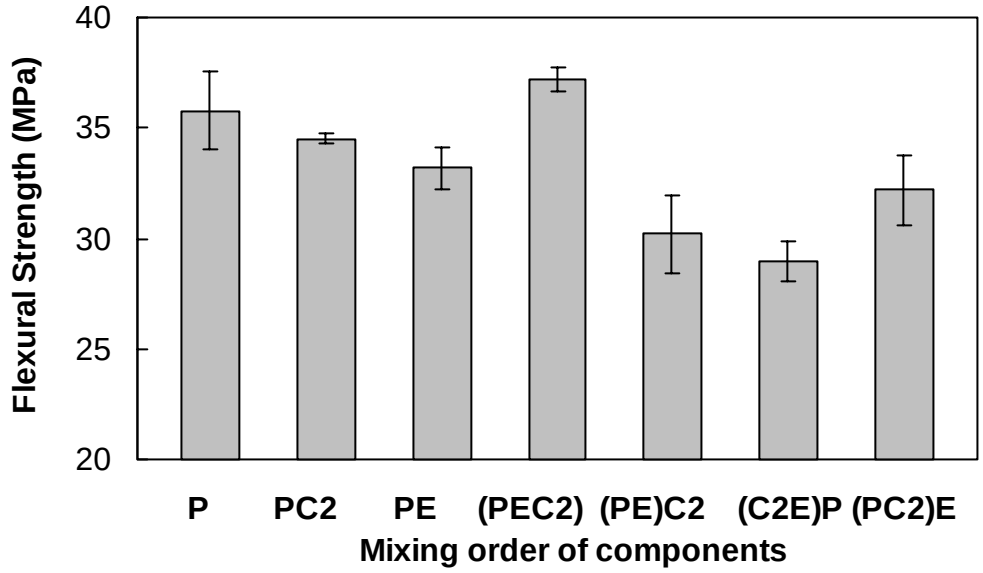

Figure 4.4.34. Effect of mixing order on flexural strength PP/E-MA-GMA/25A nanocomposites containing 5 wt% compatibilizer and 2 wt% organoclay.

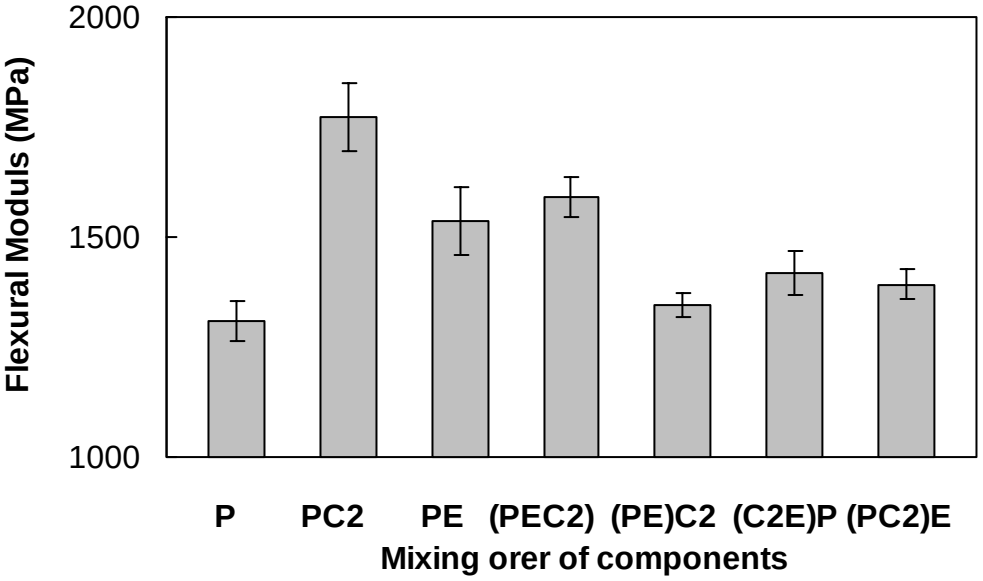

Figure 4.4.35. Effect of mixing order on flexural modulus PP/E-MA-GMA/25A nanocomposites containing 5 wt% compatibilizer and 2 wt% organoclay.

4.4.3. Impact Properties

Impact properties were determined by notched Charpy impact test according to the standards of ISO 179-2. After opening 2 mm of “V” type notched, test was performed for at least five specimens.

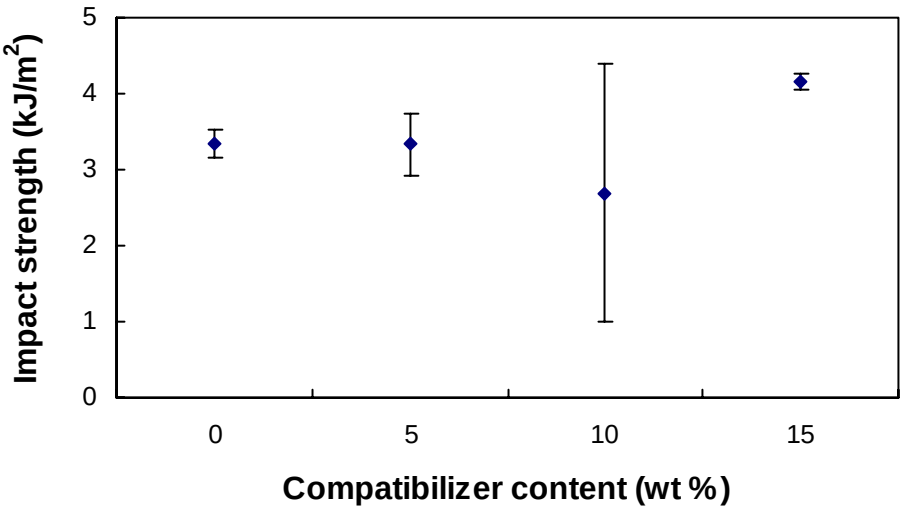

Figure 4.4.36. Effect of compatibilizer content on impact strength of PP/Lotader® 2210 (E-nBA-MAH) blend.

Polypropylene is a semi-crystalline polymer with desired properties, its toughness, especially notched impact strength. On the other hand, this toughness is not generally sufficient for applications as engineering plastics. Blends of polypropylene with rubbers (elastomer toughening) and polypropylene based composite materials have been extensively studied in order to improve its physical properties. Toughened PP with some commonly used rubbers can provide fairly high toughness. However, at the same time, the loss of stiffness cannot be neglected. On the other hand, toughening PP with rigid particles instead of rubber particles cannot usually be done effectively, although their

tensile strength and stiffness increase. It is difficult to prepare a PP with a good balance of toughness and stiffness. However, incorporation of the filler, such as organoclays, into PP/elastomer blends can restore the required stiffness and strength [61, 32].

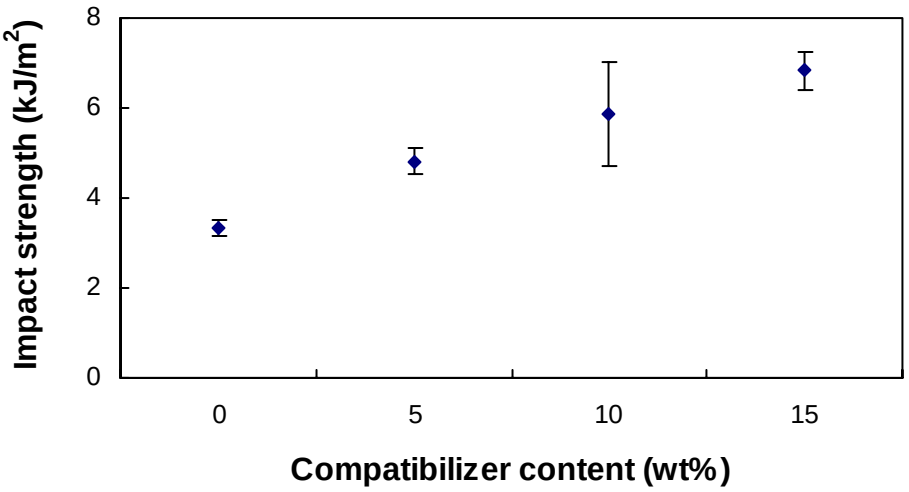

Figure 4.4.37. Effect of compatibilizer content on impact strength of PP/Lotader® 8900 (E-MA-GMA) blend.

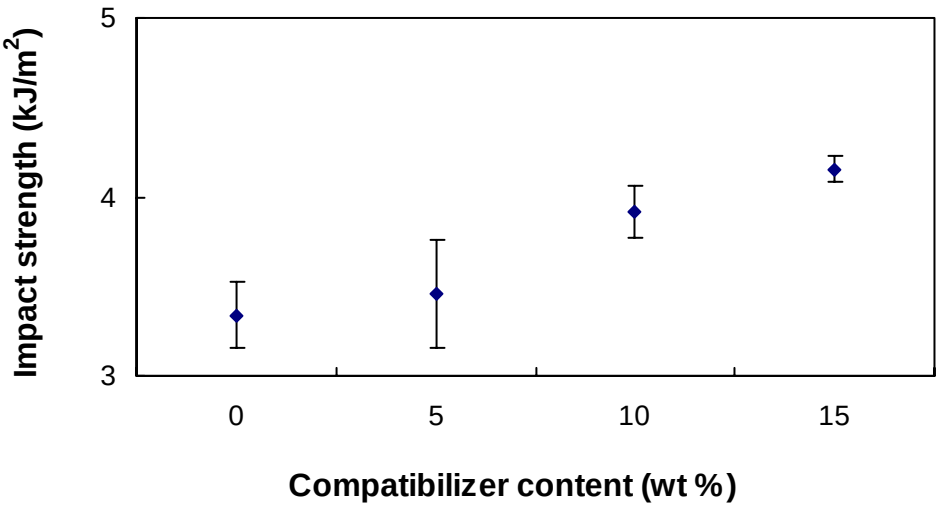

Figure 4.4.38. Effect of compatibilizer content on impact strength of PP/Lotader® 8840 (E-GMA) blend.

All studies conclude that toughening of semicrystalline polymers like PP is a complex mechanism including the initial elastic loading of the matrix/rubber blend, the internal or external cavitations of the dispersed rubber particles, followed by craze initiation and shear banding of the matrix [41].

Figure 4.4.36-4.4.38 show the effect of elastomer content on impact strengths of PP/Lotader® 2210 (E-nBA-MAH), PP/Lotader® 8900 (E-MA-GMA) and PP/Lotader® 8840 (E-GMA) blends. As it is expected, impact strength of neat PP increases by addition of elastomer. It is known that with increasing rubber content the brittle-ductile transition temperature is shifted to lower temperatures which promote toughening [48]. Also, in SEM micrographs, a second phase formed by elastomers in PP matrix are seen. Rubber particles are responsible for void initiation internally on the particles or at the rubber-matrix boundary [49].

The impact strength values of PP/organoclay and ternary nanocomposites containing 5 wt% compatibilizer and 2 wt% organoclays are illustrated in Figure 4.4.39. As observed from the Figure, the addition of organoclay increases the impact strength of PP. The nanocomposites containing (E-MA-GMA) the highest impact strength value for each organoclay type. XRD data indicate that this compatibilizer provides the best dispersibility of clay in the matrix. Also, as seen in SEM micrograms, the dispersibility of elastomer domains are more homogeneous in ternary nanocomposites containing E-MA-GMA, which provides higher impact strength.

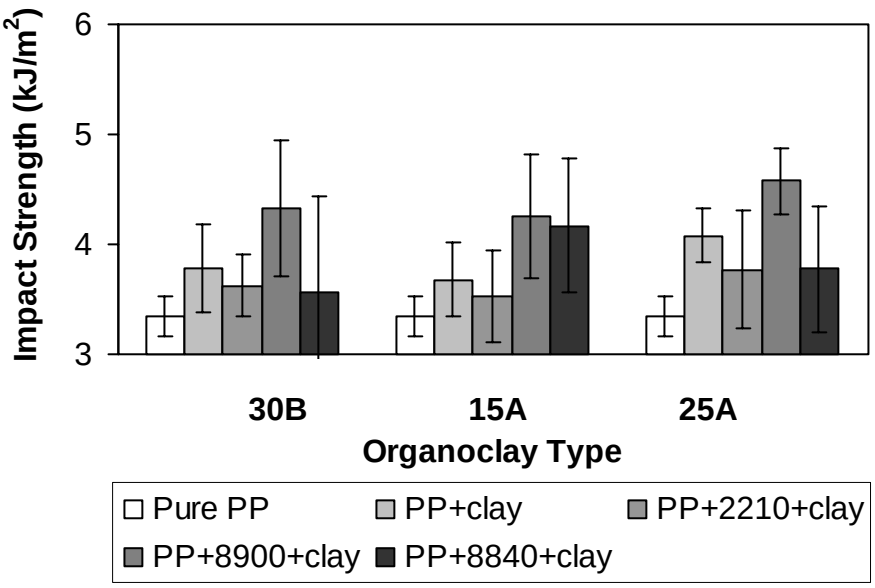

Figure 4.4.39. Impact strength values of ternary PP/compatibilizer/organoclay nanocomposites.

Figure 4.4.40 and 4.4.41 show the effect of mixing order on impact strength of PP/E-MA-GMA/15A and PP/E-MA-GMA/25A nanocomposites containing 5 wt% compatibilizer and 2 wt% organoclay, respectively. The impact strength values are close to each other for all different mixing sequences. It can be said that the mixing order of components does not affect the impact strength remarkably, as opposed to tensile and flexural properties.

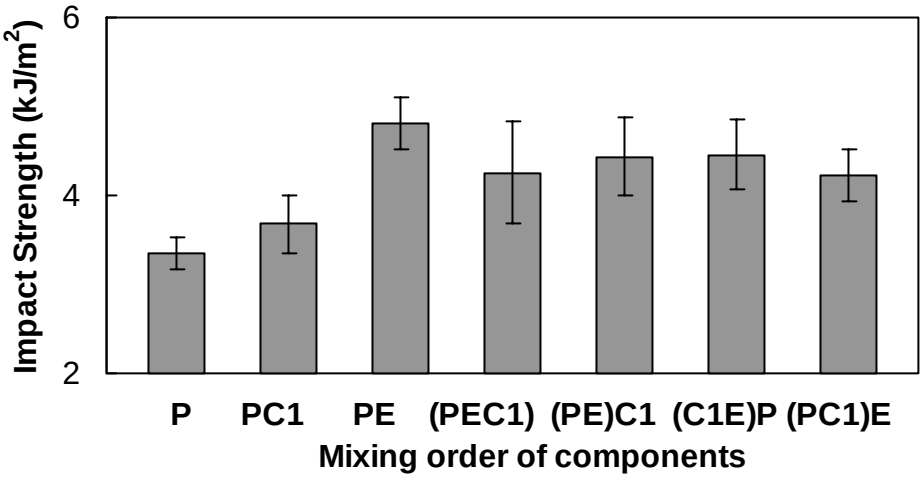

Figure 4.4.40. Effect of mixing order on impact strength PP/E-MA-GMA/15A nanocomposites containing 5 wt% compatibilizer and 2 wt% organoclay.

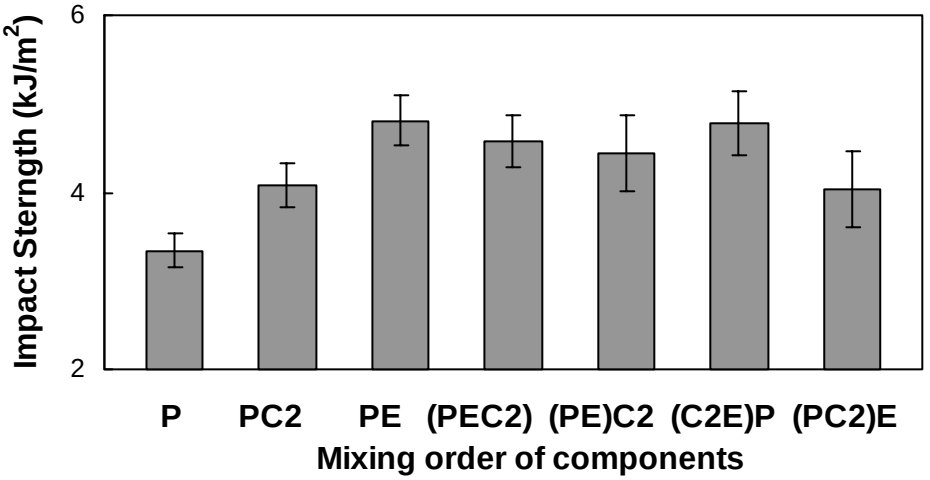

Figure 4.4.41. Effect of mixing order on impact strength PP/E-MA-GMA/25A nanocomposites containing 5 wt% compatibilizer and 2 wt% organoclay.

CHAPTER 5

CONCLUSIONS

In this study, polypropylene/organoclay nanocomposites were produced by using compatibilizers with the aid of melt mixing method. The effects of different types of compatibilizers, different types of organoclays and different mixing sequences of components on morphology, thermal properties, flow characteristics as well as mechanical properties of the nanocomposites were investigated.

First of all, in order to investigate the morphology of all materials produced in this study, X-ray diffraction analysis was carried out. According to the XRD results, intercalated structures were obtained in both PP/Cloisite® 15A/compatibilizer and PP/Cloisite® 25A/compatibilizer ternary nanocomposites. In PP/Cloisite® 15A and PP/Cloisite® 25A systems containing 5 wt % compatibilizer, the characteristic diffraction peaks of original clays shift to smaller angles, since addition of compatibilizer facilitates the dispersion of clay particulates in the PP matrix in systems with 15A and 25A. The highest increase in the interlayer spacings of organoclays were observed in the PP/E-MA-GMA/15A (23%) and PP/E-MA-GMA/25A (88.3%) systems.

SEM micrographs, show that the fractured surface of neat PP is smooth with linear propagation lines. Clay agglomerates are seen in SEM micrographs of materials with organoclays. SEM micrographs of the materials with elastomer indicates compatibility between elastomers and PP matrix. Agglomeration of clay particles leads to poor dispersion and poor mechanical properties.

Nevertheless, the SEM micrographs of all ternary nanocomposites are similar to each other making it difficult to reach conclusions based on SEM alone.

According to the TEM micrograms, the ternary nanocomposites of PP/Cloisite® 25A/E-MA-GMA processed by different mixing orders have both intercalated structure. The clay dispersion in (PEC2) nanocomposite, in which all materials were fed to the extruder simultaneously in the first run, is better than the (PE)C2 nanocomposite, in which PP and elastomer were fed to the extruder in the first run, due to maximized three-way interaction.

Differential scanning calorimetry measurements were performed in order to compare both the temperatures of melting and crystallization and the percentage crystallinity of the materials. The melting and crystallization temperatures are very close to each other. Thus, 5 wt% compatibilizer and 2 wt% organoclay do not affect the melting and crystallization temperatures significantly. It can be said that compatibilizers and organoclays have no significant nucleation activity in PP, except for the compatibilizer (E-nBA-MAH). The maximum crystallinity was observed in the blend of PP/(E-nBA-MAH) (42%) and the ternary nanocomposites of PP/E-nBA-MAH/25A (44%).

The effect of organoclay is more dominant than the effect of compatibilizer on the MFI values (viscosity) of ternary nanocomposites. Addition of organoclay decreases the MFI value of neat PP, whereas addition of compatibilizer slightly increases the MFI value with respect to the MFI of PP. In ternary nanocomposites, the MFI's are close to the MFI's of PP/organoclay blends.

Finally, when compared with pure PP, the mechanical properties such as tensile strength, tensile modulus, flexural strength, flexural modulus and impact

strength show remarkable improvement. The systems PP/E-nBA-MAH/30B, PP/E-MA-GMA/15A and PP/E-MA-GMA/25A have the highest improvements according to the results mechanical tests owing to high levels of intercalation in these ternary nanocomposites.

The mixing sequence of MO1 (PEC) in which all the materials were simultaneously fed to the extruder in the first run, exhibits the highest improvement in modulus and strength, since in this case the three-way interactions are maximized.

REFERENCES

1. Jordan J., Jacob K., Tannenbaum R., Shara M., Jasiuk I., “Experimental Trends in Polymer Nanocomposites-A Review”, Materials Science and Engineering, vol 393, 1-11, 2005.

2. Mazumdar S. K., “Composites Manufacturing Materials, Product, Process Engineering”, CRC press, USA, 2002.

3. Beyer G., “Nanocomposites: A New Class of Flame Retardants for Polymers”, Polymer Additives and Compounding, 22-28, 2002.

4. Gao F., “Clay/Polymer Composites: The Story”, Materialstoday, 50-55, 2004.

5. Giannelis E. P., “Polymer Layered Silicate Nanocomposites”, Advanced Materials, 29-35, 1996.

6. Zhang J., Jiang D., Wilkie C. A., “Polyethylene and Polypropylene Nanocomposites Based upon an Oligomerically Modified Clay”, Thermochimica acta, vol. 430, 107-113, 2005.

7. Lubin G., “Handbook of Composites”, VNR Company, New York.

8. Kaw K., “Mechanics of Composite Materials”, 1st edition, CRC Press, New York, 1997.

9. Akovalı G., “Handbook of Composite Fabrication”, 1st edition, Rapra Technology Ltd., UK., 2001.

10. Mani G., Fan Q., Ugbolue S. C., Yang Y., “Morphological Studies of Polypropylene-Nanoclay”, vol. 97, 218-226, 2005.

11. Vaia, R. A., Ishii, H., Giannelis, E. P.,”Synthesis and Properties of Two-Dimensional Nanostructures by Direct Intercalation of Polymer Melts in Layered Silicates”, Chemistry of Materials, vol. 5, 1694-1696, 1993.

12. Ray S.S. and Okamoto M., “Polymer/Layered Silicate Nanocomposites: A Review from Preparation to Processing”, Progress in Polymer Science, 2003.

13. Zanetti M., Lomakin S., Camino G., “Polymer Layered Silicate Nanocomposites”, vol. 279, 1-9, 2000.

14. Giannelis E. P., “Polymer-Layered Silicate Nanocomposites: Synthesis, Properties and Applications”, Applied Organometallic Chemistry, vol. 12, 675-680, 1998.

15. Tripathi D., “Practical Guide to Polypropylene”, 1st edition, Rapra Technology Ltd., UK., 2002.

16. Seymour R. B., Carraher C. E., “Structure-Property Relationships in Polymers”, Plenum Press, New York, 1984.

17. Yuan Q., Misra R. D. K., “Impact Fracture Behavior of Clay-Reinforced Polypropylene Nanocomposites”, Polymer, vol. 47, 4421-4433, 2006.

18. Chiu F., Laı S., Chen J., Chu P., “Combined Effects of Clay Modifications and Compatibilizers on the Formation and Physical Properties of Melt-Mixed Polypropylene/Clay Nanocomposites”, Journal of Polymer Science, vol. 42, 4139-4150, 2004.

19. Ding C., Jia D., He H., Guo B., Hong H., “How Organo-Montmorillonite Truly Affects the Structure and Properties of Polypropylene”, Polymer Testing, vol. 24, 94-100, 2005.

20. Brydson J. A., “Plastics Materials”, seventh edition, B.H., Oxford, 1999.

21. Crawford R. J., “Plastics Engineering”, third edition, BH., Oxford, 1998.

22. Middleman S., “Fundamentals of Polymer Processing”, McGraw-Hill, USA, 1977.

23. Sperling L. H., “Introduction to Physical Polymer Science”, fourth edition, John Wiley & Sons Inc., New Jersey, 2006.

24. Bower D. J., “An Introduction to Polymer Physics”, Cambridge University Press, USA, 2002.

25. Stuart B. H., “Polymer Analysis”, John Wiley & Sons Inc., UK, 2002.

26. Zhang Q., Fu Q., Jiang L., Lei Y., “Preparation and Properties of Polypropylene/Montmorillonite Layered Nanocomposites”, Polymer int., vol. 49, 1561-1564, 2000.

27. Ellis T. S., D’Angelo J. S., “Thermal and Mechanical Properties of a Polypropylene Nanocomposite”, Journal of Applied Polymer Science, vol. 90, 1639-1647, 2003.

28. Koo C. M., Kim J. M., Choi M. H., Kim S. O., Chung I. J., “Mechanical and Rheological Properties of the Maleated Polypropylene-Layered Silicate Nanocomposites with Different Morphology”, Journal of Applied Polymer Science, vol. 88, 1526-1535, 2003.

29. Hambır S., Bulakh N., Jog J. P., “Polypropylene/Clay Nanocomposites: Effect of Compatibilizer on the Thermal, Crstallization and Dynamic Mechanical Behavior”, Polymer Engineering and Science, vol. 42, 1800-1807, 2002.

30. Ton-That M. T., Leelapornpisit W., Utracki L. A., Perrin-Sarazin F., Denault J., Cole K. C., Bureau M. N., “Effect of Crystallization on Intercalation of Clay-Polyolefin Nanocomposites and Their Performance”, Polymer Engineering and Science, 1085-1093, 2006.

31. Kim D. H., Park J. U., Cho K. S., Ahn K. H., Lee S. J., “A Novel Fabrication Method for Polypropylene/Clay Nanocomposites by Continuous Processing”, Macromolecular Materials and Engineering, vol. 291, 1127-1135, 2006.

32. Zhang M., Liu Y., Zhang X., Gao J., Huang F., Song Z., Wei G., Qiao J., “The Effect of Elastomeric Nano-Particles on the Mechanical Properties and Crystallization Behavior of Polypropylene”, Polymer, vol. 43, 5133-5138, 2002.

33. Utracki L. A., “Clay-Containing ,Polymeric Nanocomposites”, first edition, Rapra Technology Ltd., Shawbury, UK, 2004.

34. Gianelli W., Ferrara G., Camino G., Pellegati G., Rosenthal J., Trombini R. C., “Effect of Matrix Features on Polypropylene Layered Silicate Nanocomposites”, Polymer, vol. 46, 7037-7046, 2005.

35. Ton-That M. T., Perrin-Sarazin F., Cole K. C., Bureau M. N., Denault J., “Polyolefin Nanocomposites: Formulation and Development”, Polymer Engineering and Science, vol. 44, 1212-1219, 2004.

36. Contreras V., Cafiero M, Da Silva S., Rosales C., Perera R. and Matos M., “Characterization and Tensile Properties of Ternary Blends with PA-6 Nanocomposites”, Polymer Engineering and Science, vol. 46, 1111-1120, 2006.

37. Pandey J. K., Reddy K. R., Kumar P., Singh R. P., “An Overview on the Degrability of Polymer Nanocomposites”, Polymer Degradation and Stability, vol. 88, 234-250, 2005.

38. Svoboda P., Zeng C., Wang H., Lee J., Tomasko D. L., “Morphology and Mechanical Properties of Polypropylene/Organoclay Nanocomposites”, Journal and Applied Polymer Science, vol. 85, 1562-1570, 2001.

39. Kim G. M., Michler G. H., Rösch J. and Mülhaupt R., ”Micromechanical Deformation Processes in Toughened PP/PA/SEBS-*g*-MA Blends prepared by reactive processing”, Acta Polymerica, vol 49, 88-95, 1998.

40. Cimmino S., Coppola F., D’Orazio L., Greco R., Maglio G., Malinconico M., Mancarella C., Martuscelli E. and Ragosta G., ”Ternary Nylon-6/Rubber/Modified Rubber Blends: Effect of the Mixing Procedure on Morphology, Mechanical and Impact Properties”, Polymer, vol 27, 1874-1884, 1986.

41. Karayannidis G.P., Bikiaris D.N., Papageorgiou G.Z. and Bakirtzis V., “Rubber Toughening of Glass Fiber Reinforced Nylon-6,6 with Functionalized Block Copolymer SEBS-g-MA”, Advances in Polymer Technology, vol 21, 153-163, 2002.

42. www.nanoclay.com (Southern Clay Products), last accessed May 2007.

43. www.lotader.com (Arkema Chemicals), last accessed May 2007.

44. www.dow.com (The Dow Chemical Company), last accessed April 2007.

45. www.eserc.stonybrook.edu/ProjectJava/Bragg (Braggs Law), last accessed December 2006.

46. www.polymerprocessing.com (Polymer Processing), last accessed July 2005.

47. en.wikipedia.org (The free encyclopedia), last accessed May 2007.

48. van der Wal A., Nijhof R. and Gaymans R., "Polypropylene–Rubber Blends: 2. The Effect of the Rubber Content on the Deformation and Impact Behaviour", Polymer, vol 40, 6031-6044, 1990.

49. Bucknall C. B., Heather P.S. and Lazzeri A. J., "Rubber Toughening of Plastics Part 12 Deformation Mechanisms in Toughened Nylon 6,6", Journal of Material Science, vol 16, 2255-2261, 1989.

50. ISO 179-2:1997 "Plastics-Determination of Charpy Impact Properties-Part 2: Instrumented Impact test", International Organization for Standardization.

51. ISO 527-1: 1977 "Plastics-Determination of Tensile Properties-Part 1: General Principles", International Organization for Standardization.

52. ISO 527-2: 1997 "Plastics-Determination of Tensile Properties-Part 2: Test Conditions for Moulding and Extrusion Plastics", International Organization for Standardization.

53. ISO R1133 "Plastics-Determination of the Melt Mass-Flow Rate (MFR) and the Melt Volume-Flow Rate (MVR) of Thermoplastics, "International Organization for Standardization.

54. Kim J. H., Koo C. M., Choi Y. S., Wang K. H., Chung I. J., "Preparation and Characterization of Polypropylene/Layered Silicate Nanocomposites Using an Antioxidant", Polymer, vol 45, 7719-7727, 2004.

55. Manias E., Touny A., Wu L., Strwhecker K., Lu B., Chung T. C., "Polypropylene/Montmorillonite Nanocomposites. Review of the Synthetic Routes and Materials Properties", Chem. Mater., vol 13, 3516-3523, 2001.

56. Alexandre M., Dubois P., "Polymer-Layered Silicate Nanocomposites: Preparation, Properties and Use of a New Class of Materials", Materials Science and Engineering, vol 28, 1-63, 2000.

57. Cheremisinoff N. P., “Polymer Characterization Laboratory Techniques and Analysis”, Noyes Publication, USA, 1996.

58. Wang L. Z., “Characterization of Nanophase Materials”, Wiley-VCH, Germany, 2001.

59. Miller E. T., “Introduction to composites”, fourth edition”, Composite Institute, New York, 1990.

60. Zhang Q., Yu Z., Xie X., Mai Y., “Crystallization and Impact Energy of Polypropylene/$CaCO_3$ Nanocomposites with Nonionic Modifier”, Polymer, vol. 45, 5985-5994, 2004.

61. Bao S. P., Tjong S. C., “Impact Essential Work of Fracture of Polypropylene/Montmorillonite Nanocomposites Toughened with SEBS-g-MA Elastomer”, Composites, vol. 38, 378-387, 2007.

62. Lei S. G., Hoa S. V., Ton-That M. T., “Effect of Clay Types on the Processing and Properties of Polypropylene Nanocomposites”, Composites Science and Technology, vol. 66, 1274-1279, 2006.

APPENDIX A

DSC ANALYSIS

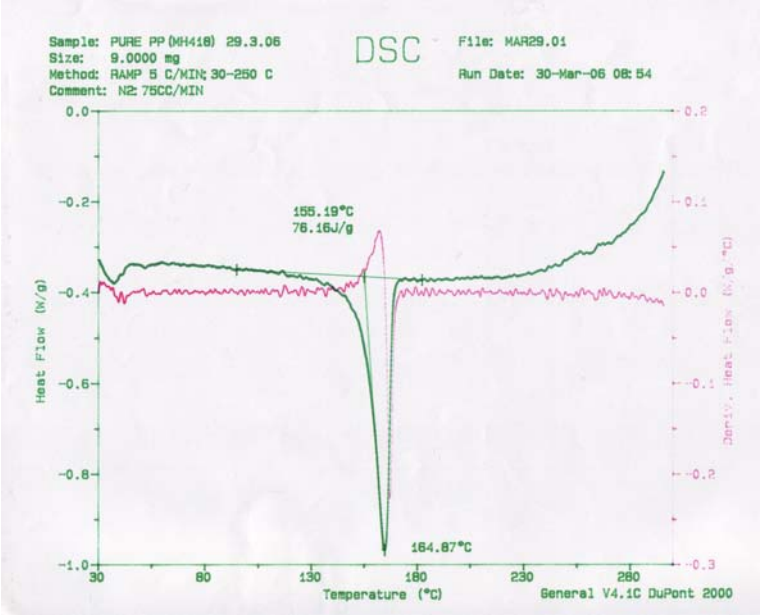

Figure A.1 DSC thermogram of Polypropylene.

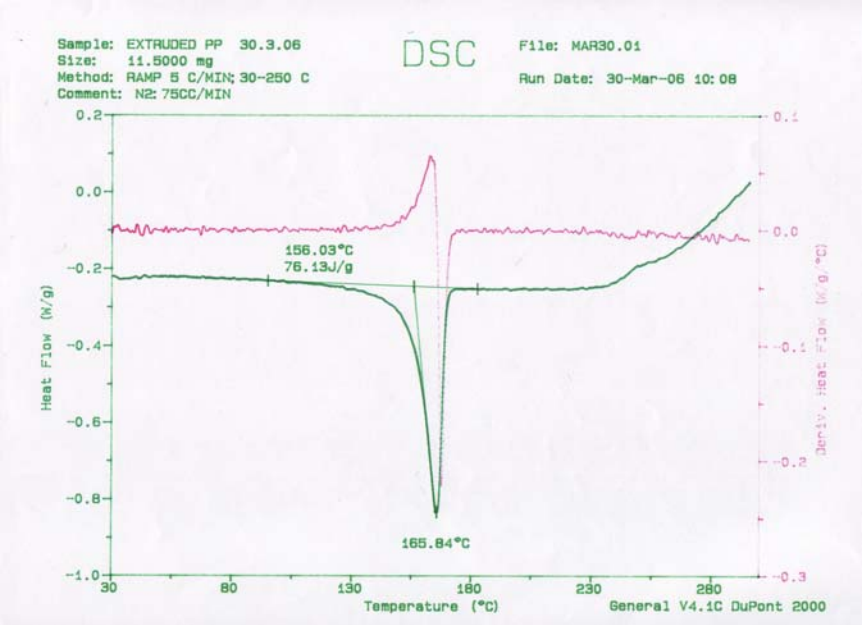

Figure A.2 DSC thermogram of twice-extruded Polypropylene.

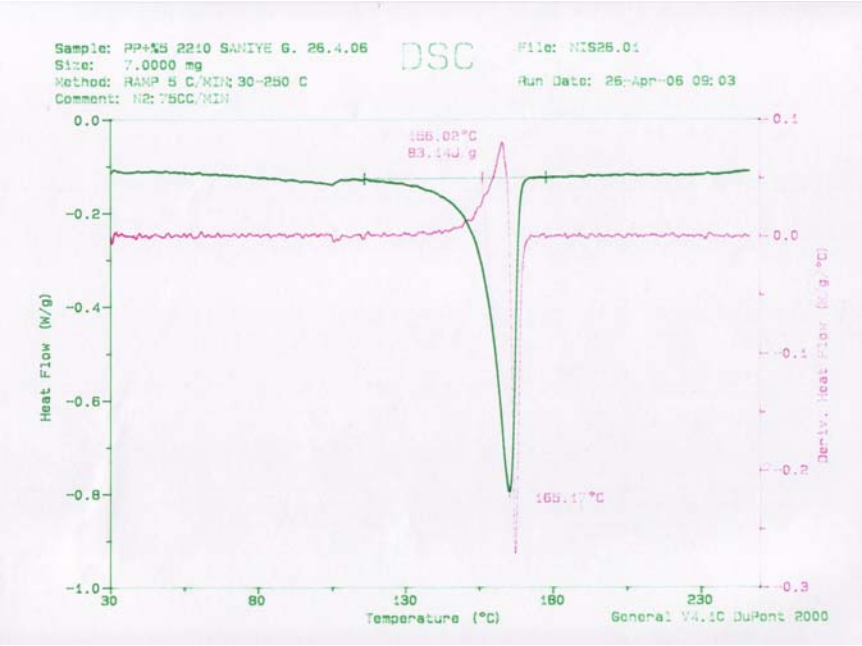

Figure A.3 DSC thermogram of PP+5% 2210.

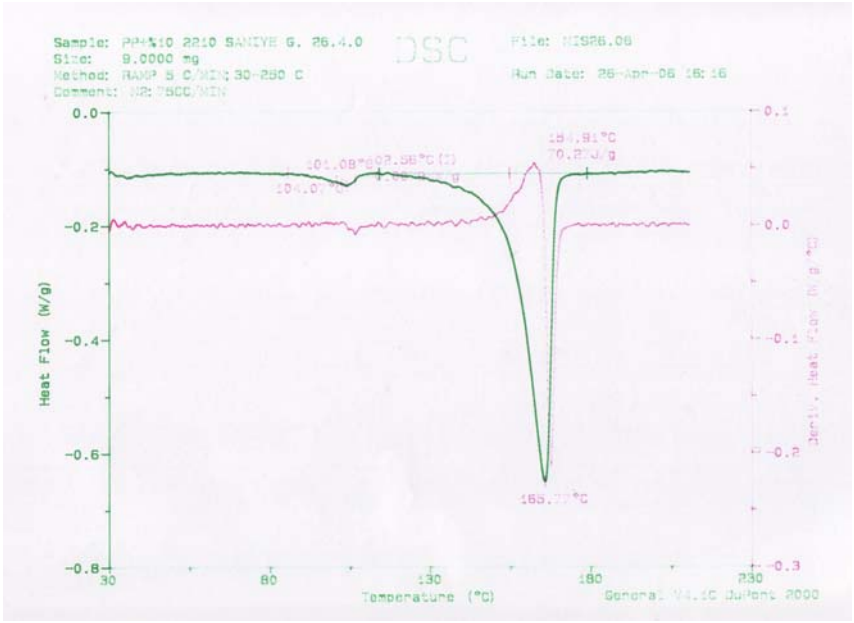

Figure A.4 DSC thermogram of PP+10% 2210.

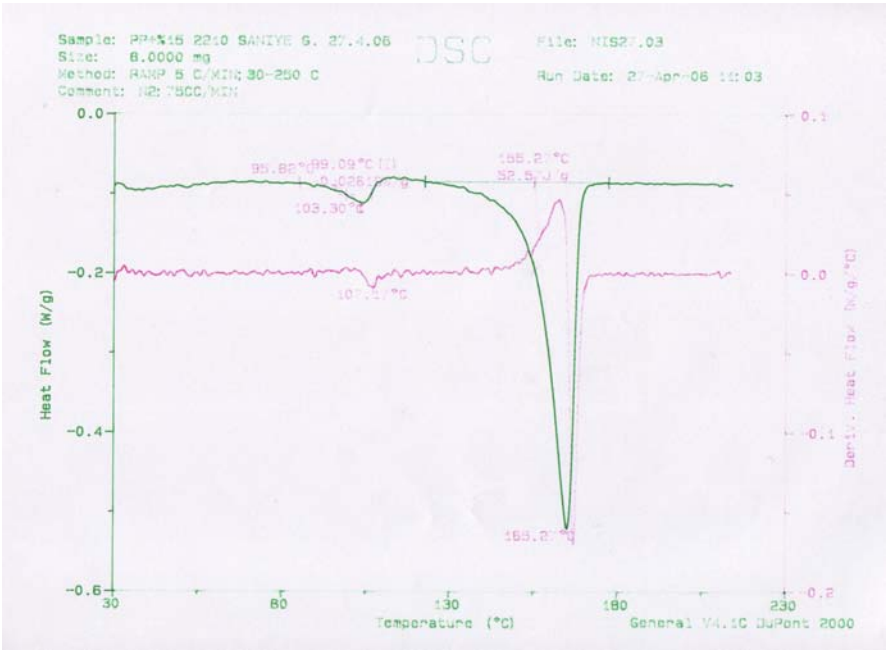

Figure A.5 DSC thermogram of PP+15% 2210.

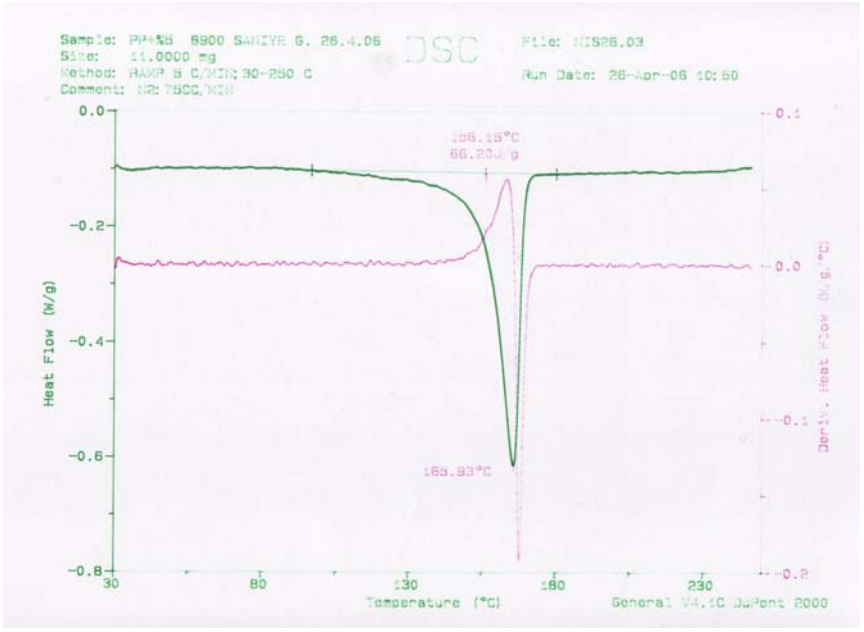

Figure A.6 DSC thermogram of PP+5% 8900.

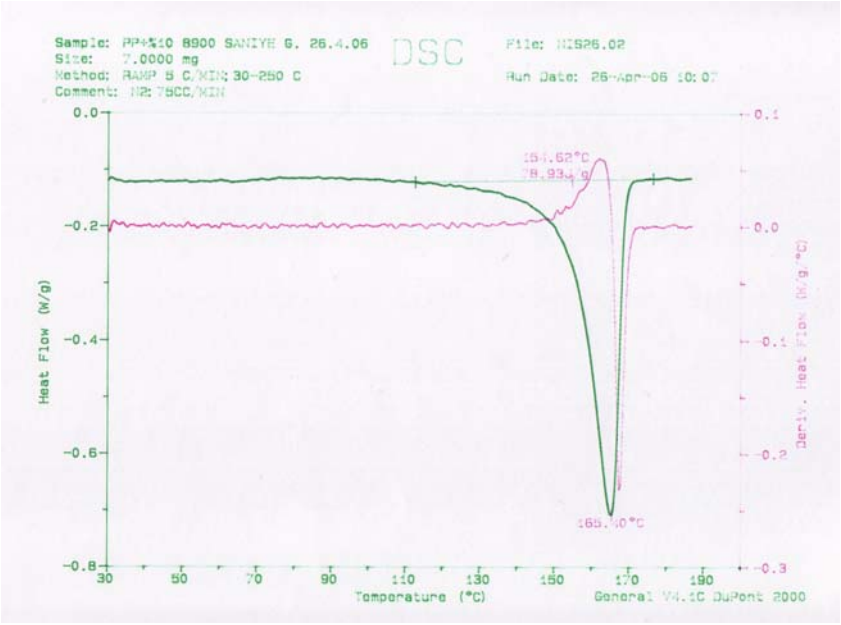

Figure A.7 DSC thermogram of PP+10% 8900.

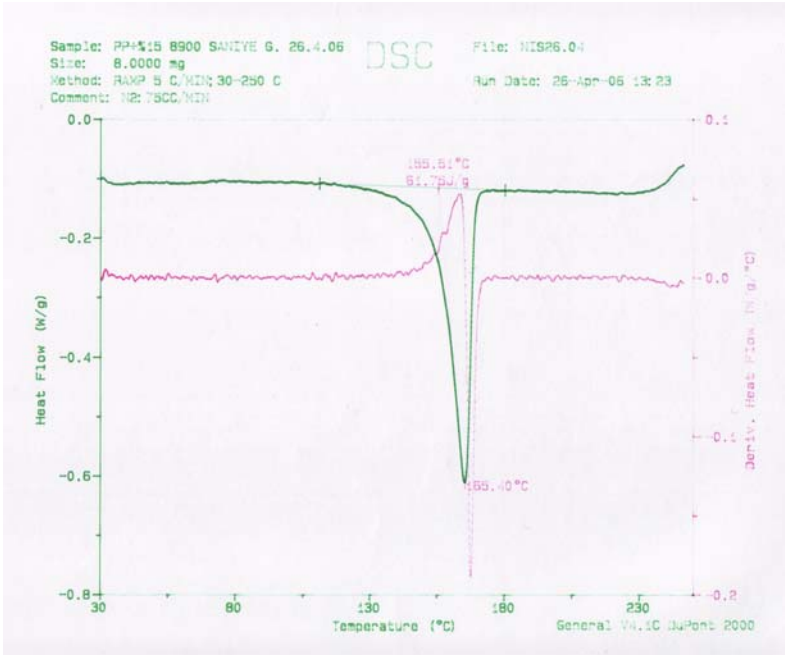

Figure A.8 DSC thermogram of PP+15% 8900.

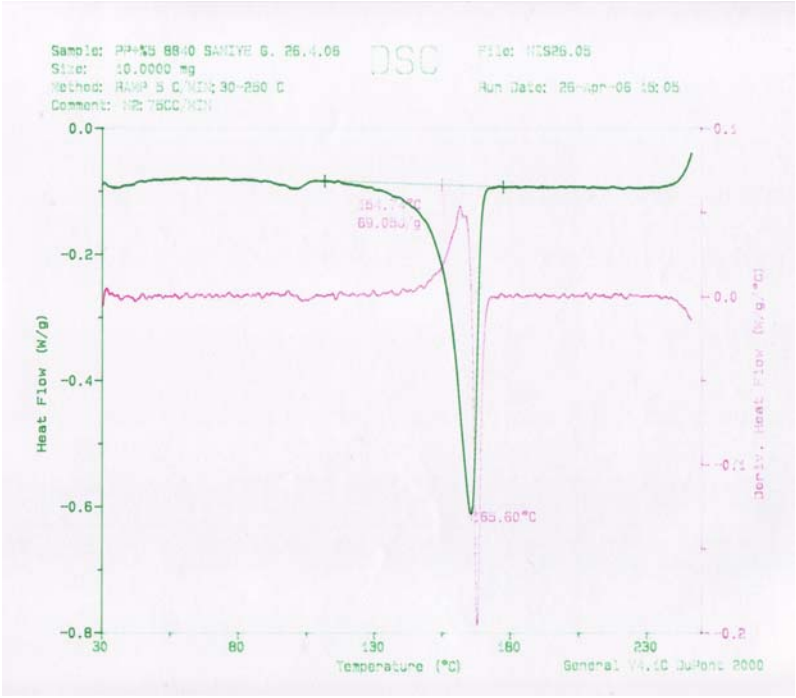

Figure A.9 DSC thermogram of PP+5% 8840.

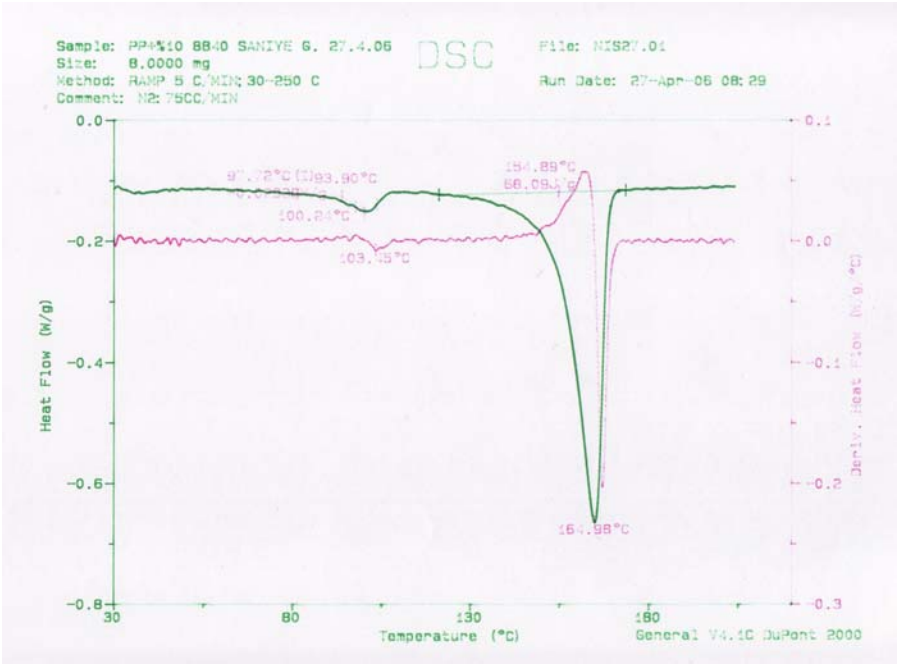

Figure A.10 DSC thermogram of PP+10% 8840.

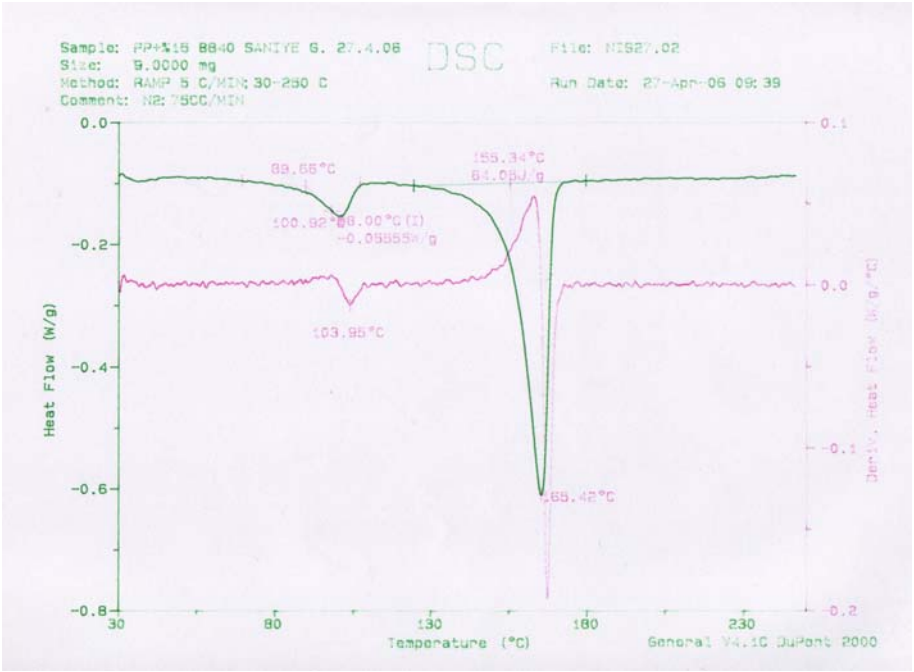

Figure A.11 DSC thermogram of PP+15% 8840.

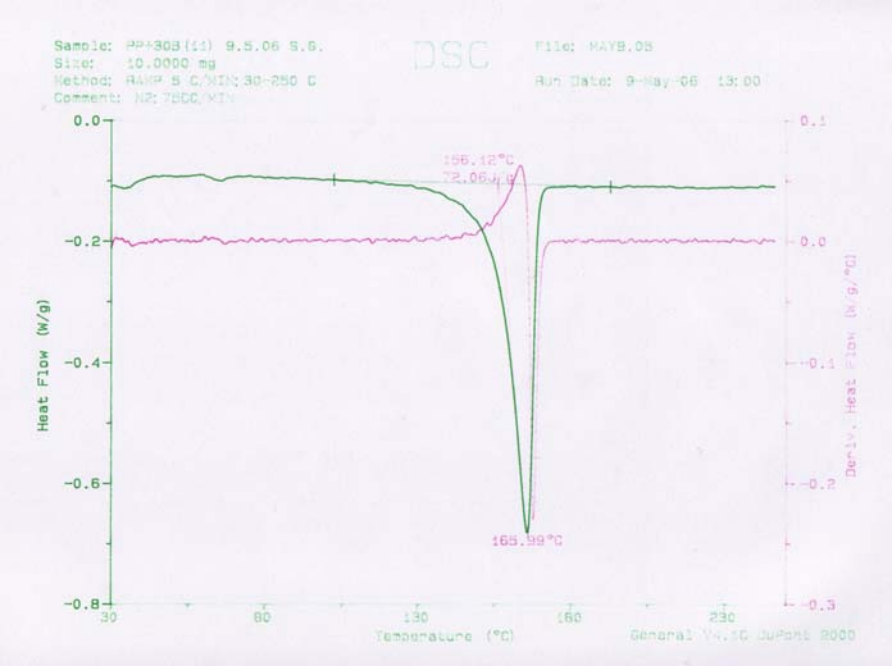

Figure A.12 DSC thermogram of PP+30B.

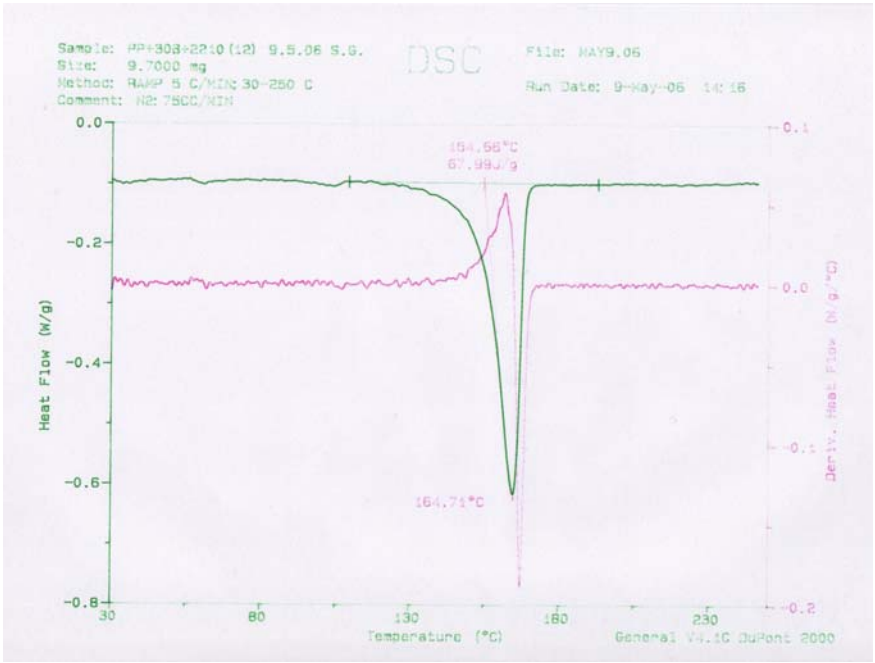

Figure A.13 DSC thermogram of PP+30B+2210.

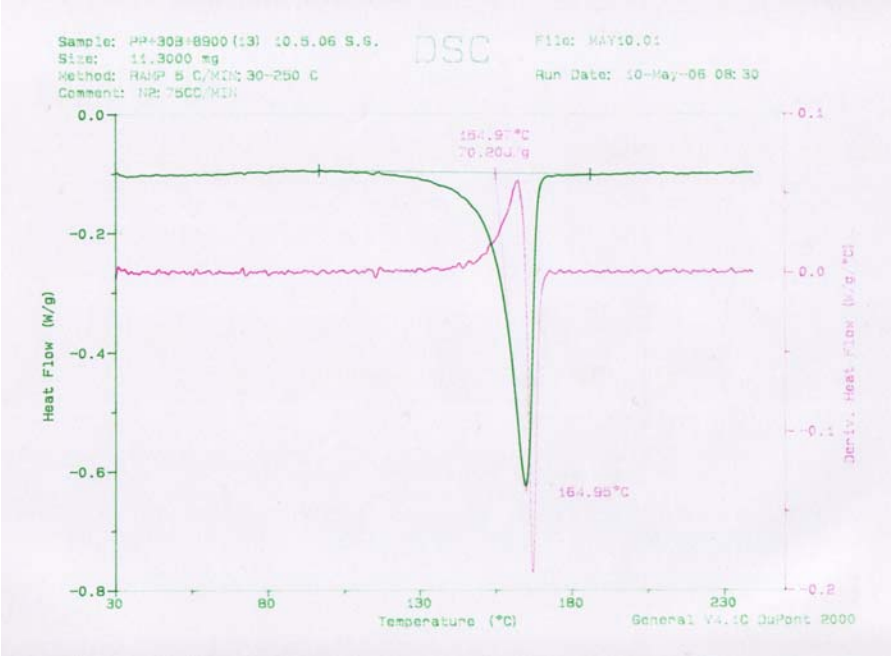

Figure A.14 DSC thermogram of PP+30B+8900.

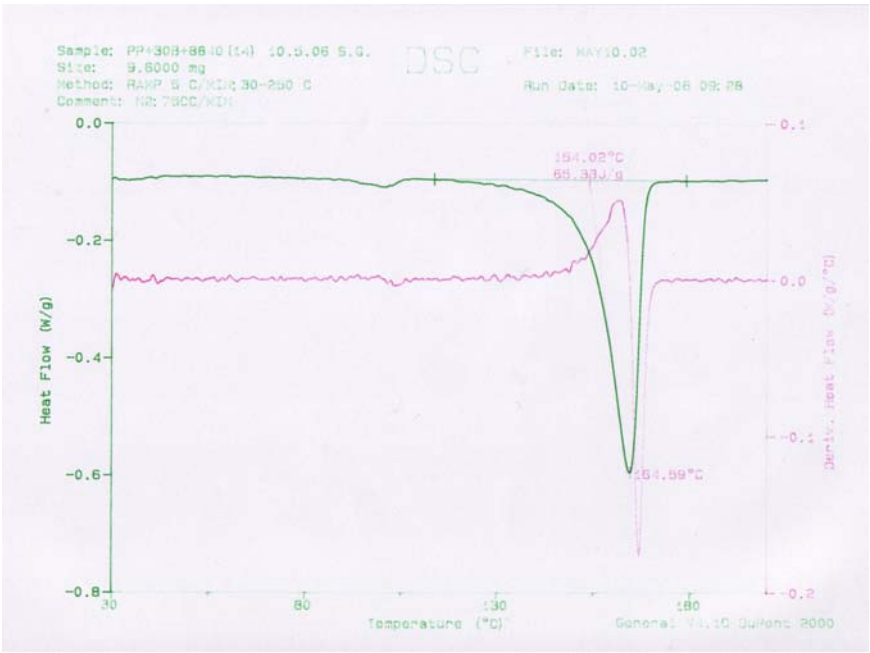

Figure A.15 DSC thermogram of PP+30B+8840.

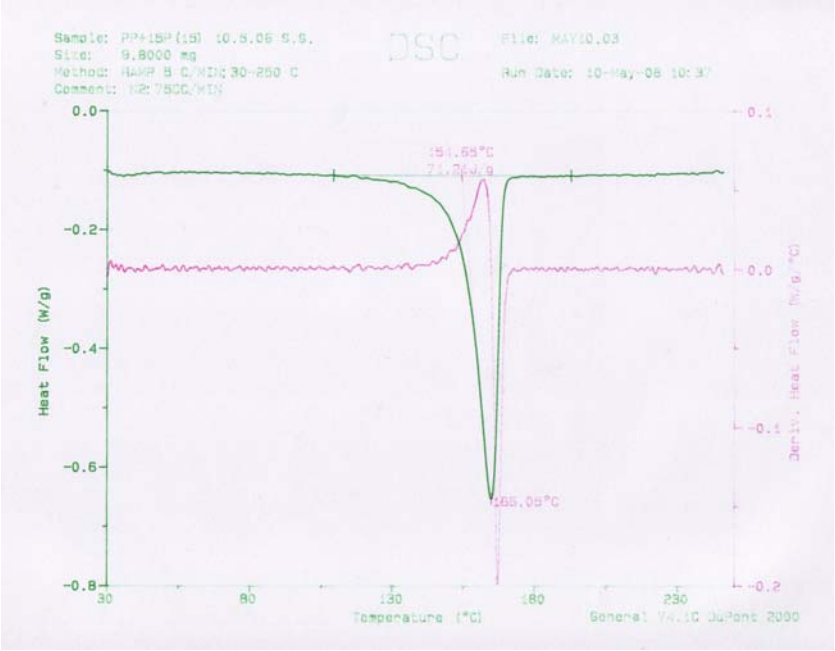

Figure A.16 DSC thermogram of PP+15A.

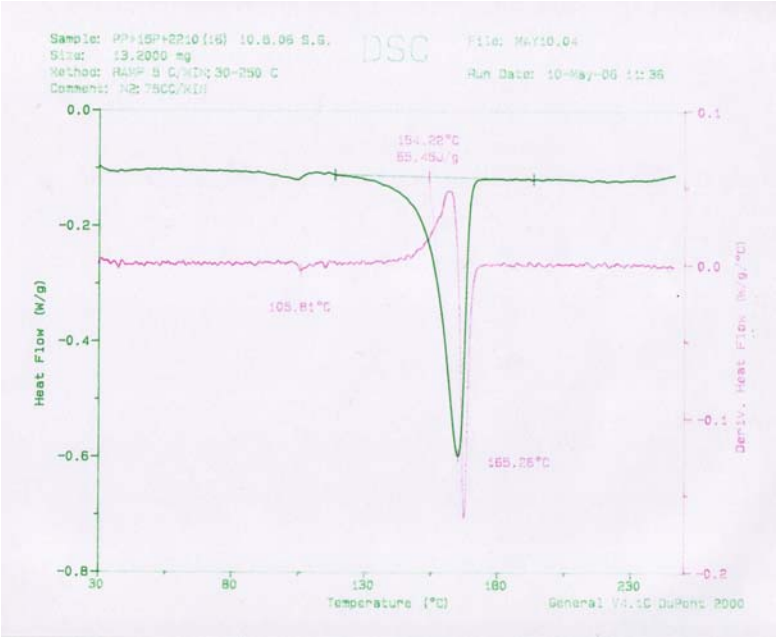

Figure A.17 DSC thermogram of PP+15A+2210.

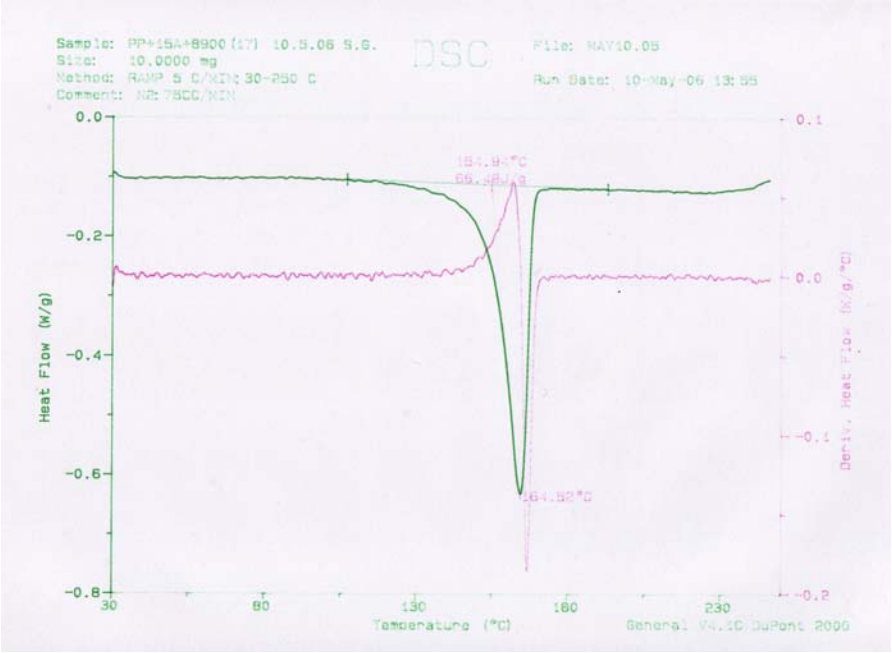

Figure A.18 DSC thermogram of PP+15A+8900.

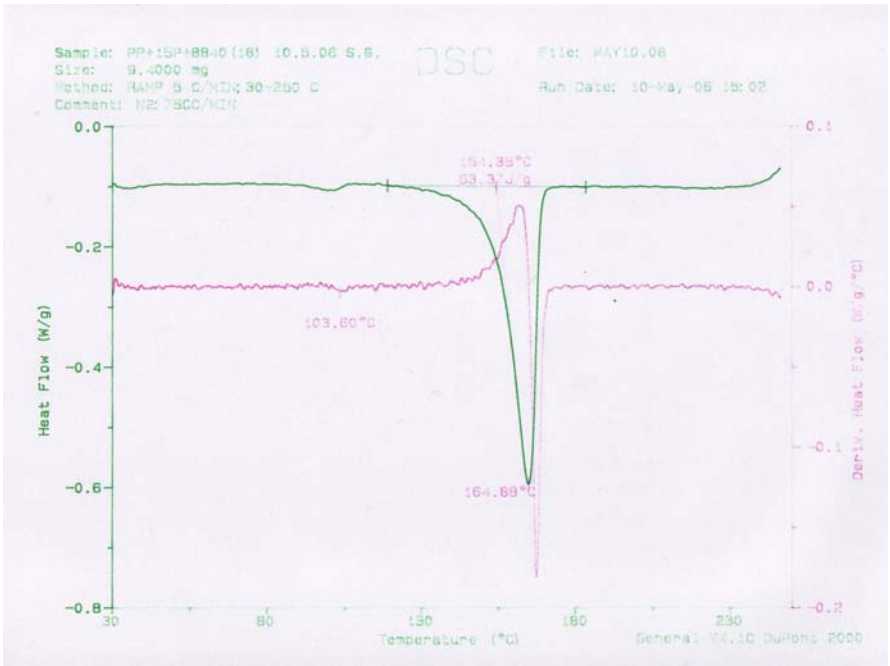

Figure A.19 DSC thermogram of PP+15A+8840.

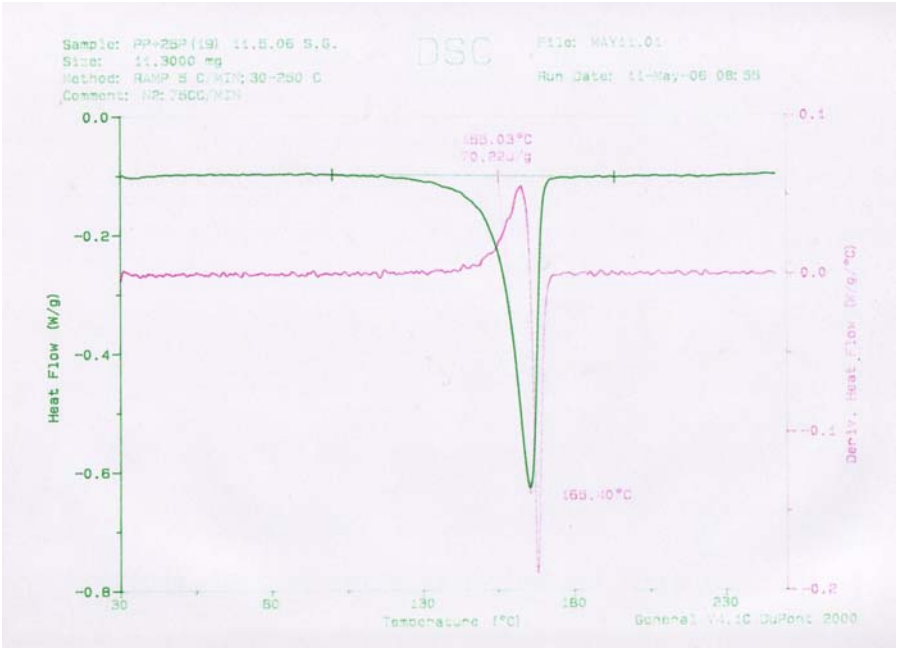

Figure A.20 DSC thermogram of PP+25A.

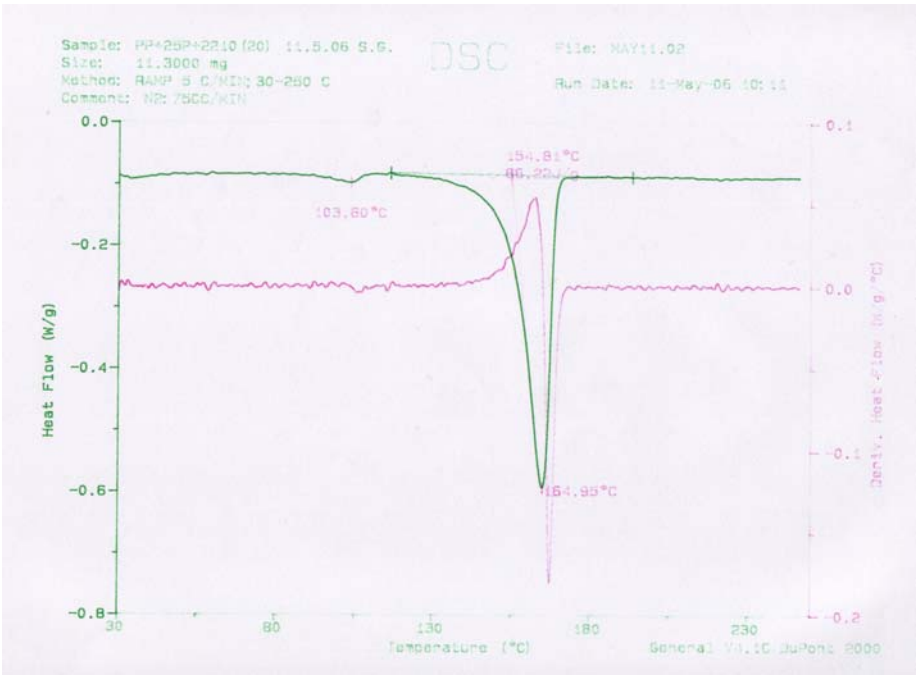

Figure A.21 DSC thermogram of PP+25A+2210.

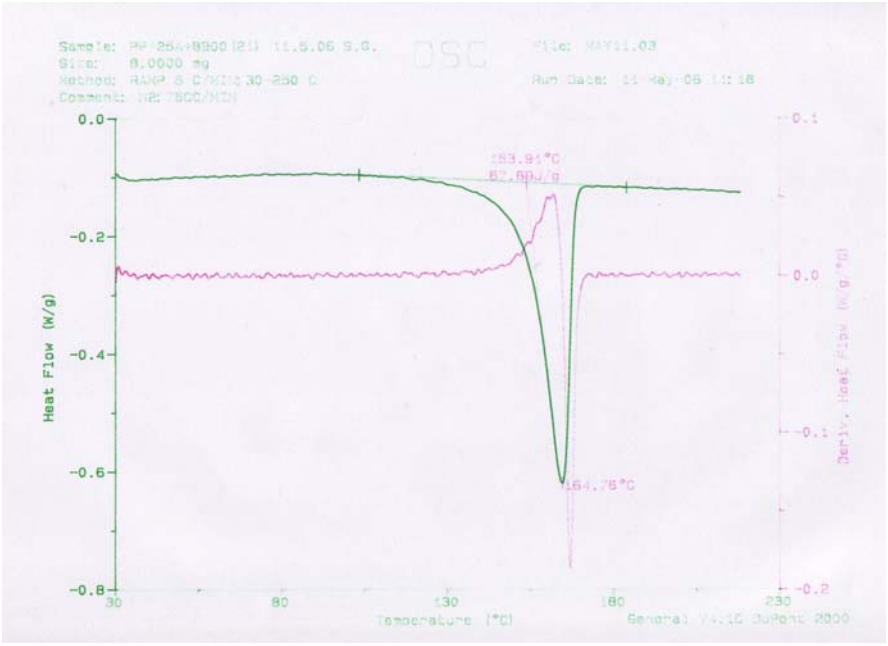

Figure A.22 DSC thermogram of PP+25A+8900.

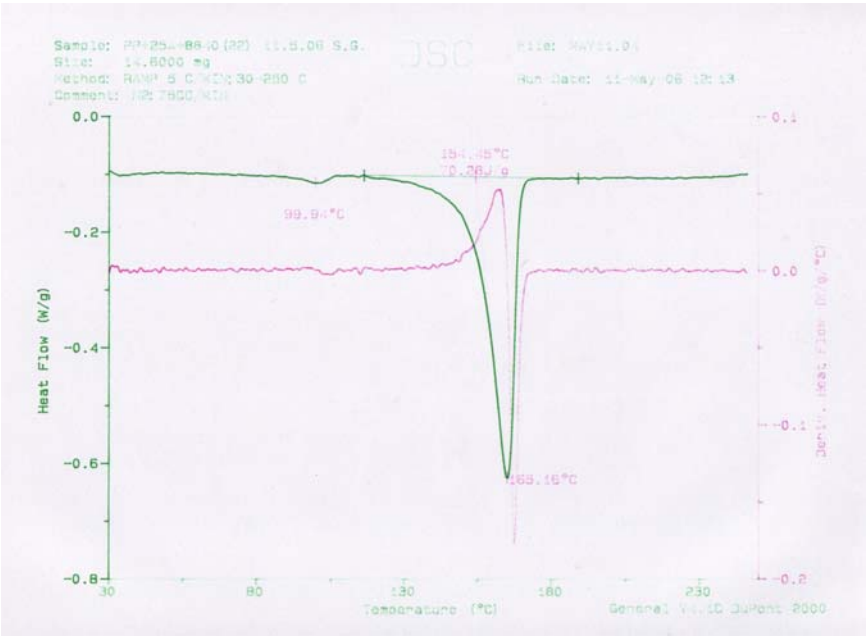

Figure A.23 DSC thermogram of PP+25A+8840.

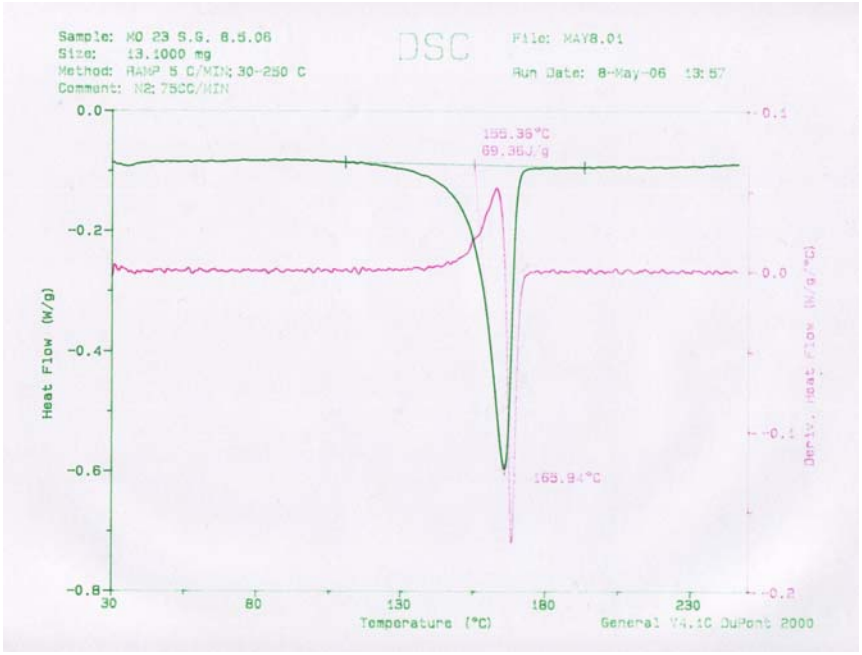

Figure A.24 DSC thermogram of MO23 (PE)C1.

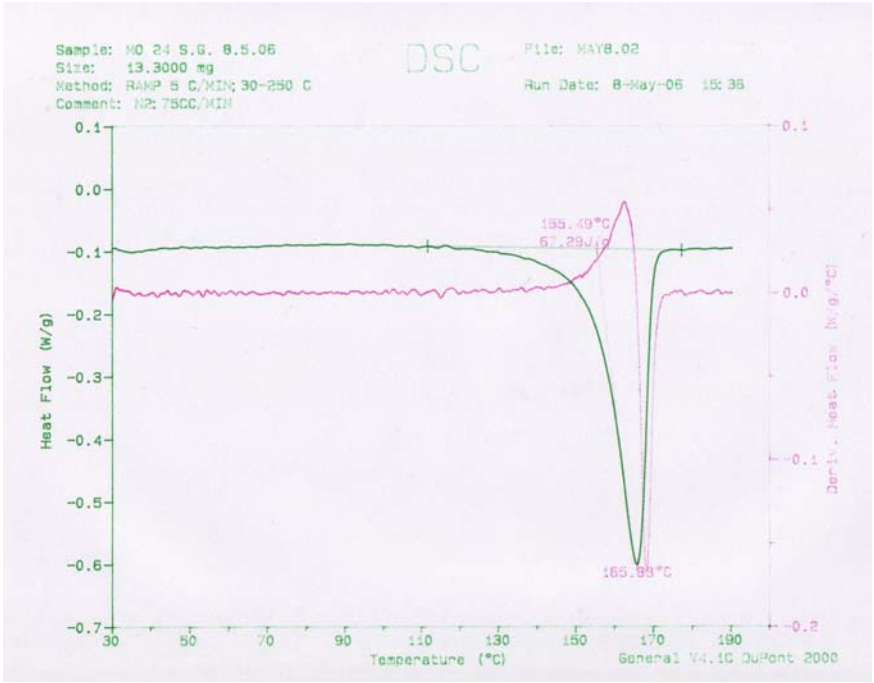

Figure A.25 DSC thermogram of MO24 (PE)C2.

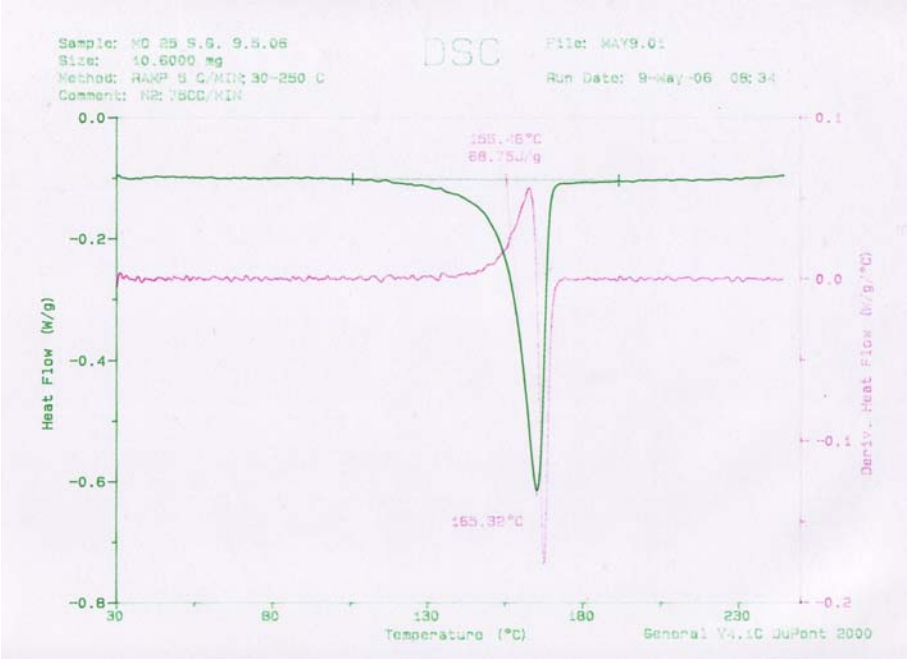

Figure A.26 DSC thermogram of MO25 (C1E)P.

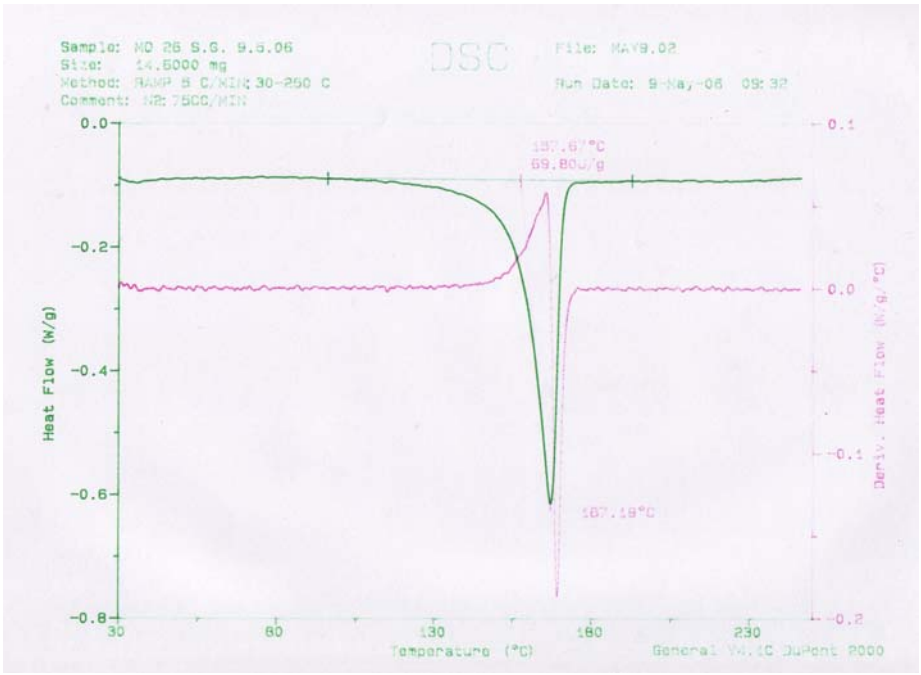

Figure A.27 DSC thermogram of MO26 (C2E)P.

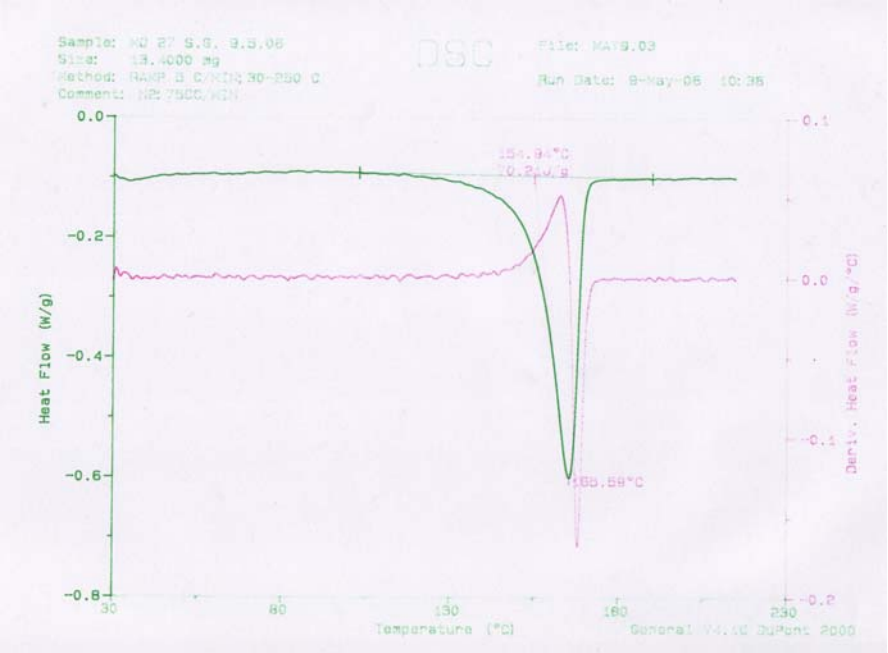

Figure A.28 DSC thermogram of MO27 (PC1)E.

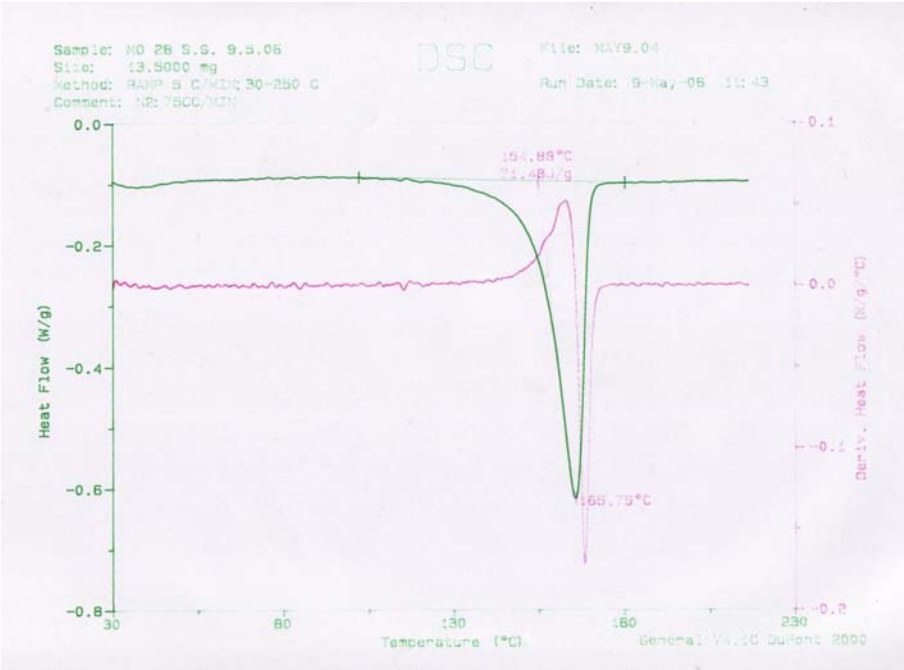

Figure A.29 DSC thermogram of MO28 (PC2)E.

APPENDIX B

RESULTS OF MECHANICAL TESTS

Table B.1. Tensile modulus data for all samples

Sample	Organoclay (wt %)	Compatibilizer (wt %)	Modulus (MPa)	st. dev.
PP	0	0	711	±48.9
PP+2210	0	5	682	±28.7
PP+2210	0	10	704	±46.6
PP+2210	0	15	644	±17.0
PP+8900	0	5	725	±23.6
PP+8900	0	10	682	±17.0
PP+8900	0	15	628	±29.4
PP+8840	0	5	725	±21.5
PP+8840	0	10	682	±19.2
PP+8840	0	15	644	±25.1
PP+30B	2	0	1125	±266.8
PP+30B+2210	2	5	1055	±57.5
PP+30B+8900	2	5	1082	±105.0
PP+30B+8840	2	5	1032	±49.1
PP+15A	2	0	1120	±55.5
PP+15A+2210	2	5	1127	±50.3
PP+15A+8900	2	5	1030	±60.7
PP+15A+8840	2	5	1010	±53.6
PP+25A	2	0	1161	±67.9
PP+25A+2210	2	5	1120	±55.9
PP+25A+8900	2	5	1140	±40.6
PP+25A+8840	2	5	1055	±57.5
(PE)C1	2	5	579	±19.2
(PE)C2	2	5	550	±13.0
(C1E)P	2	5	537	±22.8
(C2E)P	2	5	562	±42.5
(PC1)E	2	5	552	±30.9
(PC2)E	2	5	552	±26.2

Table B.2. Tensile strength data for all samples

Sample	Organoclay (wt %)	Compatibilizer (wt %)	Tensile Strength (MPa)	st. dev.
PP	0	0	48.5	±2.9
PP+2210	0	5	51.2	±5.7
PP+2210	0	10	51.9	±3.6
PP+2210	0	15	49.6	±2.8
PP+8900	0	5	51.3	±0.7
PP+8900	0	10	51.5	±2.1
PP+8900	0	15	46.7	±4.6
PP+8840	0	5	50.5	±5.0
PP+8840	0	10	49.5	±2.0
PP+8840	0	15	47.7	±1.8
PP+30B	2	0	50.3	±2.6
PP+30B+2210	2	5	51.8	±0.8
PP+30B+8900	2	5	49.7	±3.5
PP+30B+8840	2	5	50.4	±1.3
PP+15A	2	0	51.0	±0.9
PP+15A+2210	2	5	51.1	±0.6
PP+15A+8900	2	5	49.4	±1.1
PP+15A+8840	2	5	50.5	±1.9
PP+25A	2	0	51.4	±1.7
PP+25A+2210	2	5	51.7	±1.7
PP+25A+8900	2	5	49.9	±1.9
PP+25A+8840	2	5	50.5	±0.7
(PE)C1	2	5	47.8	±0.9
(PE)C2	2	5	48.8	±0.8
(C1E)P	2	5	48.51	±1.0
(C2E)P	2	5	45.80	±1.5
(PC1)E	2	5	48.5	±0.4
(PC2)E	2	5	48.3	±1.3

Table B.3. Tensile strain at break data for all samples

Sample	Organoclay (wt %)	Compatibilizer (wt %)	Strain at break (%)	st. dev.
PP	0	0	289.2	±7.4
PP+2210	0	5	326.9	±29.0
PP+2210	0	10	325.8	±21.5
PP+2210	0	15	344.1	±30.7
PP+8900	0	5	317.3	±7.3
PP+8900	0	10	339.7	±21.0
PP+8900	0	15	320.4	±5.8
PP+8840	0	5	300.1	±46.5
PP+8840	0	10	311.8	±13.1
PP+8840	0	15	326.1	±15.9
PP+30B	2	0	310.7	±10.5
PP+30B+2210	2	5	310.2	±9.7
PP+30B+8900	2	5	309.1	±11.4
PP+30B+8840	2	5	316.0	±10.8
PP+15A	2	0	322.1	±8.6
PP+15A+2210	2	5	335.6	±5.0
PP+15A+8900	2	5	311.7	±13.9
PP+15A+8840	2	5	327.2	±7.8
PP+25A	2	0	313.2	±13.6
PP+25A+2210	2	5	322.3	±14.2
PP+25A+8900	2	5	303.8	±15.3
PP+25A+8840	2	5	311.9	±8.9
(PE)C1	2	5	338.7	±28.0
(PE)C2	2	5	353.2	±32.1
(C1E)P	2	5	347.1	±29.0
(C2E)P	2	5	345.7	±44.3
(PC1)E	2	5	359.6	±29.2
(PC2)E	2	5	360.8	±1.2

Table B.4. Flexural modulus data for all samples

Sample	Organoclay (wt %)	Compatibilizer (wt %)	Flexural Modulus (MPa)	st. dev.
PP	0	0	1309	±45
PP+2210	0	5	965	±142
PP+2210	0	10	1251	±123
PP+2210	0	15	1305	±61
PP+8900	0	5	1537	±77
PP+8900	0	10	1343	±61
PP+8900	0	15	1343	±43
PP+8840	0	5	1343	±43
PP+8840	0	10	1269	±70
PP+8840	0	15	1673	±81
PP+30B	2	0	1500	±118
PP+30B+2210	2	5	1298	±114
PP+30B+8900	2	5	1283	±39
PP+30B+8840	2	5	1366	±61
PP+15A	2	0	1913	±49
PP+15A+2210	2	5	1416	±59
PP+15A+8900	2	5	1596	±79
PP+15A+8840	2	5	1541	±95
PP+25A	2	0	1772	±76
PP+25A+2210	2	5	1419	±91
PP+25A+8900	2	5	1589	±45
PP+25A+8840	2	5	1562	±88
(PE)C1	2	5	1318	±39
(PE)C2	2	5	1346	±28
(C1E)P	2	5	1384	±39
(C2E)P	2	5	1418	±51
(PC1)E	2	5	1489	±43
(PC2)E	2	5	1393	±36

Table B.5. Flexural strength data for all samples

Sample	Organoclay (wt %)	Compatibilizer (wt %)	Flexural Strength (MPa)	st. dev.
PP	0	0	35.8	±1.8
PP+2210	0	5	28.6	±2.7
PP+2210	0	10	27.3	±2.8
PP+2210	0	15	28.8	±1.1
PP+8900	0	5	33.2	±0.9
PP+8900	0	10	30.9	±0.4
PP+8900	0	15	28.0	±1.4
PP+8840	0	5	30.2	±1.2
PP+8840	0	10	28.5	±0.8
PP+8840	0	15	32.3	±1.5
PP+30B	2	0	33.9	±4.4
PP+30B+2210	2	5	28.6	±2.8
PP+30B+8900	2	5	28.8	±2.8
PP+30B+8840	2	5	28.1	±2.0
PP+15A	2	0	34.3	±1.3
PP+15A+2210	2	5	29.7	±1.3
PP+15A+8900	2	5	38.7	±1.5
PP+15A+8840	2	5	33.3	±0.9
PP+25A	2	0	34.5	±0.2
PP+25A+2210	2	5	30.8	±2.3
PP+25A+8900	2	5	37.2	±0.6
PP+25A+8840	2	5	31.7	±1.3
(PE)C1	2	5	27.6	±1.1
(PE)C2	2	5	30.2	±1.7
(C1E)P	2	5	29.3	±1.4
(C2E)P	2	5	29.0	±0.9
(PC1)E	2	5	30.8	±1.3
(PC2)E	2	5	32.2	±1.6

Table B.6. Impact strength data for all samples

Sample	Organoclay (wt %)	Compatibilizer (wt %)	Impact Strength (kJ/m^2)	st. dev.
PP	0	0	3.3	±0.2
PP+2210	0	5	3.3	±0.4
PP+2210	0	10	2.7	±1.7
PP+2210	0	15	4.2	±0.1
PP+8900	0	5	4.8	±0.3
PP+8900	0	10	5.9	±1.2
PP+8900	0	15	6.8	±0.4
PP+8840	0	5	3.5	±0.3
PP+8840	0	10	3.9	±0.1
PP+8840	0	15	4.2	±0.1
PP+30B	2	0	3.8	±0.4
PP+30B+2210	2	5	3.6	±0.3
PP+30B+8900	2	5	4.3	±0.6
PP+30B+8840	2	5	3.6	±0.9
PP+15A	2	0	3.7	±0.3
PP+15A+2210	2	5	3.5	±0.4
PP+15A+8900	2	5	4.3	±0.6
PP+15A+8840	2	5	4.2	±0.6
PP+25A	2	0	4.1	±0.2
PP+25A+2210	2	5	3.8	±0.5
PP+25A+8900	2	5	3.6	±0.3
PP+25A+8840	2	5	3.8	±0.6
(PE)C1	2	5	4.4	±0.4
(PE)C2	2	5	4.2	±0.4
(C1E)P	2	5	4.5	±0.4
(C2E)P	2	5	4.8	±0.4
(PC1)E	2	5	4.2	±0.3
(PC2)E	2	5	3.7	±0.4